SOFIA UNIVERSITY "ST. KLIMENT OHRIDSKI"
FACULTY OF CHEMISTRY AND PHARMACY

DEPARTMENT OF ANALYTICAL CHEMISTRY

Ivayla Nedialkova Pantcheva-Kadreva

METAL COMPLEXES OF CARBOXYLIC POLIETHERS MONENSIN AND SALINOMYCIN: STRUCTURE, PROPERTIES AND BIOLOGICAL ACTIVITY

ABSTRACT

OF THE HABILITTATION THESIS

for acquiring DSc Degree

4. Natural sciences, mathematics and informatics

4.2. Chemistry (Analytical chemistry)

Sofia

2023

Ivayla Nedialkova Pantcheva-Kadreva

METAL COMPLEXES OF CARBOXYLIC POLIETHERS MONENSIN AND SALINOMYCIN: STRUCTURE, PROPERTIES AND BIOLOGICAL ACTIVITY

ABSTRACT

OF THE HABILITTATION THESIS

for acquiring DSc Degree

Scientific jury: **prof. Adriana Bakalova, PhD**
prof. Ivelina Georgieva, PhD
prof. Irina Karadjova, PhD
prof. Ognyan Petrov, PhD
assoc. prof. Martin Tsvetkov, PhD
assoc. prof. Neli Mintcheva, PhD
assoc. prof. Silviya Angelova, PhD

The dissertation contains 155 pages, illustrated with 59 figures, 30 tables, and 5 Appendixes. The bibliographic reference covers 188 literature sources.

The DSc Thesis was discussed, accepted and directed for defense in front of a scientific jury by the Council of the Analytical Chemistry Department, Faculty of Chemistry and Pharmacy, Sofia University "St. Kliment Ohridski", held on 27.10.2023

The public defense of the DSc Thesis will take place on ..... from ..... h in the Meeting Hall of the Faculty of Chemistry and Pharmacy, Sofia University "St. Kliment Ohridski", Sofia, 1, J. Boucher" Blvd.

The defense materials are available to those interested in the office of the Faculty of Chemistry and Pharmacy at Sofia Unuversity "St. Kliment Ohridski", 1, J. Boucher Blvd., Office 107, and on the website of FCP.

Content

1. Introduction

More animals have been medicated with ionophores, such as monensin,
for control of disease than any other medicinal agents in the history of veterinary medicine.
Chapman, Jeffers, Williams, 2010

Diseases caused by microorganisms and parasites are subject of extensive interdisciplinary research aiming to obtain effective medicines. The introduction of antibiotics into clinical practice gives a powerful impetus to the treatment of a number of infectious diseases, but in recent years humanity is facing an extremely serious problem - the emergence of multiresistant strains of microorganisms. For the treatment of caused conditions, there is a limited number of formulations with broad-spectrum activity. For that reason, the use of several chemotherapeutics with a specific effect is required. Taking a combination of drugs leads to an overload of the body, accompanied by the manifestation of the side effects of each individual medicine and the appearance of cross-resistance. In this sense, the infected organism is exposed to additional stress and a number of its vital functions can be negatively affected by the side effects of antibiotics. Therefore, today's efforts are mainly directed to the development of combined preparations that exhibit a therapeutic effect against multi-resistant infectious agents.

An important challenge that should be emphasized in the search for new active medicines is to optimize the properties of substances in order to increase their selectivity. Currently, the main disadvantage of some of the preparations is their non-specific mode of action, resulting in their effect not only on target microorganisms (positive, healing effect on the patient), but also affect the patient himself (negative or side effect of the drug). The problem of finding effective broad-spectrum antibiotics raises a number of open questions for modern medical scienceover the world, incl. our country and requires the research intensification involving scientists from different fields (chemistry, biology, molecular biology, human and veterinary medicine).

An approach that has been successfully developed in recent decades is based on modifying the properties of already proven in medicine substance by their complexation with metal ions. In clinical practice, a number of compounds are known, which, applied in the form of metal complexes, possess a more pronounced therapeutic effect. The increased activity of metal complexes directly relates to the principle that lower an organism, it is more dependent on concentration of metal ions. In this sense, a minor influence on the metal homeostasis in the "lower-higher organism" system would significantly affect the conditions of the lower

(microorganism or parasite) organism, but would have a minimal impact on the higher (host – human or animal). In order to find effective candidates to combat multidrug-resistant strains of microorganisms, the approach to the synthesis of metal complexes of biologically active substances possesses its pronounced advantages.

Of the antibiotics applied today, those that have found application in human medicine are most intensively studied. For drugs used in veterinary medicine, there is no enough detailed information. In most cases, it was obtained indirectly through the similarity with the effect of compounds administered to humans. The lack of sufficient data about veterinary preparations requires to expand the field of study of their properties. Detailed studies are needed on their effect on microorganisms and animal species, as well as on their possible impact on the human health in contact with the infection source or when ingesting food of animal origin.

The groups of antibiotics most widely used in veterinary medicine is that of the natural polyether ionophores, which are drugs at the first choice in the treatment of coccidiosis, a disease caused by the parasites i. In recent years, it has been established that, in addition to coccidiostatic activity, these substances possess also pronounced antibacterial and fungicidal properties. Of particular interest is the discovery in 2009 that the representative of this class of compounds - salinomycin - is among the top three agents of choice (out of 16,000 compounds) in the treatment of tumor stem cells in breast cancer. In this respect, increased research attention has been observed regarding the study of the potential antitumor properties of monensin, salinomycin, lasalocid - ionophores with direct application in veterinary medicine, as well as their various chemical modifications.

The main objects of the present study are the ionophores monensin and salinomycin (**Fig. 1**). Their choice is determined by the following reasons:

- monensin is the most widely aplied antibiotic in veterinary medicine;

- salinomycin possesses promising antitumor potential;

- last but not least - Bulgaria is a producer of both ionophores, which creates the conditions for a wider and targeted study of their properties.

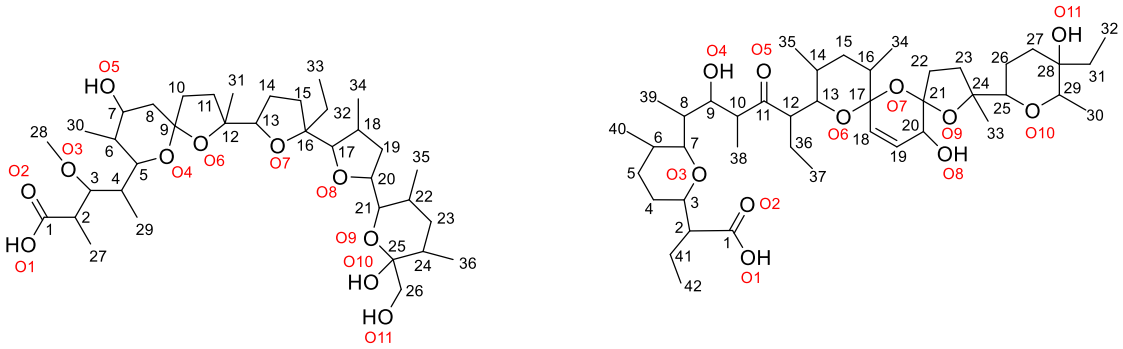

Fig. 1. Structure and numbering scheme of MonH (left) and SalH (right)

Based on the review of the scientific literature, two directions can be outlined: an area of already gained knowledge, and one in which there are "white spots" which should be studied in more details.

Monensin and salinomycin are representatives of monocarboxylic polyether ionophores; they preferentially bind monovalent metal cations; they are used in veterinary practice as coccidiostats and antibacterial agents; both antibiotics show potential in the therapy of oncological diseases; the environment affects their biological properties.

What we do not know about monensin and salinomycin: can the environment (presence of different metal ions) influence their effect through complexation? What is the behavior of the two ionophores in the presence of metal cations in a higher oxidation state? If the conditions exist to isolate new metal-containing species, how would the biological activity of monensin and salinomycin bound in these coordination compounds be affected?

An answer to these questions is provided by the present Thessis, which reviews the achievements in the field of coordination chemistry of the polyether ionophores monensin and salinomycin.

2. Aim of the DSc Thesis

The aim of the Thesis is to present the complexation processes involving the polyether ionophorous antibiotics monensin and salinomycin and the properties of the corresponding coordination species. The results are summarized in three directions:

- ✓ preparation, isolation and structural characterization of coordination compounds with metal ions in different oxidation state;
- ✓ studies of the "metal ion – ionophore" systems in solution;
- ✓ evaluation of the biological properties of the complexes and comparison of the data with those of the parent ligands.

The dissertation is based on the studies conducted by Ivayla Pancheva, PhD, in the field of coordination chemistry within 2008-2023. The data presented are fully or partially published in 27 original scientific papers, of which 21 articles – in refereed / indexed journals and 4 – in monographs chapters. A total of 204 independent citations (122 of which in the Scopus database) were noticed on the publications used in the current procedure for obtaining the scientific degree "Doctor of Sciences".

Parts of the research were a subject of 9 successfully defended diploma theses (5 in BSc and 4 in MSc) and 3 dissertations for obtaining the PhD degree. Currently, the 4th PhD thesis is being prepared. A large part of the experiments carried out was financially supported by the Bulgarian Scientific Research Fund (DO-02-84/2008, KP-06-H29/3-2018)

3. Results and Discussion

Complexes of monensin and salinomycin – structure and spectral properties

In this chapter, the all complexes of monensin and salinomycin (HL), which, after optimization of the synthesis conditions, were isolated in chemically pure form and characterized by a range of spectral methods (UV-VIS, CD, IR, NMR, EPR, FAB -MS), elemental analysis and X-ray diffraction (in the presence of single crystals) are discussed. At the moment, the structural studies regarding the coordination compounds of monensin and salinomycin with metal cations in the second-fourth oxidation state are primarily Bulgarian contributions.

The results are presented in two Sections: "classical" complexes of polyether ionophores, in which the coordination of the ligand is realized bidentately ("head-tail" mode), and "non-classical" - where a different binding way of the antibiotics is observed according to the features of the complex species .

3.1. „Classical“ complexes of monensin and salinomycin

The subject of research are the coordination compounds containing alkaline earth or transition metal ions M^{2+} – $[ML_2(H_2O)_2]$, lanthanide cations M^{3+} – $[ML_3(H_2O)_3]$and Ce^{4+} – $[ML_2(OH)_2]$. They were obtained by reaction of the corresponding metal salts with monoanions of the ligands (monensinate or salinomycinate), which result from the deprotonation of MonH/SalH by an organic base (R_4NOH/Et_3N).

A feature that unites all these complexes are the donor groups of the ionophores - carboxylate and hydroxyl, located at both ends of the antibiotic molecules. Their simultaneous binding in the primary coordination shell of a given metal ion creates prerequisites for the folding of the polyether chain of the ionophore, resulting in a highly distorted macrocyclic structure. In most cases, its stabilization is ensured by a water molecule or hydroxide anion hosted in the hydrophilic cavity of the ligands and participating in the formation of a number of hydrogen bonds. In the discussion below, $[ML_2(H_2O)_2]$ and $[ML_2(OH)_2]$ will be denoted as mononuclear bis-complexes, and $[ML_3(H_2O)_3]$ – as mononuclear tris-complexes.

3.1.1. X-ray diffraction of single crystals

The monensinate complexes $[ML_2(H_2O)_2]$ (M = Mg, Ca, Co, Mn, Ni, Zn, Cd) were isolated as single crystals suitable for X-ray diffraction, which allowed the unambiguous determination of their structure in solid state (**Fig. 3.1-1**, **Table 3.1-1**). The comparison of the crystallographic

data shows that these coordination compounds are isostructural – one metal ion interacts with two ionophore anions, and a water molecule is located in antibiotic's cavity. The four M-O bonds formed with the COO^- and OH-groups of the ionophore define the equatorial plane of the complexes and the antibiotic folds into its characteristic cyclic structure. Water molecules play a dual function: they stabilize the resulting macrocycles through intramolecular hydrogen bonds and participate in donor-acceptor bonds with the metal cation. The presence of water molecules as ligands in the axial position leads to a distorted octahedral geometry of the inner coordination shell of $[MMon_2(H_2O)_2]$. The M-O bond lengths increase with increasing the metal ionic radii in the order $Ni^{2+} < Mg^{2+} < Co^{2+} < Zn^{2+} < Mn^{2+} < Cd^{2+} < Ca^{2+}$ (coord. number of. 6). The nature of the metal ion does not significantly affect the bond angles in the equatorial plane of the complexes: they are all within 3-4º as follows: from 169.55˚ (Ni^{2+}) to 172.16˚ (Ca^{2+}) (O1-M-O111), and from 169.36º (Ni^{2+}) to 173.95º (Ca^{2+}) (O101-M-11), resp. (average deviation of about 10º from the ideal angle 180º). The ionic radius of the divalent metal cations affects significantly the H_2O-M-H_2O bond angle, which decreases in the order Ni^{2+} (164.2º) > Mg^{2+} (160.4º) > Co^{2+} (159.4º) > Zn^{2+} (156.0º) > Mn^{2+} (154.4º) > Ca^{2+} (151.2º) > Cd^{2+} (149.5º). In all these coordination compounds the organic ligands are located in the *cis*-position to the metal ion.

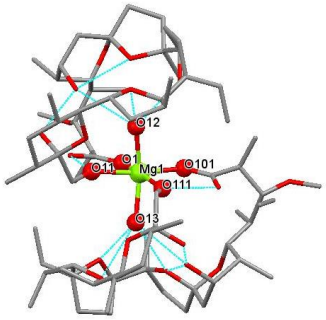

Mg^{2+}

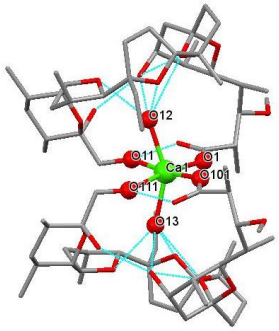

Ca^{2+}

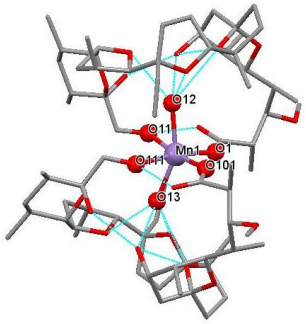

Mn^{2+}

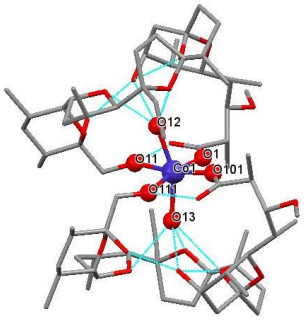

Co^{2+}

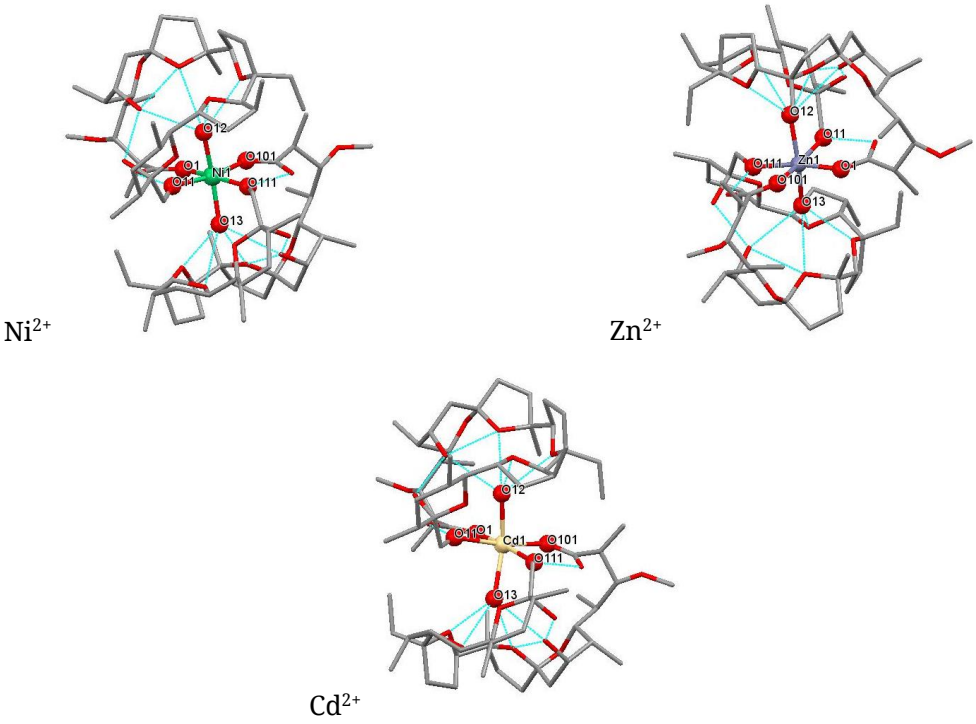

Fig. 3.1-1. Structures of monensin mononuclear complexes with divalent metal ions (intramolecular hydrogen bonds are presented as dashes, and hydrogen atoms are omitted for clarity)

Table 3.1-1. Selected bond lengths (Å) and angles (°) in mononuclear monensinates $[MMon_2(H_2O)_2]$

Bond	Metal(II) ion						
	Mg	Ca	Co	Mn	Ni	Zn	Cd
Bond length							
M-O1	2.029(3)	2.266(3)	2.057(3)	2.116(6)	2.0225(14)	2.038(5)	2.216(6)
M-O101	2.029(3)	2.253(3)	2.047(3)	2.109(6)	2.0136(14)	2.047(4)	2.233(6)
M-O11	2.130(3)	2.358(3)	2.141(3)	2.237(5)	2.0762(14)	2.188(4)	2.370(5)
M-O111	2.136(3)	2.370(3)	2.105(3)	2.235(5)	2.0817(14)	2.145(5)	2.340(6)
M-O12	2.107(3)	2.341(2)	2.125(3)	2.208(5)	2.0900(13)	2.159(4)	2.324(5)
M-O13	2.102(3)	2.340(3)	2.134(3)	2.208(5)	2.0849(14)	2.166(5)	2.337(5)
Angle							
O101-M-O1	88.84(12)	94.63(10)	86.50(15)	89.4(2)	84.00(6)	88.49(19)	89.1(2)
O101-M-O111	85.89(12)	82.54(10)	87.62(14)	86.1(2)	87.81(6)	86.4(2)	86.3(2)
O111-M-O11	99.81(12)	101.03(9)	99.91(12)	99.30(19)	101.00(6)	97.8(3)	99.02(19)

O1-M-O11	86.17(12)	82.44(9)	86.79(12)	85.9(2)	87.86(6)	87.69(19)	86.4(2)
O1-M-O111	171.29(13)	172.17(9)	170.17(12)	171.5(2)	169.37(6)	170.40(18)	171.36(19)
O101-M-O11	172.00(13)	173.94(9)	170.54(13)	172.0(2)	169.57(6)	171.6(2)	171.8(2)
O12-M-O13	160.41(12)	151.22(9)	159.39(12)	154.3(2)	164.21(6)	155.98(16)	149.55(18)

Despite the availability of crystal structures for the [$MMon_2(H_2O)_2$]complexes, they have also been characterized by a range of spectroscopic methods. The collected information is extremely useful in the absence of X-ray structural analysis, as is the case with the rest of the monensin and salinomycin complexes. The structure of the latter was deduced based on their spectral features combined with the elemental analysis data.

3.1.2. Infrared spectroscopy (IR)

IR spectroscopy is the main method for monitoring the changes in ionophore spectra that occur due to complexation. An important indicator is the band for stretching vibration of the carboxyl group (1700 cm^{-1} for MonH and 1710 cm^{-1} for SalH), which in the spectra of coordination compounds [$ML_2(H_2O)_2$] is not observed at the expense of two new bands at ~ 1550 cm^{-1} and ~ 1400 cm^{-1}, attributed to the asymmetric and symmetric stretching vibrations of the carboxylate anion (**Table 3.1-2**). The energy difference between them is of the order of 140-150 cm^{-1} and is characteristic of monodentate coordination of the COO^- group. The second region to be considered is that in the range 3500-3250 cm^{-1}, where changes related to the different behavior of the OH-groups from the ligands and water molecules are observed. No significant changes were registered in the fingerprint area (1100-500 cm^{-1}). The spectra of all coordination compounds of monensin with the studied divalent metal cations are practically indistinguishable from each other, which is in agreement with the crystallographic analysis data. Similar is the spectral behavior of copper(II) monensinate, isolated only as amorphous precipitate. The fact that complexes of salinomycin with divalent metal cations show analogous IR behavior assumes that this series is also isostructural, with the antibiotic coordinating in the same way - through the carboxylate ("head") and the hydroxyl ("tail") groups. Representative spectra of the two antibiotics and their complexes are shown in **Fig. 3.1-2** (monensin) and **Fig. 3.1-3** (salinomycin).

Table 3.1-2. Characteristic IR vibrations of MonH / $[MMon_2(H_2O)_2]$ and SalH / $[MSal_2(H_2O)_2]$

Vibration	Vibration position, cm^{-1}			
	MonH	$[MMon_2(H_2O)_2]$[a]	SalH	$[MSal_2(H_2O)_2]$[b]
ν_{OH} (H_2O)	3520	3490-3360	3500	3450-3380
ν_{OH} (лиганд)	3320	3280		
$\nu_{C=O}$ (COOH)	1700	-	1710	-
$\nu_{C=O}$ (C=O)	-	-	1710	1710-1690[c]
$\nu_{C=O}^{asym}$ (COO^-)	-	1550	-	1560-1550
$\nu_{C=O}^{sym}$ (COO^-)	-	1410-1400	-	1410-1400

[a] M^{2+} = Mg, Ca, Mn, Co, Ni, Cu, Zn, Cd;
[b] M^{2+} = Mg, Ca, Sr, Ba, Co, Ni, Cu, Zn, Cd;
[c] significantly reduced intensity

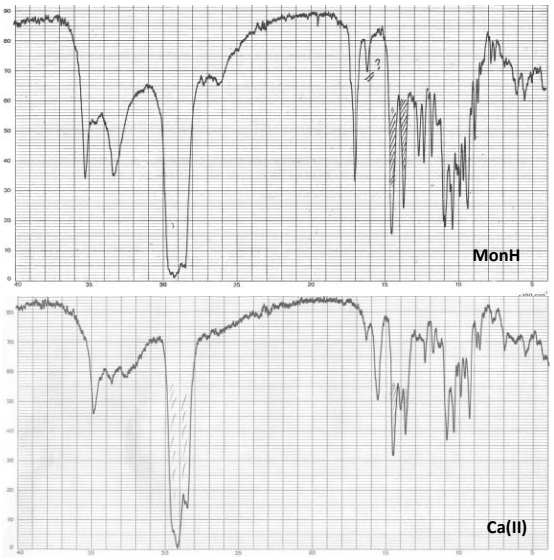

Fig. 3.1-2. IR spectra of MonH and $[CaMon_2(H_2O)_2]$

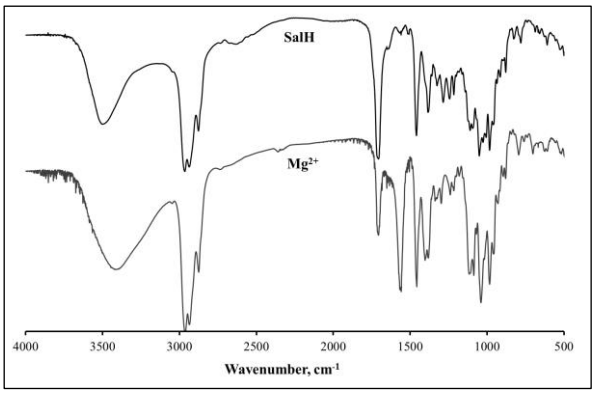

Fig. 3.1-3. IR spectra of SalH and $[MgSal_2(H_2O)_2]$

The hitherto published coordination compounds of the polyether ionophores with lanthanide ions $[ML_3(H_2O)_3]$ show similar IR spectral behavior to that of $[ML_2(H_2O)_2]$. The main conclusion is that the carboxyl group is deprotonated and new vibrations appear for the carboxylate anion (1560 cm^{-1} and 1420 cm^{-1}, corresponding to $\nu^{as}_{COO^-}$ and $\nu^{s}_{COO^-}$), suggesting its participation in the complexes as monodentate ligand. At the same time, a broadening of the bands in the fingerprint region is observed, pointing to the coordination of a heavy metal ion to the corresponding ionophore. The spectra of MonH and SalH and their complexes with La^{3+} ions are shown in **Fig. 3.1-4** and **Fig. 3.1-5**.

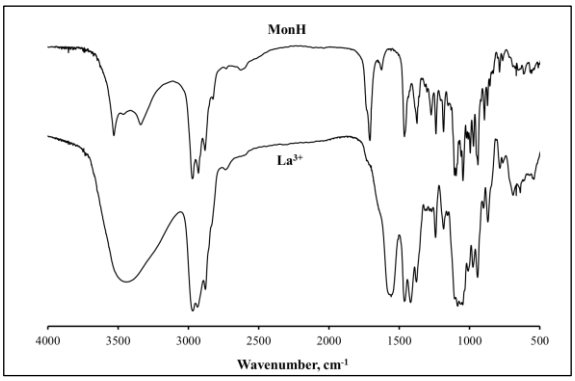

Fig. 3.1-4. IR spectra of MonH and $[LaMon_3(H_2O)_3]$

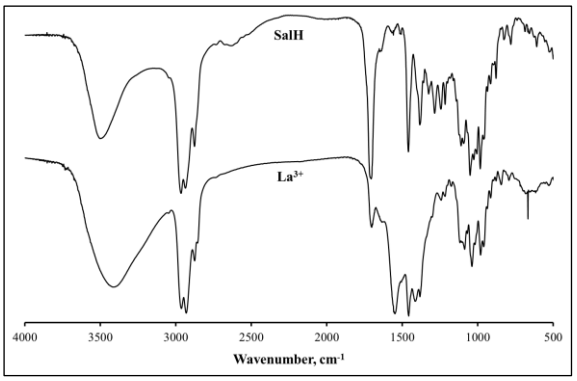

Fig. 3.1-5. IR spectra of SalH and $[LaSal_3(H_2O)_3]$

An exception to the isostructural series of $[ML_2(H_2O)_2]$ and $[ML_3(H_2O)_3]$ are the complexes of Ce^{4+} with monensin and salinomycin $[ML_2(OH)_2]$. In addition to the studies in KBr, those in solution ($CHCl_3$) were also carried out. The data confirm the deprotonation of the antibiotics by the appearance of two new bands characteristic of carboxylate anion at 1552/1414 cm^{-1} (Mon^-) and 1550/1400 cm^{-1} (Sal^-), which is in agreement with the already observed coordination mode of ionophores (**Fig. 3.1-6, 3.1-7**). In case of $[CeMon_2(OH)^2]$, a difference in the range 4000-3000 cm^{-1} is observed compared to the spectra of complexes with divalent metal ions, which is expressed by the appearance of a single broadened signal and points out to the possible absence of coordinated water. Regarding the cerium(IV) salinomycinate, there are no significant changes compared to the uncoordinated antibiotic, and an unequivocal conclusion for the presence of water cannot be made. The IR spectra of both ligands and $[CeL_2(OH)_2]$ in chloroform differ slightly compared to those recorded in solid state. This fact indicates that the compounds retain their structure in both phases, with a minimal amount of the antibiotics in the complexes being protonated due to a solvent impurity of HCl.

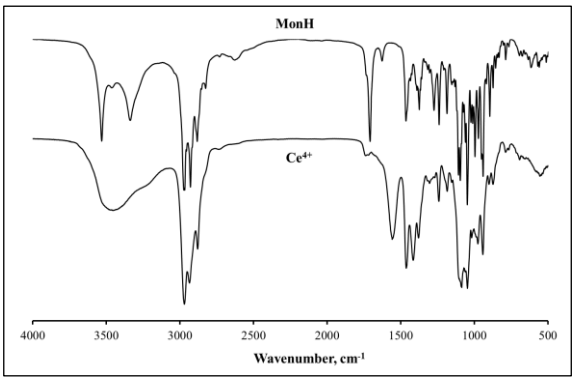

Fig. 3.1-6. IR spectra of MonH and $[CeMon_2(OH)_2]$

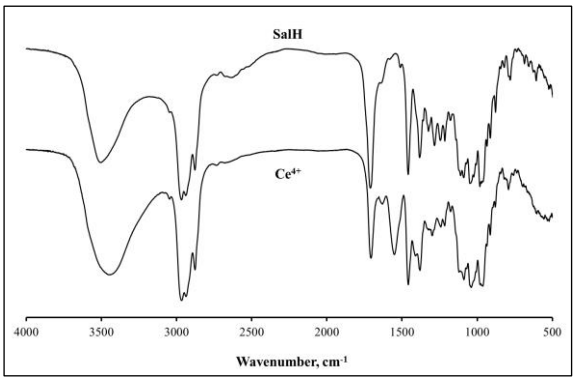

Fig. 3.1-7. IR spectra of SalH and $[CeSal_2(OH)_2]$

3.1.3. Fast atom bombardment mass spectrometry (FAB-MS) or electrospray ionization mass spectrometry (ESI-MS)

The "classical" complexes of monensin and salinomycin were analyzed by mass spectrometry. Over the years, two techniques have been used – FAB-MS or ESI-MS. **Tables 3.1-3 and 3.1-4** summarize the data concerning the main ions proving the formation of coordination compounds of the antibiotics and/or the inclusion of a metal cation in certain molecular fragments[1]. Representative MS spectra and fragmentation patterns of $[CaMon_2(H_2O)_2]$ and $[LaMon_3(H_2O)_3]$ are shown in **Fig. 3.1-8 - 3.1-11**.

Table 3.1-3. Major ions observed in the mass spectra of mononuclear complexes of monensin and salinomycin with divalent metal cations (FAB-MS)

Monensin	m/z		Salinomycin	m/z
$[MgMon_2Na]^+$	1385.2		$[MgSal_2Na]^+$	1546.9
$[CaMon_2Na]^+$	1401.3		$[MgSal]^+$	773.5
$[CaMon]^+$	709.2		$[CaSal_2Na]^+$	1562.9
$[Mn\text{-}Mon]^+$	724.4		$[CaSal]^+$	789.5
$[Co\text{-}Mon]^+$	728.4		$[SrSal]^+$	837.4
$[NiMon_2(H_2O)_2]Na^+$	1455.8		$[BaSal]^+$	887.4
$[NiMon_2]Na^+$	1419.8		$[CoSal]^+$	808.4
$[Ni\text{-}Mon]^+$	727.8		$[NiSal]^+$	808.7
$[ZnMon_2]Na^+$	1491.7		$[CuSal]^+$	813.5
$[Zn\text{-}Mon]^+$	733.4		$[ZnSal]^+$	814.9
$[Cd\text{-}Mon]^+$	783.3		$[CdSal]^+$	863.4

[1] *For the complexes of salinomycin $[MSal_2(H_2O)_2]$ and those of Ce(IV) with the two ligands – $[CeL_2(OH)_2]$, only the molecular ions of $[SalH]Na^+$ or $[MonH]Na^+$ are observed. A probable reason is the easier decomposition of the coordination compounds under the standard conditions of the technnique despite the confirmation of their formation by IR spectroscopy.*

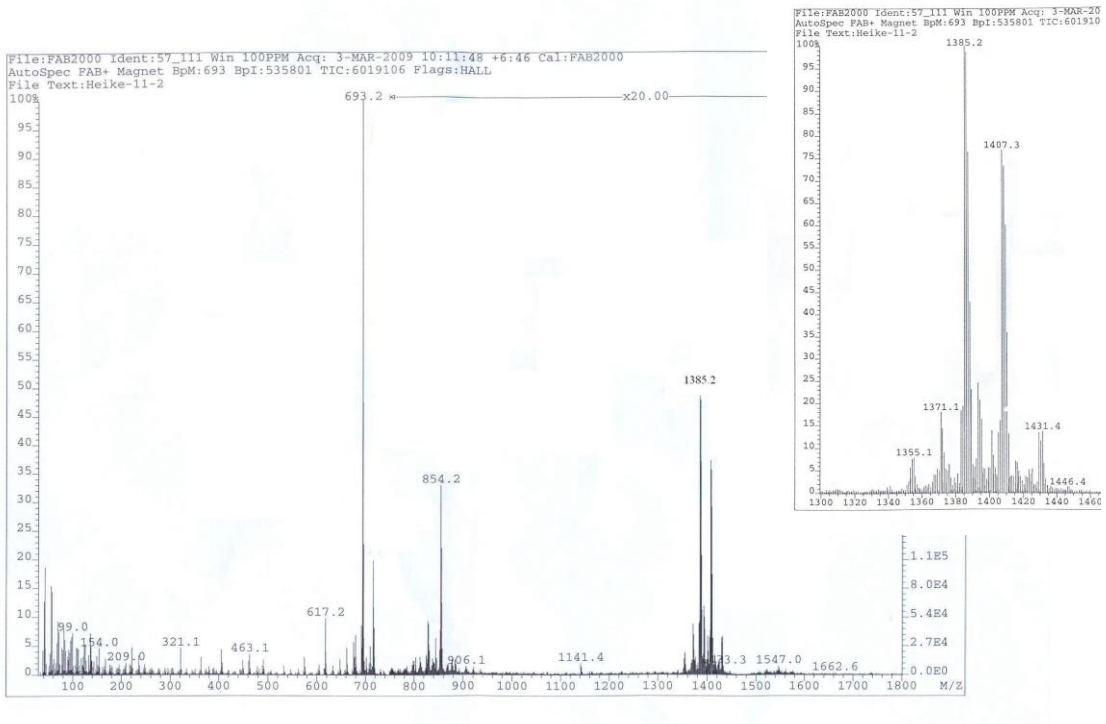

Fig. 3.1-8. FAB-MS spectrum of $[CaMon_2(H_2O)_2]$

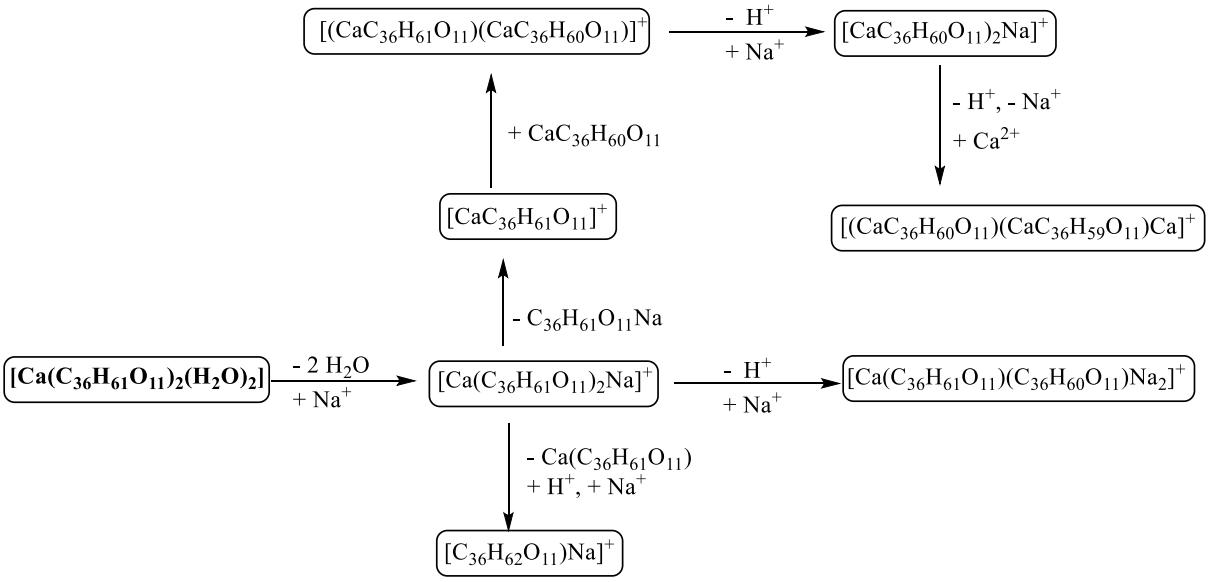

Fig. 3.1-9. Fragmentation pattern of $[CaMon_2(H_2O)_2]$

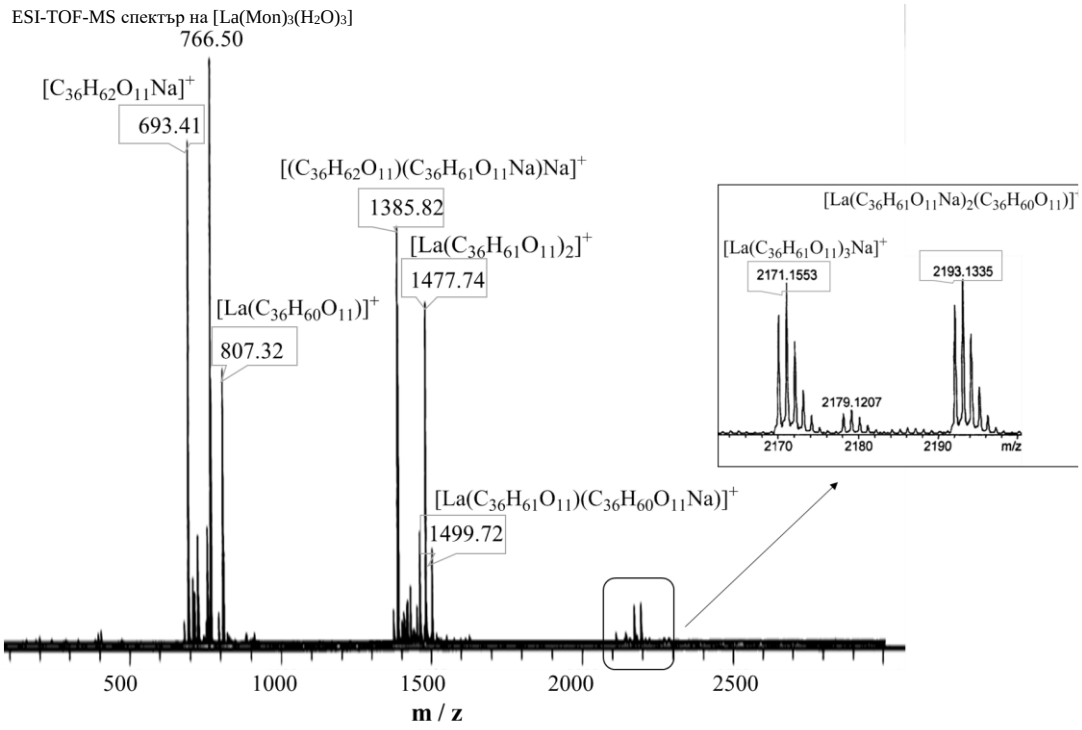

Fig. 3.1-10. ESI-MS spectrum of [LaMon$_3$(H$_2$O)$_3$]

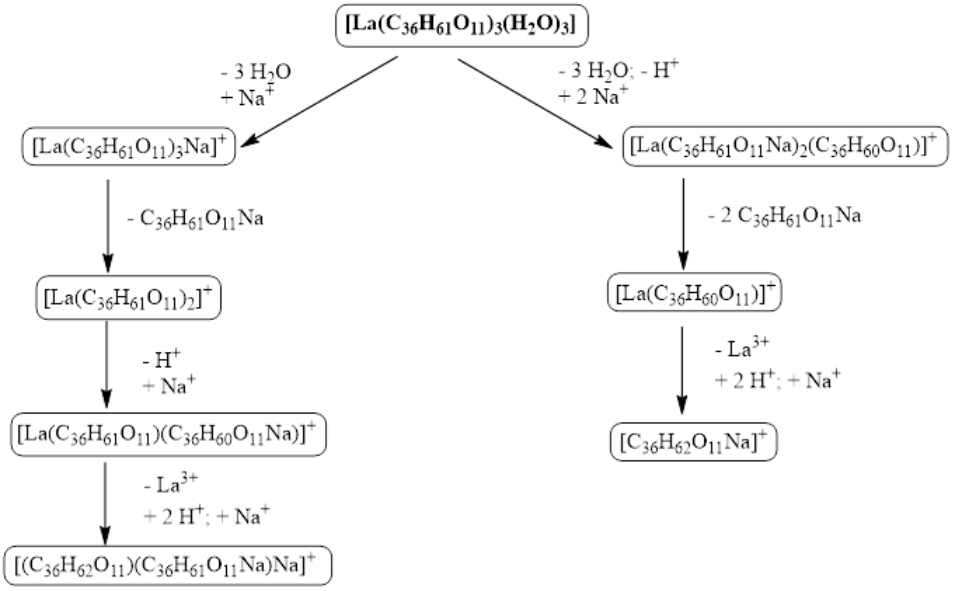

Fig. 3.1-11. Fragmentation pattern of [LaMon$_3$(H$_2$O)$_3$]

Table 3.1-4. Mass spectrometry data for monensin complexes with Ln^{3+} (ESI-MS)

Complex	Molecular ion, m/z		
	$[M(C_{36}H_{60}O_{11})]^+$	$[M(C_{36}H_{61}O_{11})_2]^+$	$[M(C_{36}H_{60}O_{11})_3H_2Na_2]^+$
$[YMon_3(H_2O)_3]$	757.3	1427.8	2121.1
$[LaMon_3(H_2O)_3]$	807.3	1477.7	2171.2
$[PrMon_3(H_2O)_3]$	809.3	1479.7	2195.1
$[NdMon_3(H_2O)_3]$	810.3	1482.7	2197.1
$[SmMon_3(H_2O)_3]$	820.3	1490.8	2207.1
$[EuMon_3(H_2O)_3]$	821.3	491.7	2206.1
$[GdMon_3(H_2O)_3]$	826.3	1496.8	2211.2
$[ErMon_3(H_2O)_3]$	836.3	1506.8	2221.2

3.1.4. Nuclear magnetic resonance (NMR)

The diamagnetic monensinates and salinomycinates of divalent metal cations have been characterized by NMR using one- and two-dimensional techniques. The alkaline earth complexes of salinomycin were studied in solid phase (due to their very limited solubility), and all the others – in solution. The chemical shift of the ^{13}C signals in the two ligands which undergo the most significant changes upon complexation is discussed below (**Tables 3.1-5, 3.1-6, 3.1-7**).

The most significant change in the spectra of monensinates is observed for the 1C, which is significantly shifted to a lower field compared to MonH (Δ = 4.37-4.85 ppm; $\Delta = \delta_{complex} - \delta_{MonH}$). Such a change confirms the presence of a deprotonated carboxyl group in the ligand coordinated to the metal(II) centers. Carbon atoms in the close vicinity of O1 and O11 (bound directly to the divalent cation) also undergo a weak field shift to – 2C (Δ = 1.76-2.35 ppm), 25C (Δ = 0.73-1.69 ppm), 27C (Δ = 1.05-1.28 ppm), 29C (Δ = 0.73-1.10). The formation of H-bonds between water molecules (H_2O-12 and H_2O-13) and ether oxygens O5-O8 leads to a significant shift of some of the ^{13}C resonances in the spectra of the complexes. Experimental data show that both positive and negative chemical shift changes are observed depending on the ligand conformation upon complexation. The NMR data corroborate the coordination mode of monensin which is analogous in the $[MMon_2(H_2O)_2]$series, and confirm that complexes retain their structure in solid state and in solution.

Similar to monensin, in the spectra of diamagnetic salinomycinates, the signal for 1C - Δ_{Cd} ~7 ppm (**Table 3.1-5**) and Δ_{IIA} ~5 ppm (**Table 3.1-6**) also undergoes the most significant

change, which confirms the deprotonation of the carboxylic group and its involvement in interaction with the metal(II) center. The position of most of the remaining signals varies within ± 0.5 ppm, with a shift of certain resonances to a stronger or weaker field (1-3 ppm). Taken together, these observations indicate that structure of salinomycin undergoes some conformational changes upon formation of the corresponding complex compounds.

Table 3.1-4. Chemical shift (δ, ppm) of signals in $^{13}C\{^{1}H\}$-NMR (150 MHz, $CDCl_3$) spectra of MonH and $[MMon_2(H_2O)_2]$

C-atom	MonH	Mg^{2+}	Ca^{2+}	Zn^{2+}	Cd^{2+}
1COO(H)	177.09	181.94	181.81	181.66	181.46
*9C	107.79	107.65	107.55	107.68	107.48
*25C	96.99	98.38	98.63	97.72	98.68
*16C	86.18	87.91	87.12	87.23	87.17
12CH	85.14	85.11	85.29	85.06	84.97
17CH	85.11	85.44	84.35	85.06	84.66
13CH	83.42	85.06	83.91	83.66	84.33
3CH	81.56	82.28	82.49	81.82	82.05
20CH	77.01	77.58	77.46	77.44	77.31
21CH	73.83	72.94	73.56	73.31	73.32
7CH	70.74	70.61	70.71	70.56	70.51
$26CH_2$	67.98	67.85	66.35	66.38	66.80
5CH	67.01	65.66	68.21	67.58	67.78
$28CH_3$-O	58.03	57.75	57.94	57.94	57.86
2CH	41.94	43.70	44.29	42.41	43.97
$10CH_2$	38.36	38.51	38.75	38.42	38.50
4CH	36.70	37.08	37.40	36.82	37.20
$23CH_2$	36.59	36.50	36.73	36.55	36.57
24CH	35.68	36.30	35.90	35.55	35.74
6CH	34.54	34.31	34.23	34.40	34.24
18CH	34.45	34.31	34.23	34.31	34.37
$8CH_2$	34.03	34.36	34.33	34.21	34.20
$11CH_2$	33.73	34.12	33.83	33.91	33.84
22CH	32.80	33.40	33.34	33.01	33.18
$19CH_2$	32.58	32.75	31.25	32.61	32.62
$15CH_2$	31.49	29.26	32.83	30.80	32.62
$32CH_2$	31.19	30.66	30.79	30.80	30.79
$14CH_2$	27.88	27.60	27.78	27.74	27.66
$31CH_3$	27.69	27.93	27.43	27.81	27.44
$35CH_3$	17.54	17.39	17.63	17.54	17.49
$36CH_3$	16.32	16.88	16.97	16.71	16.80
$34CH_3$	15.75	15.84	15.74	15.80	15.60
$27CH_3$	15.66	16.94	16.81	16.71	16.80
$30CH_3$	10.75	10.67	10.76	10.58	10.66
$29CH_3$	10.37	11.23	11.36	11.38	11.10
$33CH_3$	8.61	8.84	8.73	8.72	8.70

Table 3.1-5. ^{13}C-NMR (150 MHz, acetonitrile-d_3) chemical shifts (δ, ppm) in the spectra of SalH and $[CdSal_2(H_2O)_2]$

C-atom	SalH	Cd^{2+}		C-atom	SalH	Cd^{2+}
11C=O	215.53	216.77		8CH	37.06	36.92
1COO(H)	177.86	184.98		14CH	33.66	33.89
19CH=	133.65	132.59		$23CH_2$	31.53	32.37
18CH=	123.43	122.23		$31CH_2$	31.92	32.09
*21C	107.72	107.44		$27CH_2$	30.19	30.24
*17C	100.14	100.24		6CH	29.06	29.15
*24C	89.04	88.84		$33CH_3$	26.03	26.07
29CH	77.83	78.14		$5CH_2$	26.94	27.13
13CH	78.60	78.76		$41CH_2$	23.47	23.56
3CH	75.51	76.84		$26CH_2$	22.72	22.41
25CH	75.05	74.67		$4CH_2$	20.77	21.16
7CH	72.73	72.13		$35CH_3$	17.86	18.19
*28C	71.47	71.87		$36CH_2$	18.68	19.39
9CH	69.89	69.63		$34CH_3$	15.99	16.07
20CH	68.10	67.70		$30CH_3$	15.31	15.24
12CH	56.80	57.28		$38CH_3$	13.47	13.70
2CH	49.25	49.24		$37CH_3$	14.15	14.09
10CH	49.09	48.69		$42CH_3$	12.20	12.71
16CH	41.42	41.73		$40CH_3$	11.65	12.09
$15CH_2$	39.09	39.39		$39CH_3$	7.83	7.97
$22CH_2$	37.49	36.57		$32CH_3$	6.79	6.94

Table 3.1-6. Characteristic ^{13}C CPMAS chemical shifts (δ, ppm) in the spectra of SalH u alkaline-earth salinomycinates $[MSal_2(H_2O)_2]$

C-atom	SalH	Mg^{2+}	Ca^{2+}	Sr^{2+}	Ba^{2+}
1COO(H)	177.59	183.04	182.90	182.55	182.80
19CH=	131.23	133.76	133.44	132.95	133.48
18CH=	121.84	121.75	121.38	121.93	122.13
*21C	107.19	107.00	106.95	107.19	107.25
*17C	99.89	99.69	99.66	99.54	99.62
*24C	87.55	88.45	88.43	88.83	88.87
3CH	75.49	76.13	76.03	76.04	76.20
*28C	71.60	71.22	70.98	71.19	71.12
2CH	50.15	50.14	49.91	50.26	50.40
8CH	37.33	37.26	37.12	37.08	37.00
14CH	32.58	33.13	33.03	33.04	32.86
6CH	28.66	28.76	28.87	28.80	28.86
$41CH_2$	23.19	23.45	23.37	23.61	23.53
$32CH_3$	7.23	7.25	7.24	7.19	7.23

Among the lanthanide complexes, only $[CeL_2(OH)_2]$ was subjected to NMR analysis, and the participation of monensinate and salinomycinate anions was confirmed by ^{1}H-NMR in $CDCl_3$. The signals of the coordination compounds are significantly broadened compared to those of the two acids due to the presence of the metal cation. A more significant difference was observed for MonH and $[CeMon_2(OH)_2]$ than for SalH and $[CeSal_2(OH)_2]$. The narrow and intense band at 6.25 ppm in the MonH spectrum (attributed to the OH groups) is shifted to lower field in the complex (6.76 ppm). Concomitantly, the signal attributed to CH-2 (2.62 ppm, MonH) significantly broadened to merge with the baseline, confirming the proximity of the heavy cerium ion to the carboxylate group of the antibiotic. On the other hand, the proton spectrum of SalH is much more complicated, because the signals of some characteristic protons located at the two opposite ends of the organic molecule overlap significantly. For this reason, no significant structural information can be extracted by comparing the spectra of SalH and its complex. The analogous spectral behavior of the two antibiotics in their complex compounds with di- and tri-valent metal ions gives reason to assume here also an identical (to monensin) binding of salinomycin in $[CeSal_2(OH)_2]$.

3.1.5. Electron paramagnetic resonance (EPR)

The following paramagnetic coordination compounds of monensin and salinomycin were investigated by EPR spectroscopy: $[CuL_2(H_2O)_2]$, $[GdMon_3(H_2O)_3]$ u $[CeL_2(OH)_2]$.

Copper(II) complexes: the spectra in solid phase (**Fig. 3.1-12**) consist of hyperfine structure due to the interaction of the unpaired electron of Cu^{2+} (d^9) with the nuclear spin of ^{63,65}Cu (I = 3/2). EPR parameters are typical for mononuclear Cu(II)-containing species: $g_{||} = 2.34$, $A_{||} = 152\times10^{-4}$ cm^{-1}, $g_{\perp} = 2.06$ – monensin; $g_{||} = 2.31$, $A_{||} = 149\times10^{-4}$ cm^{-1}, $g_{\perp} = 2.05$ – salinomycin. The ratio $g_{||} > g_{\perp}$ points that the single electron occupies predominantly the $d_{x^2-y^2}$ orbital. The high value of $g_{||}$ and the relatively low one for $A_{||}$ corroborate the data for oxygen-containing copper(II) complexes placed in distorted tetragonal field. No exchange interaction between the paramagnetic centers is observed (G = 5.56) and the metal ion – oxygen bonds are primarily of ionic origin ($\alpha^2 = 0.76$).

Gadolinium(III) monensinate: in both EPR spectra of the complex (solid and liquid (THF) state, Fig. **3.1-13**) an analogous symmetric signal with g ≈ 1.99 and line width ΔHpp ≈ 155 mT is observed, which shows the stability of the complex in both phases; in addition, the EPR spectrum of the gadolinium complex in solid phase contains weakly intense signals at g = 5.97 and g = 2.77, the origin of which cannot be unambiguously assigned.

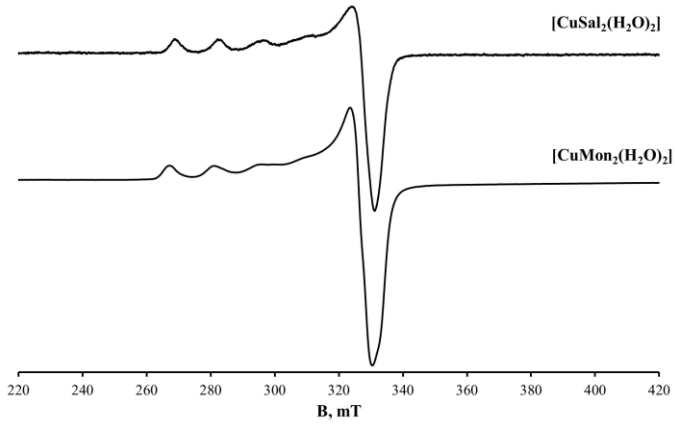

Fig. 3.1-12. EPR spectra of [$CuMon_2(H_2O)_2$] (77 K) and [$CuSal_2(H_2O)_2$] (295 K)

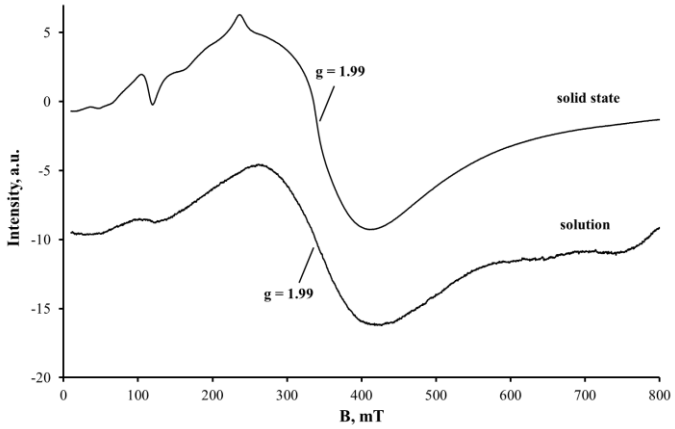

Fig. 3.1-13. EPR spectra на [$GdMon_3(H_2O)_3$] в твърдо и течно състояние

Cerium(IV) complexes: both samples (**Fig. 3.1-14**) show narrow signals (ΔHpp ~ 1.2 mT) with low intensity and g-values in the range of 2.004-2.030. The signal at g ~ 2.011 overlaps with the signal at g = 2.004 and becomes “visible” only at low temperature. Measurements at 100 K show higher signal intensity according to the Curie-Weiss law. EPR parameters are assigned to defect centers in the studied complexes. The signal with g = 2.004 can be attributed to the presence of oxygen-containing radicals, while those at g ~ 2.011 and g ~ 2.030 are most likely components of an asymmetric signal characteristic of radicals containing the Ce^{4+}-oxygen pair. It should be emphasized that the concentration of defect centers in both complexes is very low, but the measurements indirectly confirm the +4 oxidation state of the cerium cation.

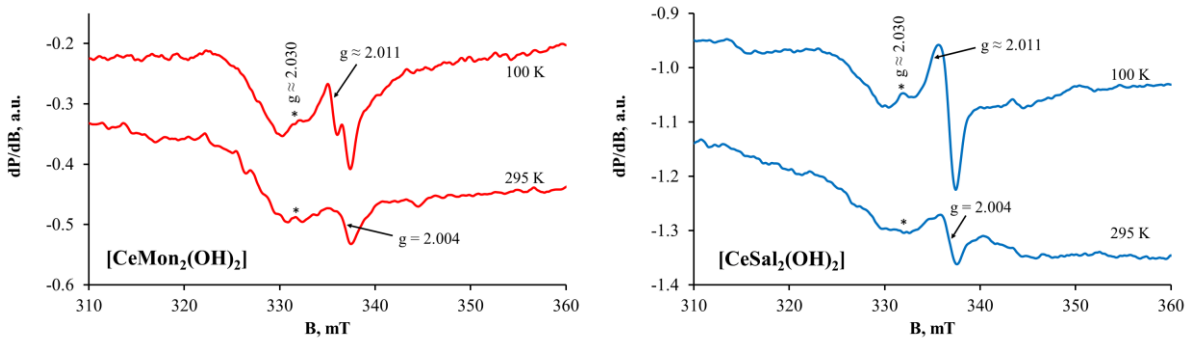

Fig. 3.1-14. EPR spectra of $[CeMon_2(OH)_2]$ and $[CeSal_2(OH)_2]$

3.1.6. Complementary experiments for particular complex compounds

Some of the isolated "classical" coordination compounds of monensin and salinomycin were subjected to specific studies that enriched the data set for the respective complex species.

Fluorescence study with $[TbMon_3(H_2O)_3]$: upon excitation with λ = 450-470 nm, the emission spectrum (**Fig. 3.1-15**) exhibits bands that correspond to the main transitions for Tb^{3+} ions – from $^5D_4$ to ^4F_J, as expected the most intense is the transition $^5D_4$ - $^7F_5$ at 545 nm. The band for the $^5D_4$ - $^4F_6$ transition, which is not very intense but is often observed in the spectra of Tb(III)-containing compounds, is absent.

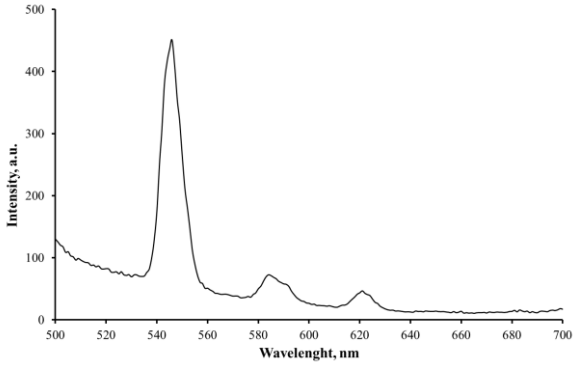

Fig. 3.1-15. Emission spectrum of $[TbMon_3(H_2O)_3]$

Transmission electron microscopy (TEM) imaging of $[CaSal_2(H_2O)_2]$, $[LaMon_3(H_2O)_3]$ and $[CeL_2(OH)_2]$: the samples are amorphous and the elements are uniformly distributed on their surface. The particle size varies from 100-200 nm in Ca^{2+} and La^{3+} complexes to 200-300 nm in those of Ce^{4+} (**Fig. 3.1-16**).

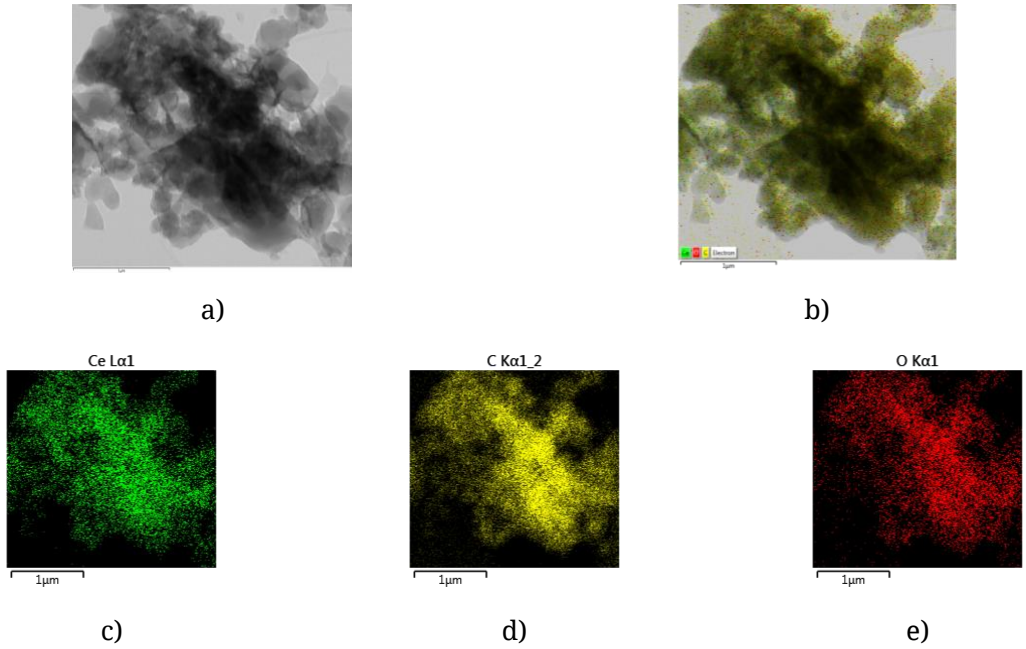

Fig. 3.1-16. TEM images (a, b) and distribution of Ce, C u O (c-e) in $[CeSal_2(OH)_2]$

Thermal analysis (TGV-DTA, TGV-MS) of $[CeL_2(OH)_2]$: no endothermic peaks below 200 °C were observed for both complexes, which ruled out the presence of water molecules in their composition (**Fig. 3.1-17**). The endothermic peak at ~200 °C for $[CeMon_2(OH)_2]$ corresponds to its melting point (196 °C), followed by its gradual decomposition. The weak endothermic peak in the range 128-150 °C corresponds to the melting point of $[CeSal_2(OH)_2]$ (142-144 °C), but the decomposition starts at a lower temperature compared to the monensinate analogue. Water loss was observed below 100 °C, although the complexes were dried and stored in a desiccator prior to all analyses. These water molecules are weakly bound and do not relate either to the structural features of the antibiotics or to the coordination environment of the cerium(IV) ions.

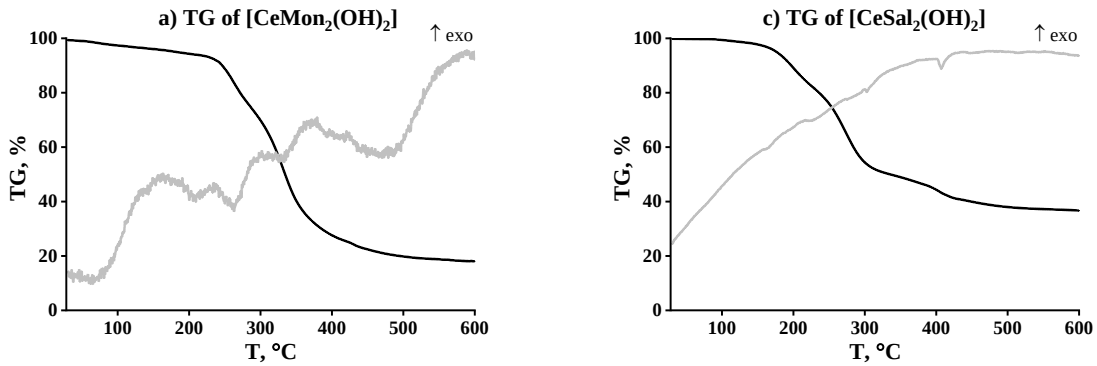

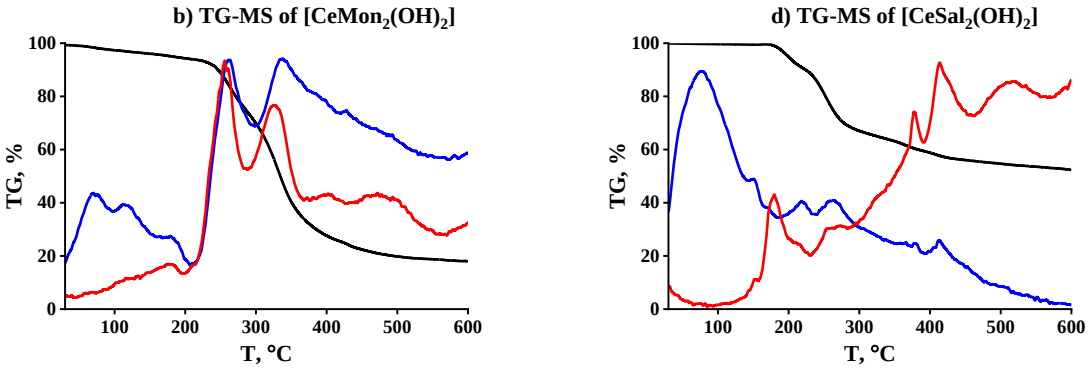

Fig. 3.1-17. TG-DTA and TG-MS of $[CeMon_2(OH)_2]$ (a, b) and $[CeSal_2(OH)_2]$ (c, d)

Electronic spectroscopy (UV-Vis) of $[CeL_2(OH)_2]$: the spectra of the complexes contain an asymmetric band in the range 200–500 nm (**Fig. 3.1-18**). The electronic configuration of Ce^{4+} is analogous to that of Xe^0 and the observed absorption can only be explained by the presence of O → Ce charge transfer transitions:

$[CeMon_2(OH)_2]$ a_{270} = 1.71 $L \cdot g^{-1} \cdot cm^{-1}$ ε_{270} = 2590 $L \cdot mol^{-1} \cdot cm^{-1}$;

$[CeSal_2(OH)_2]$ a_{282} = 2.65 $L \cdot g^{-1} \cdot cm^{-1}$ ε_{282} = 4434 $L \cdot mol^{-1} \cdot cm^{-1}$.

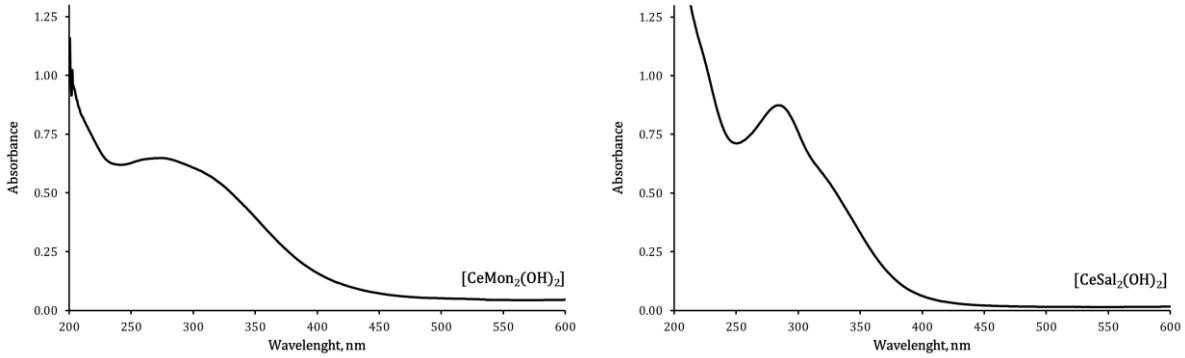

Fig. 3.1-18. UV-Vis spectra of $[CeL_2(OH)_2]$ (MeOH, concentration 0.3125 mg/mL)

3.1.7. Structures of the "classical" complexes of monensin and salinomycin

Mononuclear bis-complexes of M^{2+}: the analogous spectral behavior of the two antibiotics suggests the formation of salinomycinates similar to monensin coordination compounds characterized by single crystal X-ray diffraction. It is likely that salinomycin anions are also located in a *cis*-position to the divalent metal ion and a water molecule is bound in their hydrophilic cavity.

In order to investigate the possible coordination of Sal^-, we modeled the structure of $[CaSal_2(H_2O)_2]$ based on the known crystallographic data for the monensinate complexes and the two sodium forms of salinomycin. The geometry of the proposed structure was optimized using the AMBER99 force field. The inclusion of water molecules as ligands is only possible if they additionally participate in intramolecular hydrogen bonds with the 11C=O and 20C-OH groups of salinomycin. The origin of the hydrogen bonds formed significantly affects the model stability, as the other possible structures lead to unfolding of the ligand and preclude the binding of water to the metal(II) center. The carboxylate groups of salinomycin deviate from the equatorial plane of the modeled calcium complex compared to isostructural monensinates with divalent metal ions. Such behavior can be explained by the absence of a primary alcohol group in salinomycin, and thus the tertiary alcohol substituent at 28C remains the only possibility for complex formation with the simultaneous participation of the carboxylate function at the opposite end of the ligand (**Fig. 3.1-19**).

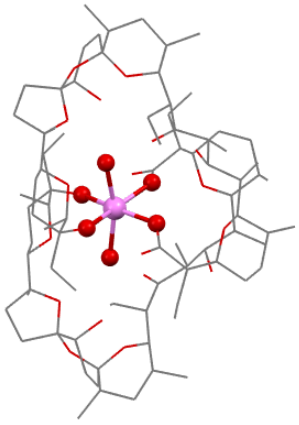

Fig. 3.1-19. Modeled structure of $[CaSal_2(H_2O)_2]$

Mononuclear tris-complexes of M^{3+}: the spectral data set combined with the elemental analysis suggests the formation of neutral coordination compounds in which one metal ion is bound to three organic ligands and (presumably) water molecules. The assumed coordination number of the lanthanide ions is 9 - six places are occupied by the bidentate anions of the antibiotics, and the remaining three - by the water molecules in their cavity (**Fig. 3.1-20**). The precise geometry of the complexes cannot be discussed without X-ray structural data on single crystals, which have not yet been obtained despite the various crystallization techniques that have been applied.

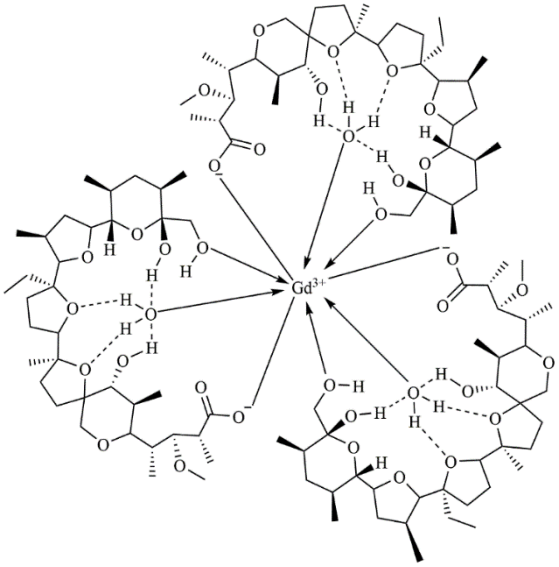

Fig. 3.1-20. Suggested structure of lanthanide complexes of polyether ionophores ([$GdMon_3(H_2O)_3$] as an example)

Mononuclear bis-complexes of Ce^{4+}: Based on the elemental analysis and spectral properties of [$CeL_2(OH)_2$], it is presumed that their structures resemble those of monensin and salinomycin complexes with divalent metal ions, i.e. two deprotonated antibiotics coordinate bidentately to the metal(IV) center. To achieve the overall electroneutrality, Ce^{4+} is also bound to two hydroxide ions originating from the weak base excess used in the synthetic procedures. The structure of [$CeMon_2(OH)_2$] was constructed using the crystallographic data for [$NiMon_2(H_2O)_2$], with Ni^{2+} replaced by Ce^{4+} and one hydrogen from each water molecule removed (**Fig. 3.1-21**). The geometry of the resulting complex was optimized and the M-O bond lengths ranged from 2.04 Å in Ce-OH^- to 2.35 and 2.45 Å in COO^--Ce and Ce-OH. The *cis*-oriented organic ligands occupy the equatorial plane of the complex and the axially placed hydroxide ions complete the inner coordination shell. The surroundings of the metal center can be considered as a distorted octahedron with the following angles: 77.2° (COO^--Ce-OH), 87.4° (OH-Ce-OH), 118.2° (COO^--Ce-COO^-) and 178.4° (OH^--Ce-OH^-).

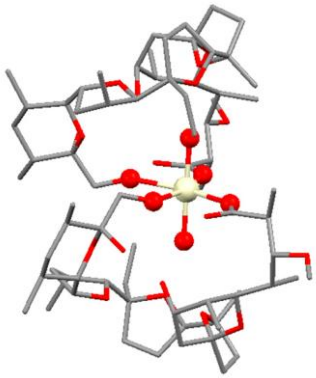

Fig. 3.1-21. Optimized structure of [$CeMon_2(OH)_2$]

3.2. "Non-classical" complexes of monensin and salinomycin

This Section reviews those individual systems in which polyether ionophores form specific coordination compounds isolated and characterized in the solid phase:

- mononuclear mono-complexes of monensin with Hg^{2+} and of Salinomycin with Pb^{2+};
- mononuclear mono-complexes of ionophores with Ce^{4+};
- mixed-metal complexes of sodium monensin with Co^{2+}, Mn^{2+} u Cu^{2+}.

3.2.1. Complexes [HgMon(H_2O)] and [PbSal(NO_3)]

The ions of mercury(II) and lead(II) form complexes of different composition compared to those so far discussed. The first cation reacts with monensinate anion, and the second - with salinomycinate. The reaction proceeds in a mixed solvent with the formation of [HgMon(H_2O)] and [PbSal(NO_3)]. The structure of the mercury(II) complex was proved by X-ray diffraction, while that of lead(II) was deduced indirectly by the physicochemical data. Exploring the Pb(II)-monensin and Hg(II)-salinomycin systems did not lead up to now to the isolation of chemically pure individual coordination compounds.

The [HgMon(H_2O)] complex contains a monensinate dianion that is tetradentately coordinated to Hg^{2+} via bidentate carboxylate (O1 and O2), deprotonated secondary hydroxyl (O10), and primary hydroxyl (O11) groups (**Fig. 3.2-1**). The two pairs of oxygen atoms (O1 / O2 and O10 / O11) are at a "head-to-tail" position, which ensures the cyclization of the antibiotic. These oxygen atoms occupy the equatorial plane in the inner coordination sphere of the mercury(II) cation, and a water molecule (O12) is coordinated at an axial position, leading to a distorted square-pyramidal geometry of the complex and stabilization of the macrocycle through hydrogen bonds.

The Hg-O bond lengths vary widely from 2.050 Å (Hg-O1) to 2.921 Å (Hg-O2) and reflect the strong interaction of the metal ion with 1O / 11O and its weaker one with 2O / 10O / 12O . Unlike the divalent metal complexes of the monensinate anion $[MMon_2(H_2O)_2]$, Hg^{2+} interacts preferably with the secondary hydroxylate oxygen atom rather than the primary hydroxyl group, and a bidentate mode of coordination of the carboxylate function is observed for the first time, albeit with greatly increased Hg-O2 bond length.

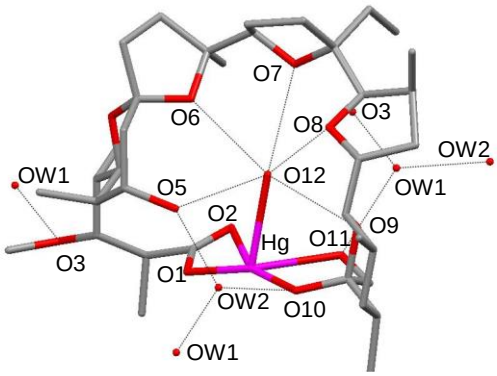

Fig. 3.2-1. Structure of $[HgMon(H_2O)]$ (hydrogen atoms are omitted for clarity)

The IR spectrum of $[HgMon(H_2O)]$ is in agreement with its crystal structure (**Table 3.2-1**). In the spectrum of lead(II) salinomycinate, a monodentate binding of the COO-group is observed, and the neutrality of the complex is achieved by the inclusion of nitrate ions from the starting metal salt. The presence of peaks for $[Hg(C_{36}H_{61}O_{11})]^+$ (m/z 871.4) and $[Hg(C_{36}H_{60}O_{11})]Na]^+$ (m/z 893.4) and for $[Pb(C_{42}H_{69}O_{11})]^+$ (m/z = 957.5) in the corresponding FAB-MS spectra also support the formation of the coordination compounds.

Table 3.2-1. Characteristic IR vibrations in the spectra of MonH / $[HgMon(H_2O)]$ and SalH / $[PbSal(NO_3)]$

Vibration	Vibration position, cm^{-1}			
	MonH	$[HgMon(H_2O)]$	SalH	$[PbSal(NO_3)]$
ν_{OH} (H_2O)	3520	3500	3500	3380
ν_{OH} (ligand)	3320	3400-3200		
$\nu_{C=O}$ (COOH)	1700	-	1710	-
$\nu_{C=O}$ (C=O)	-	-	1710	1710-1690[8]
$\nu_{C=O}^{asym}$ (COO^-)	-	1650	-	1520
$\nu_{C=O}^{sym}$ (COO^-)	-	1410	-	1410
NO_3^-	-	-	-	1300

In the ^{13}C-NMR spectrum of [HgMon(H_2O)] (**Table 3.2-2**), the carbon atoms that are close to the metal(II) center undergo a weaker shift compared to the complex [$CdMon_2(H_2O)_2$] (**Table 3.1-4**). The observed differences for 1C, 25C and 27C are probably due to the tetradentate coordination of monensin, with the smaller numerical values also suggesting a different conformation of the ligand in the studied compounds.

Table 3.2-2. Chemical shift (δ, ppm) of $^{13}C\{^1H\}$-NMR (150 MHz, $CDCl_3$) signals for MonH and [HgMon(H_2O)]

C-atom	MonH	Hg^{2+}		C-atom	MonH	Hg^{2+}
1COO(H)	177.09	178.15		24CH	35.68	32.83
*9C	107.79	107.62		6CH	34.54	34.40
*25C	96.99	97.91		18CH	34.45	34.41
*16C	86.18	86.34		8CH_2	34.03	34.04
12CH	85.14	85.30		11CH_2	33.73	33.67
17CH	85.11	84.26		22CH	32.80	32.83
13CH	83.42	82.93		19CH_2	32.58	32.46
3CH	81.56	81.53		15CH_2	31.49	31.34
20CH	77.01	77.34		32CH_2	31.19	30.37
21CH	73.83	73.60		14CH_2	27.88	27.32
7CH	70.74	70.74		31CH_3	27.69	27.52
26CH_2	67.98	67.64		35CH_3	17.54	17.52
5CH	67.01	67.20		36CH_3	16.32	16.61
28CH_3-O	58.03	57.91		34CH_3	15.75	15.84
2CH	41.94	41.56		27CH_3	15.66	15.76
10CH_2	38.36	38.53		30CH_3	10.75	10.35
4CH	36.70	36.74		29CH_3	10.37	10.91
23CH_2	36.59	36.54		33CH_3	8.61	8.36

The NMR data for the lead(II) complex of salinomycin (**Table 3.2-3**), namely the shift of 1C, 2C, 23C, 28C, 33C to a weaker field, and of 12C, 13C, 26C – to a stronger one , suggest the participation of the carboxylate 1aO, hydroxyl 28O and ether (3O, 4O) oxygen atoms in interaction with the metal ion. The weak solubility of the complex in water indicates that probably the nitrate ions are direct participants in the primary coordination shell of Pb^{2+} (not playing the role of counterions). The recorded NOESY spectra for [$CdSal_2(H_2O)_2$] and [PbSal(NO_3)] confirm the different stoichiometry of the two compounds, because for the first complex, negative values for NOE's corresponding to molecular mass higher than 1500 D are observed, while for the second, positive NOE's for all signals correspond to M(II)-ligand molar ratio = 1:1 and lower molecular weight .

Table 3.2-3. ^{13}C-NMR (150 MHz, acetonitrile-d_3) chemical shifts (δ, ppm) in the spectra of SalH and [PbSal(NO_3)]

C-atom	SalH	Pb^{2+}		C-atom	SalH	Pb^{2+}
11C=O	215.53	215.75		8CH	37.06	36.43
1COO(H)	177.86	184.60		14CH	33.66	33.55
19CH=	133.65	133.03		23CH_2	31.53	33.91
18CH=	123.43	123.95		31CH_2	31.92	31.92
*21C	107.72	108.96		27CH_2	30.19	30.47
*17C	100.14	99.99		6CH	29.06	28.97
*24C	89.04	89.33		33CH_3	26.03	28.97
29CH	77.83	78.11		5CH_2	26.94	27.02
13CH	78.60	77.41		41CH_2	23.47	24.85
3CH	75.51	75.24		26CH_2	22.72	20.47
25CH	75.05	76.05		4CH_2	20.77	21.50
7CH	72.73	72.30		35CH_3	17.86	17.95
*28C	71.47	73.74		36CH_2	18.68	17.02
9CH	69.89	70.60		34CH_3	15.99	16.06
20CH	68.10	67.22		30CH_3	15.31	14.8
12CH	56.80	54.58		38CH_3	13.47	13.34
2CH	49.25	55.08		37CH_3	14.15	13.81
10CH	49.09	49.59		42CH_3	12.20	13.01
16CH	41.42	41.74		40CH_3	11.65	11.59
15CH_2	39.09	38.90		39CH_3	7.83	7.48
22CH_2	37.49	36.64		32CH_3	6.79	6.83

Based on the observed properties of lead(II) salinomycinate and its elemental analysis, the proposed composition is [PbSal(NO_3)], and its structure is presented in **Fig. 3.2-2**.

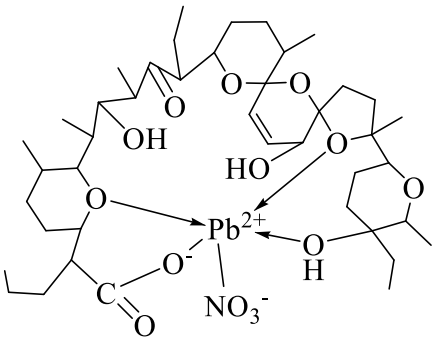

Fig. 3.2-2. Structure of [PbSal(NO_3)]

3.2.2. Complexes of monensin and salinomycin [CeL(NO_3)$_2$(OH)]

Mononuclear mono-complexes of monensin and salinomycin with Ce^{4+} ions were isolated and characterized. The spectral properties of [CeL(NO_3)$_2$(OH)] complexes are very close to those of [CeL$_2$(OH)$_2$] due to the close coordination behavior of antibiotics. The main

differences are due to the another composition of the two types of complexes, since in the mono-complexes, the inclusion of two moles of nitrate ions per mole of complex was observed.

The IR spectra of $[CeL(NO_3)_2(OH)]$ in KBr confirm the deprotonation of MonH and SalH, but also contain two new bands in the range of 1520-1280 cm^{-1} attributed to the stretching vibrations of NO_3^- (1505/1289 cm^{-1} for $[Ce(Mon(NO_3)_2(OH)$, **Fig. 3.2-3**; 1512/1288 cm^{-1} for $[CeSal(NO_3)_2(OH)]$, **Fig. 3.2-4**). The difference between the two signals (216-224 cm^{-1}) indicates that the nitrate ions are directly bound to the metal center. The band at 378 cm^{-1} (monensin) and 380 cm^{-1} (salinomycin) (in CsI) is due to the deformation vibration of NO_3^-, involved in the formation of four-membered chelate structures, suggesting their bidentate mode of coordination. Comparison of the solution ($CHCl^3$) and solid state spectra showed that the complexes retain their structure in both phases, with a negligible degree of antibiotics protonation.

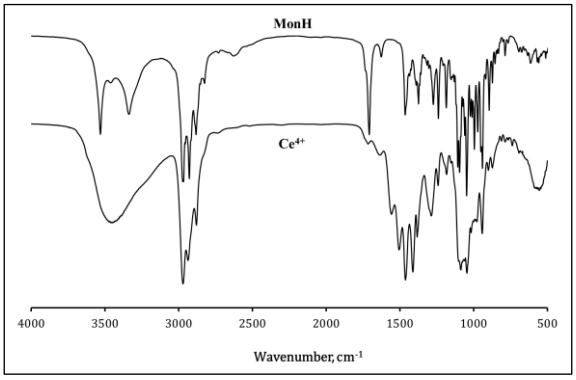

Fig. 3.2-3. IR spectra of MonH and $[Ce(Mon(NO_3)_2(OH)]$

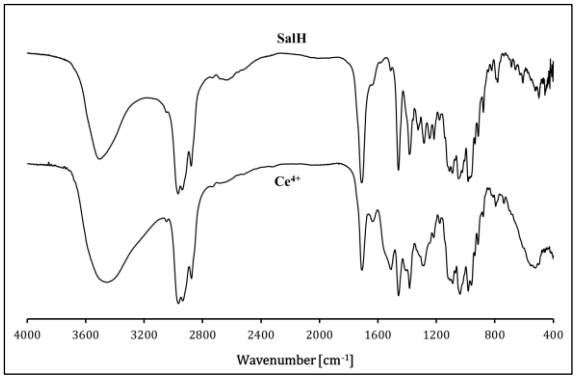

Fig. 3.2-4. IR spectra of SalH and $[Ce(Sal(NO_3)_2(OH)]$

In the UV-Vis spectra of $[CeL(NO_3)_2(OH)]$, an asymmetric band (250-500 nm) attributed to O → Ce charge transfer transitions is again observed (**Fig. 3.2-5**). The ^{1}H-NMR signals for the hydroxyl group attached to 25C and for 2CH are broadened in the spectrum of $[CeMon(NO_3)_2(OH)]$ but retain their position relative to the parent antibiotic. The overlap of the bands for SalH and $[CeSal(NO_3)_2(OH)]$ does not allow to retrieve significant information about the coordination mode of salinomycin.

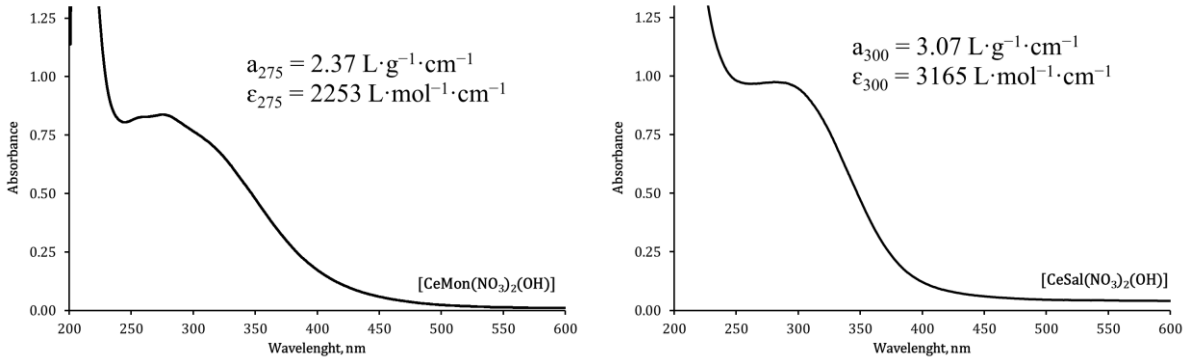

Fig. 3.2-5. UV-Vis spectra of [CeL(NO$_3$)$_2$(OH)] (MeOH, concentration 0.3125 mg/mL)

The EPR spectrum of [CeMon(NO$_3$)$_2$(OH)] completely matches that of [CeL$_2$(OH)$_2$] (g = 2.004, 2.011, 2.030). In the spectrum of [CeSal(NO$_3$)$_2$(OH)], the signal with g = 2.004 is not observed, instead of two others with effective g-factors of 2.002 and 1.96, resp. The first signal is attributed to a carbon-containing radical, while the second is informative for the presence of radicals containing the Ce^{3+}-O pair. Similar to [CeL$_2$(OH)$_2$], all signals are of very low intensity (**Fig. 3.2-6**).

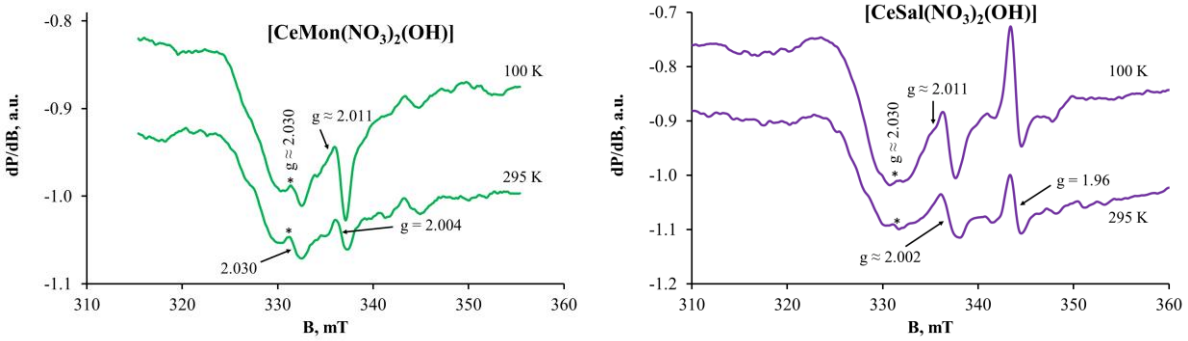

Fig. 3.2-6. EPR spectra of [CeMon(NO$_3$)$_2$(OH)] and [CeSal(η$_2$-NO$_3$)$_2$(OH)]

The TG-DTA and TG-MS studies (**Fig. 3.2-7**) exclude the presence of water molecules in the primary coordination sphere of [CeL(NO$_3$)$_2$(OH)]. In contrast to the mononuclear bis-complexes of Ce^{4+}, here the TG-DTA curves contain an exothermic peak at 258 °C (monensin) and 153 °C (salinomycin) due to the oxidation processes with the participation of nitrate anions. The data show that the degradation of the complexes starts before their melting with intensive release of H$_2$O, CO$_2$ and NO (TG-MS).

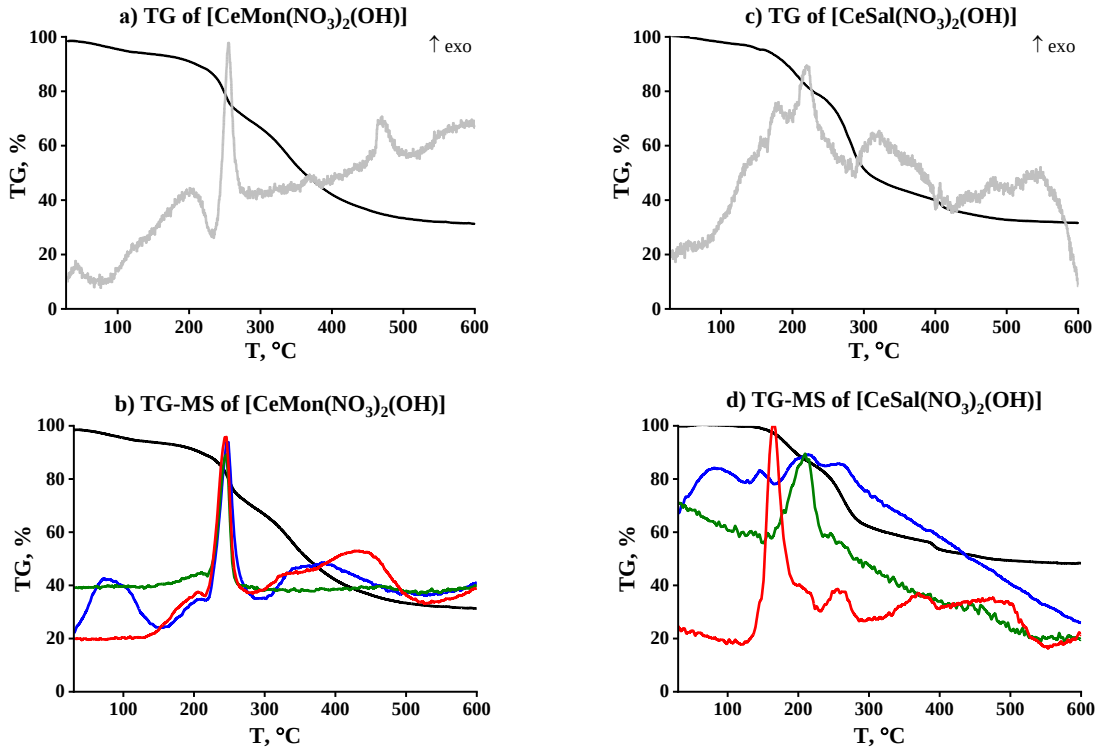

Fig. 3.2-7. TG-DTA and TG-MS of $[CeL(NO_3)_2(OH)]$

The structure of mononuclear mono-complexes of Ce^{4+} was explored by molecular dynamics and subsequent quantum-chemical calculations. The results show that the metal cation is located near the cavity of the ionophores, which are polydentately bound. The electroneutrality of the coordination compounds is achieved by the additional binding of two nitrates and one hydroxide anion. The coordination number of Ce^{4+} is 9, but it is realized in a different way in the two complexes (**Table 3.2-4, Fig. 3.2-8**).

Table 3.2-4. Coordination mode of ligands in $[CeL(NO_3)_2(OH)]$

Ligands denticity	Final structure
pentadentate monensin; cyclisation one monodentate / one bidentate nitrates monodentate hydroxide	$[CeMon(\eta_2\text{-}NO_3)(NO_3)(OH)]$
tetradentate salinomycin; no cyclisation two bidentate nitrates monodentate hydroxide	$[CeSal(\eta_2\text{-}NO_3)_2(OH)]$

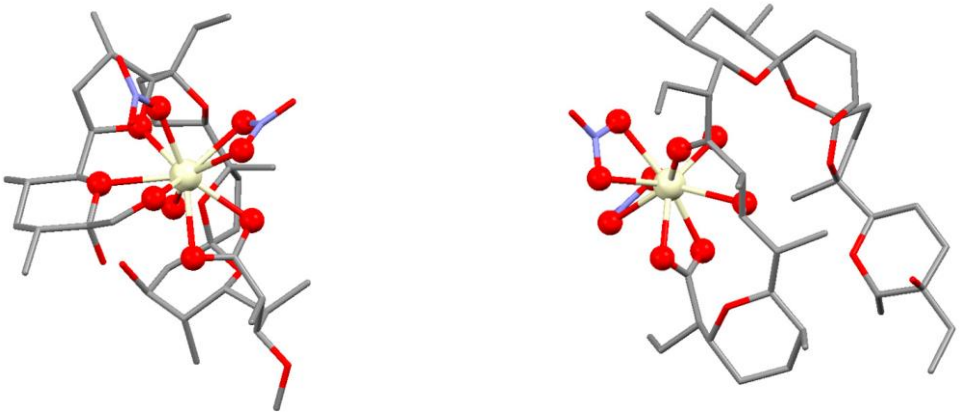

Fig. 3.2-8. Optimized structure of the mononuclear mono-complexes of Ce^{4+} with monensin (left) and salinomycin (right) (hydrogen atoms are omitted for clarity)

3.2.3. Mixed-metal complexes of sodium monensin

Studies with sodium monensin were performed in the presence of Co^{2+}, Mn^{2+} and Cu^{2+}. The metal ion – ligand interaction takes place in a mixed nonaqueous solvent (MeCN/MeOH); the isolated complexes are of composition $[M(MonNa)_2Cl_2]$.

The structures of $[M(MonNa)_2Cl_2]$ are presented in **Fig. 3.2-9**. **Table 3.2-5** summarizes selected bond lengths and angles of the complexes. In all three compounds, two molecules of sodium monensinate coordinate one transition metal ion. Each MonNa molecule acts as a monodentate neutral ligand via one carboxylate oxygen atom bound to the transition cation, forming metal-oxygen bonds. The other two sites in the inner coordination sphere of the metal ion are occupied by chloride anions originating from the starting metal salt. The neutral complexes of manganese(II) and cobalt(II) crystallize as monohydrates, while that of copper(II) contains an acetonitrile molecule. Intramolecular hydrogen bonds of different origin are formed in the crystal structures, and intermolecular H-bonds are not observed.

In the $[M(MonNa)_2Cl_2]$ complexes, the coordination number of transition metal ions is 4. The bond lengths and angles of M-O and M-Cl are typical for monodentate coordination of the carboxylate anions. The length of M-O and M-Cl bonds decreases in the order $Mn^{2+} > Co^{2+} > Cu^{2+}$ with decreasing the corresponding ionic radius. The main difference between the three structures is the geometry of the primary coordination shell: while the manganese(II) and cobalt(II) ions are arranged in a slightly distorted tetrahedral field with bond angles varying from 105.82° to 109.74°, the copper(II) ion is placed in a distorted planar-square environment with bond angles in the range of 94.12-95.66°.

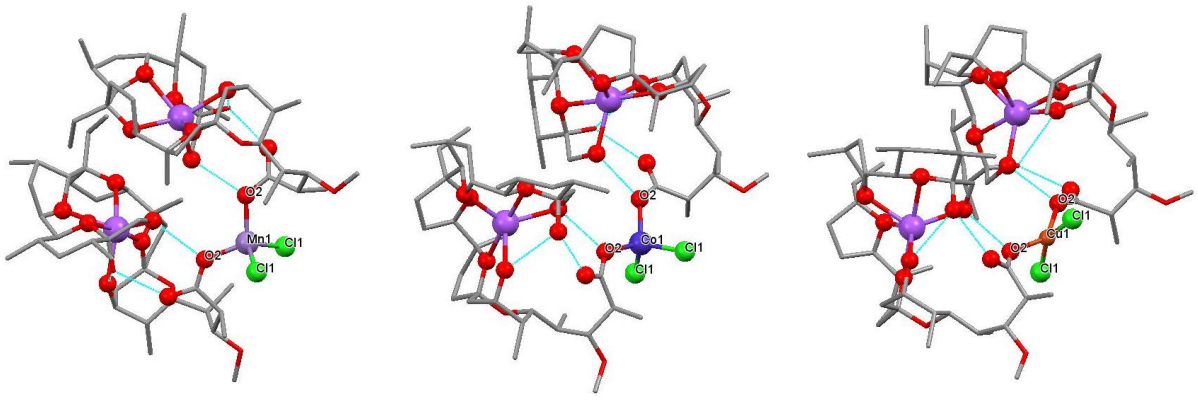

Mn^{2+} Co^{2+} Cu^{2+}

Fig. 3.2-9. Structures of mixed-metal monensinates (intramolecular hydrogen bonds are depicted by a dash, and hydrogen atoms are omitted for clarity)

Table 3.2-5. Selected bond lengths (Å) and angles (°) in mixed-metal complexes of monensin

$[Mn(MonNa)_2Cl_2]\times H_2O$		$[Co(MonNa)_2Cl_2]\times H_2O$		$[Cu(MonNa)_2Cl_2]\times MeCN$	
Mn-O2	2.071(3)	Co-O2	1.975(6)	Cu-O2	1.960(4)
Mn-Cl1	2.3103(19)	Co-Cl1	2.231(3)	Cu-Cl1	2.181(2)
Na-O4	2.333(4)	Na-O4	2.332(8)	Na-O4	2.331(5)
Na-O6	2.342(3)	Na-O6	2.342(6)	Na-O6	2.339(4)
Na-O11	2.364(3)	Na-O11	2.351(8)	Na-O11	2.338(5)
Na-O8	2.406(3)	Na-O8	2.411(7)	Na-O8	2.403(5)
Na-O7	2.442(3)	Na-O7	2.467(7)	Na-O7	2.448(5)
Na-O9	2.480(3)	Na-O9	2.475(6)	Na-O9	2.474(4)
O2-Mn-O2	113.80(17)	O2-Co-O2	110.6(4)	O2-Cu-O2	137.9(3)
O2-Mn-Cl1	107.92(11)	O2-Co-C11	109.4(2)	Cl1-Cu-Cl1	152.6(3)

The sodium ion remains in the monensin cavity and cannot be displaced by the corresponding transition metal ion. The alkali center is coordinated by six oxygen atoms and the inner coordination sphere possesses a highly distorted octahedral geometry, with the Na-O

bonds varying between 2.33 and 2.48 Å in all three complexes (**Table 3.2-5**). The results corroborate the data on the crystal structures of sodium monensinate.

The IR data for the mixed-metal monensinates are consistent with the structures dissolved by the X-ray diffraction (**Table 3.2-6**). Main attention should be paid to the difference between the asymmetric and symmetric stratching vibrations of the carboxylate anion, which is $\Delta\nu$ = 180-200 cm^{-1} in the complexes, confirming the monodentate mode of coordination of the deprotonated carboxylic group. The second range is that of the stretching OH vibrations (3600-3200 cm^{-1}), where a different number of bands are observed depending on the presence of crystal water and the coordination and/or hydrogen bonds formed.

The paramagnetic complexes $[Mn(MonNa)_2Cl_2]$ and $[Cu(MonNa)_2Cl_2]$ were further characterized by EPR spectroscopy. The spectrum of manganese(II) complex in methanol (77 K, **Fig. 3.2-10**) contains a well-resolved sextet (g = 2.07; A_{Mn} = 93 G), the hyperfine splitting being due to electronic interaction with the ^{55}Mn nucleus (I = 5/2). The observed signal is characteristic of mononuclear complexes of Mn^{2+} in an octahedral environment, realized most likely by additional coordination of solvent molecules in the tetrahedral complex. The EPR spectra of $[Cu(MonNa)_2Cl^2]$ were recorded in solution and solid state (77 K). They are characterized by a hyperfine structure due to the interaction of the unpaired electron with the nuclear spin of $^{63,65}Cu$. The values of the g- and A-parameters are typical for mononuclear copper(II) complexes bound to O- and Cl-donor atoms and located in a field with distorted tetragonal symmetry: $g_{||}$ = 2.38, $A_{||}$ = 96 × 10^{-4} cm^{-1}, $g_{\perp}$ = 2.09 (solid sample); $g_{||}$ = 2.42, $A_{||}$ = 127×10^{-4} cm^{-1}, $g_{\perp}$ = 2.08 (MeOH).

Table 3.2-6. Characteristic IR vibrations in the spectra of MonH, MonNa and $[M(MonNa)_2Cl_2]$

Vibration	Vibration position, cm^{-1}				
	MonH	MonNa	$[M(MonNa)_2Cl_2]$		
			Mn^{2+}	Co^{2+}	Cu^{2+}
ν_{OH} (H_2O)	3520	3500-3300	3560	3560	3550
ν_{OH} (free)	3320		3490	3490	3490
ν_{OH} (H-bond/coord.)			3250	3250	3190
$\nu_{C=O}$ (COOH)	1700	-	-	-	-
$\nu_{C=O}^{asym}$ (COO^-)	-	1540	1600	1600	1590
$\nu_{C=O}^{sym}$ (COO^-)	-	1390	1400	1400	1410

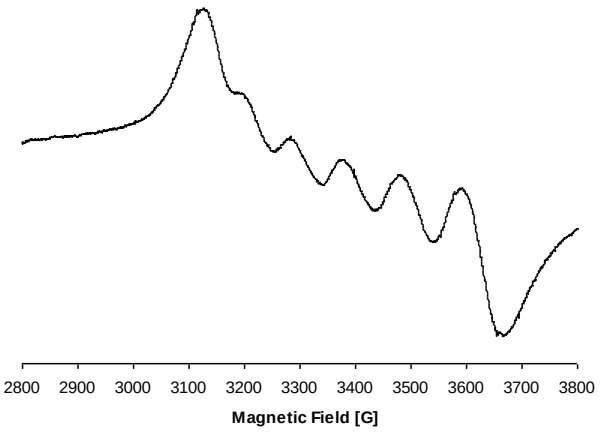

Fig. 3.2-10. EPR spectrum of $[Mn(MonNa)_2Cl_2]$ (77 K, MeOH)

3.3. Summary

A total of 32 "classical" and 7 "non-classical" complexes of monensin and salinomycin with metal cations in the second-fourth oxidation state were isolated and characterized.

The experimental data, combined with single crystal X-ray diffraction and theoretical calculations, display the isostructurality of the coordination compounds in the individual series, where the antibiotics always act bidentately, forming cyclic "head-to-tail" structures:

$[ML_2(H_2O)_2]$:	monensin	M^{2+} = Mg, Ca, Co, Mn, Ni, Cu, Zn, Cd;
	salinomycin	M^{2+} = Mg, Ca, Sr, Ba, Co, Ni, Cu, Zn, Cd;
$[ML_3(H_2O)_3]$:	monensin	M^{3+} = Y, La, Ce, Pr, Nd, Sm, Eu, Gd, Tb, Er;
	salinomycin	M^{3+} = La, Pr, Nd;
$[ML_2(OH)_2]$:	monensin	M^{4+} = Ce;
	salinomycin	M^{4+} = Ce.

In those complexes where a different coordination mode is observed, monensin and salinomycin react as polydentate ligands. The coordination compounds $[HgMon(H_2O)]$ and $[M(MonNa)_2Cl_2]$ (M^{2+} = Co, Mn, Cu) have been analyzed by single crystal X-ray diffraction, the structures of $[CeL(NO_3)_2(OH)]$ have been modeled using molecular dynamics and quantum-chemical calculations.

4. Results and Discussion:
Complexation of monensin and salinomycin in solution - experimental and theoretical studies

Having in hands a series of complexes of monensin and salinomycin with metal ions in different oxidation states a question raised about the coordination ability of the ligands in solution under different reaction conditions. The data had shown that circular dichroism (CD) can be successfully applied to study the properties of monensin as a chiral molecule, and combined with theoretical calculations, they can increase our knowledge for its behavior in solution. The circular dichroic spectrum of salinomycin does not change in the presence of metal cations and its complexation ability was investigated by a theoretical model.

4.1. Experimental CD study of the interaction of monensin with di- and trivalent metal ions

In circular dichroism experiments, it was found that the ultraviolet (UV-CD) spectrum of monensin is sensitive to the conformational changes of the ligand upon its complexation with divalent metal cations. This study was later supplemented with circular dichroic data in the visible (Vis-CD) and near-infrared (NIR-CD) regions. UV-CD analysis was carried out for the most of the trivalent metal ions. The studies were carried out with conventional equipment and/or with synchrotron radiation circular dicroism (SRCD).

4.1.1. CD spectroscopy in the ultraviolet region (UV-CD)

Initially we recorded the SRCD spectra of MonH, $[CoMon_2(H_2O)_2]$ and $[MnMon_2(H_2O)_2]$ isolated as solids and dissolved in methanol (optical path length b = 0,1045 mm). We observed different spectra for all three systems. Next, the methanolic solutions containing the deprotonated antibiotic Mon^- (with Et_4NOH) and the Co^{2+}/Mn^{2+} – Mon^- systems at a molar ratio of l:2 (b = 0.014 mm) were analysed. The good agreement between the two experiments (**Fig. 4.1-1**) showed that the molecular species distribution was identical for the two systems (dissolved solid phase and complexes obtained *in situ*). The different CD behavior of monensin and the monensinant anion in the presence of Co^{2+}/Mn^{2+} (despite their very close X-ray structural data) gave us the reason to include in these studies the remaining divalent metal cations for which crystal structures are available (**Fig. 4.1- 2**).

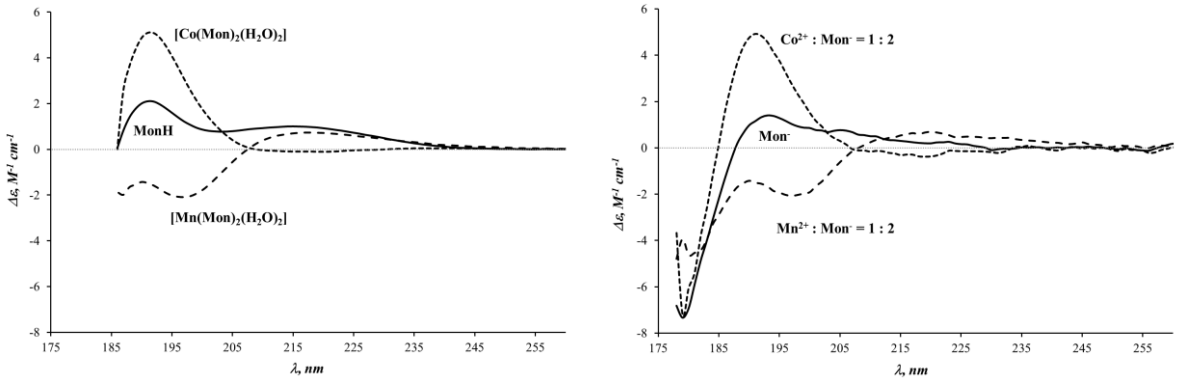

Fig. 4.1-1. SRCD spectra of: MonH, $[CoMon_2(H_2O)_2]$ and $[MnMon_2(H_2O)_2]$ (left); monensinate (Mon^-) and solutions, containing Co^{2+}:Mon^- = 1:2 and Mn^{2+}:Mon^- = 1:2 (right); 20 mM ligand analytical concentration

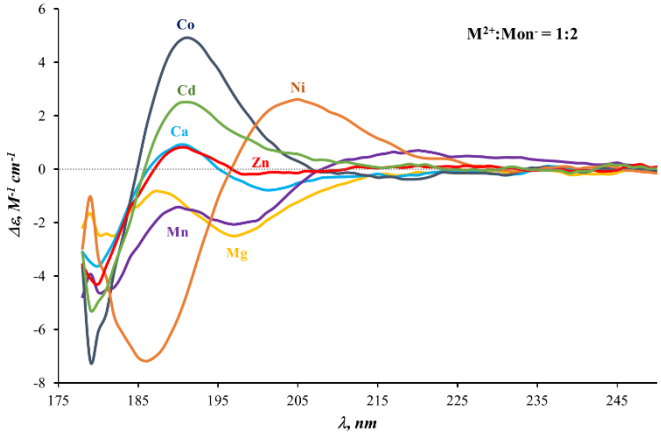

Fig. 4.1-2. SRCD spectra of reaction mixtures, containing monensin and divalent metal ions at molar ratio M:L = 1-2 (b = 0.014 mm, 20 mM ligand analytical concentration)

The results showed a significant sensitivity and selectivity of the circular dichroism to the binding of monensin to divalent metal cations, therefore we performed a series of experiments at different molar ratio of M^{2+}-Mon^- varying from 1:10 to 6:1. The titration curves for the Co^{2+}-Mon− system are presented in Fig. **4.1-3**.

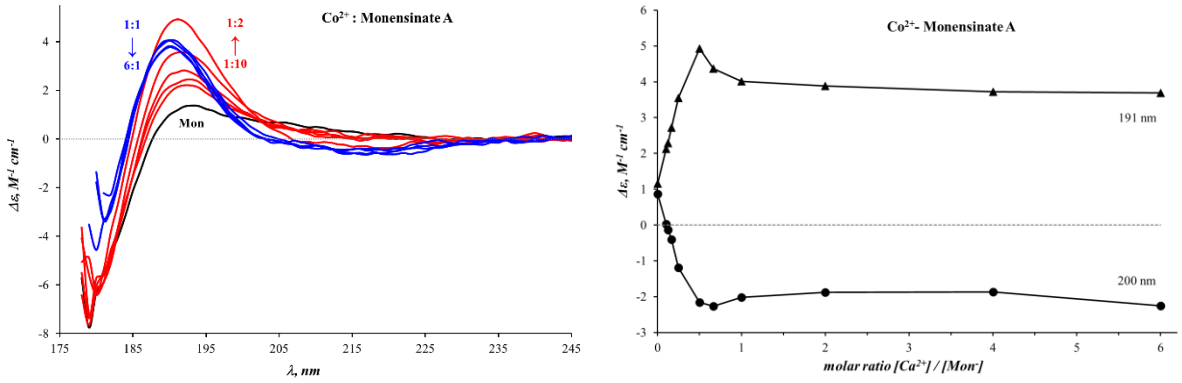

Fig. 4.1-3. Spectra of Et_4NMon (черно) with deficiency (red) and excess (blue) of Co^{2+} ions (left); spectral changes at a given wavelength as a function of Co^{2+}–Mon^- molar ratio (right); 20 mM analytical ligand concentration, b = 0.014 mm

The positive band of Et_4NMon (Mon^-) at 193 nm gradually increases in intensity with increasing amount of Co^{2+} and reaches a maximum at 191 nm at a metal–ligand molar ratio of 1:2. At the same time, the positive signal for Et_4NMon in the range of 200-220 nm decreases to the appearance of a negative band of low intensity. A further increase in the concentration of cobalt(II) ions leads to the formation of a second type of species with a positive absorption at 190 nm and a weak negative signal in the range 200-220 nm. The spectral changes observed at the deficit of the metal ion are mainly due to the formation of the complex $[CoMon_2(H_2O)_2]$, whose structure is already known. The formation of the second type of species was observed experimentally for the first time at a molar ratio of Co^{2+} – Mon^- = 1:1, and further addition of Co^{2+} did not change its spectral characteristics. Because of the close spectral pattern of the two types of spectra (although they differ in shape and intensity), we suggest that in the new particles the monensinate ion possesses a similar coordination behavior as that in $[CoMon_2(H_2O)_2]$.

The SRCD spectra of the solutions containing Mon^- and the rest of the divalent metal metal ions studied under the same reaction conditions also suggest the formation of two types of complex species depending on the molar ratio between the metal ion and the ligand. The MRA-analysis (matrix rank analysis) on the data set for the studied systems and the evaluation of the residual CD signals showed that the use of only two species (free ligand and ML_2) still leads to a sufficiently high residual ellipticity that differs from the baseline. Therefore, a minimum of three species is required to satisfactorily describe the ongoing spectral changes (**Fig. 4.1-4** for Co^{2+}).

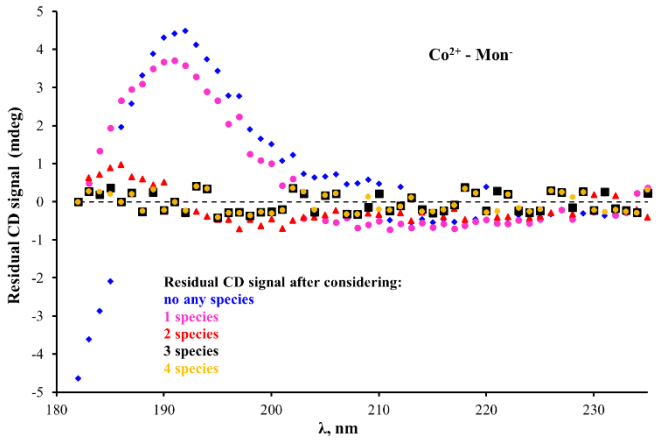

Fig. 4.1-4. Residual CD signals for the system Co^{2+}-Mon^{-} depending on the number of assumed species in solution

The experimentally observed dependence of the intensity of the CD signals on the molar ratio M^{2+}-Mon^{-} (**Fig. 4.1-3**, right) cannot be attributed only to the existence of one type of complex species. Considering the change in the dependence slope (and in some cases the sign) and the molar ratio at which it occurs, the third species in the system could be attributed to the formation of mono-complexes of the ML^{+} composition. Thus, by means of circular dichroism spectroscopy, for the first time we were able to observe a new type of monensin species with divalent metal cations and to prove that, at an excess of metal ions, the ligand can bind more than half an equivalent of M^{2+}. It is worth noting that the discussed changes are less pronounced for the monensin – Zn^{2+} / Ca^{2+} systems, and no formation of second species is observed for Cd^{2+}. A reason for this can be sought in the closeness of the CD spectra for ML_2 and ML^{+} with these ions, but we can also rule out the formation of CdL^{+} in methanol solutions.

Assuming that the monensinate ion forms two types of complex species, the following equilibriums in methanol leading to $MMon_2(H_2O)_2]$ (**ML_2**) and $[MMon(H_2O)]^{+}$ (**ML^{+}**) may proceed (L^{-} = Mon^{-}, the water molecules are excluded for clarity):

$$M^{2+} + 2\ L^{-} \rightleftharpoons \mathbf{ML_2}\ \text{(equilibrium I)}$$

$$M^{2+} + \mathbf{ML_2} \rightleftharpoons \mathbf{2\ ML^{+}}\ \text{(equilibrium II)}$$

Using the PSEQUAD program, the individual spectra of the **ML_2** and **ML^{+}** species (**Fig. 4.1-5**), the conditional stability constants β_2' / β_1' and the constant K' characteristic of the relative stability of the mono- and bis-complexes were calculated (**Table 4.1-1**). K' is defined by equation (1).

$$K' = \frac{[ML]^2}{[M]\cdot[ML_2]} = \frac{K1'}{K2'} \qquad (1),$$

where [X] is the equilibrium concentration of X species in solution (free ligand L, metal ion M, **ML$_2$** and **ML$^+$** complexes). The stepwise stability constants K_1' and K_2' are calculated according to (2):

$$K_1' = \sqrt{K' \cdot \beta_2'};\ K_2' = \sqrt{\frac{\beta_2'}{K'}} \qquad (2)$$

Table 4.1-1. Stability of monensin complexes with divalent cations at constant CD spectrum of the ligand anion (standard deviation is given in parentheses)

	Mn^{2+}	Co^{2+}	Ni^{2+}	Zn^{2+}	Cd^{2+} [а]	Mg^{2+}	Ca^{2+} [б]
$\lg\beta_1'$(ML)	4.8 (0.2)	5.9 (0.5)	16.0 (0.3)	6.7 (0.6)	0.9 (*)	4.9 (0.4)	3.3 (0.2)
$\lg\beta_2'$(ML$_2$)	7.8 (0.3)	10.2 (0.8)	24.5 (0.5)	12.1 (1.0)	4.8 (0.2)	7.4 (0.4)	4.7 (*)
$\lg K_2'$	3.0	4.3	8.5	5.32	3.9	2.5	1.4*
K'	63	40	3.2×10^7	27.54	1.0×10^{-3}	1251	79

[а] at constant spectra of Mon^- and **ML$^+$**: $\lg\beta_1'$ = 3.4 (0.3); $\lg\beta_2'$ = 5.8 (0.3)
[б] assuming one type of species: $\lg\beta_1'$ = 4.0 (0.4) or $\lg\beta_2'$ = 4.3 (0.4)

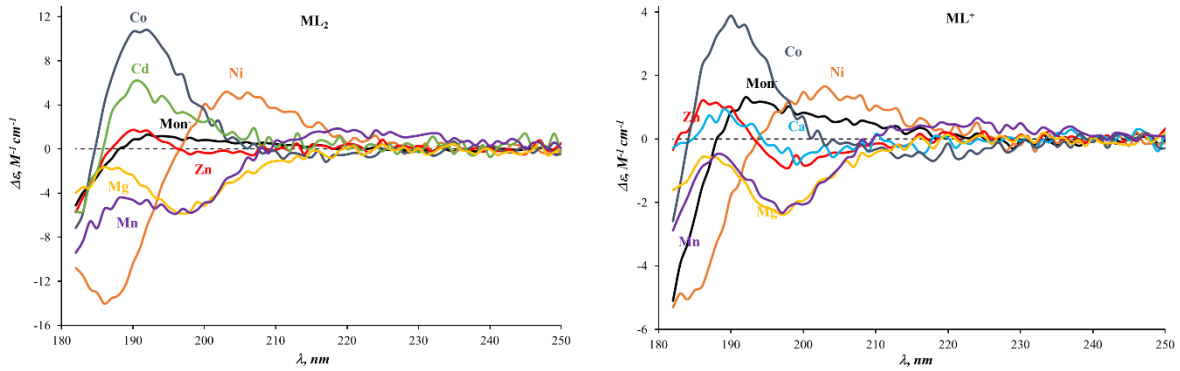

Fig. 4.1-5. Individual SRCD spectra of **ML$_2$** and **ML$^+$** (PSEQUAD)

For the most studied systems, the PSEQUAD approach showed good agreement between the calculated and experimentally observed spectra providing the existence of two complex species. It should be noted that the complexation process is almost irreversible (and we cannot fully trust the computational accuracy), but the decrease in the stability of the **ML$_2$** species follows the order $Ni^{2+} > Zn^{2+} > Co^{2+} \sim Mg^{2+} \sim Mn^{2+}$ (> $Cd^{2+} > Ca^{2+}$). The stability of **ML$^+$** complexes is very similar to **ML$_2$** series ($Ni^{2+} > Zn^{2+} > Co^{2+} \sim Mg^{2+} \sim Mn^{2+}$ (> $Ca^{2+} > Cd^{2+}$)). It is also necessary to account that the equilibrium in solution is shifted in favor of **ML$^+$** over **ML$_2$**, although the only complexes isolated in solid phase are the electroneutral **ML$_2$**. The presence of two types of

monensinate species provoked our interest in yet another direction, namely to evaluate the behavior of $\mathbf{ML_2}$ and $\mathbf{ML^+}$ in the presence of a competing divalent metal cation.

In the first set of experiments, to a reaction mixture containing a given metal ion (M^1) and Mon^- at a 1:2 molar ratio, we added increasing amounts of a second metal ion (M^2). Spectral changes showed that in this process the equilibrium shifts from $\mathbf{M^1L_2}$ to $\mathbf{M^2L^+}$, and *vice versa* – an excess of M^1 converts $\mathbf{M^2L_2}$ to $\mathbf{M^1L^+}$. In a pointed manner, from the $\mathbf{M^1L_2}$ complex of any metal ion, an equilibrium can be reached in which the competing cation is dominant in the form of $\mathbf{M^2L^+}$. These results outlined a general trend that under competition conditions, monensin bound in the $\mathbf{ML_2}$ complex can interact with those divalent metal ions that are in excess in its close environment.

In the second experimental set, we investigated the competition processes involving only the $\mathbf{ML^+}$ species. For this purpose, pairs of solutions were prepared in a molar ratio M^1-Mon^- = 4:1 and M^2-Mon^- = 4:1, ensuring the dominant formation of the corresponding particles $\mathbf{M^1L^+}$ and $\mathbf{M^2L^+}$, and the corresponding SRCD spectra were recorded for each independent system. Then we analyzed the solutions spectra containing M^1, M^2 and Mon^- at a 4:4:1 molar ratio, considering that the observed signal results from the different contribution of individual $\mathbf{M^1L^+}$ and $\mathbf{M^2L^+}$ particles. We thus estimated the partition coefficients that account for the competition between the divalent metal ions, i.e. the tendency of monensin to selectively bind M^{2+} as ML^+ (**Table 4.1-2**). The relative affinity of monensinate anion in these systems decreases in the order $Ni^{2+} > Co^{2+} \sim Ca^{2+} > Mn^{2+} \sim Mg^{2+} \sim Zn^{2+} \sim Cd^{2+}$.

The comparison between the stability of the $\mathbf{ML_2}$ / $\mathbf{ML^+}$ complexes and the behavior of monensin in recent experiments showed a significant change in the position of the zinc(II) ions in the respective series. At this stage, we cannot explain the observed difference, but probably other additional factors (origin of the counterion of the metal salt, solvolysis, etc.) that may affect the studied processes should be also taken into account.

Table 4.1-2. Competition between M^{2+} on formation of $\mathbf{ML^+}$

Competitive ion M^2	Contribution (%) of M^1-Mon to the resultant SRCD spectrum at M^1:M^2:Mon^- = 4:4:1						
	Ni	Co	Ca	Mn	Mg	Zn	Cd
Co	75						
Ca	75	55					
Mn	90	75	65				

Mg	90	75	70	55			
Zn	90	75	90	85	55		
Cd	95	80	70	75	60	60	

Based on the PSEQUAD-calculated individual spectra of the two types of monensinate species (**Fig. 4.1-5**), it is evident that circular dichroism spectroscopy can distinguish between the individual complexes with divalen mettal cations, as their spectral behavior is definitely different. Such discrimination can be explained by subtle changes in ligand conformation due to the geometrical requirements of the metal ion. From the similarities between the SRCD spectra of the corresponding pairs $\mathbf{ML}^+$ and $\mathbf{ML_2}$, we assume that the excess of metal(II) ions leads to the formation of positively charged complex particles with the composition $[MMon(H_2O)]^+$, where the monensinate anion coordinates in the same way as in $[MMon_2(H_2O)_2]$. The metal ion most likely does not occupy the ligand cavity, which is also supported by the similarity in the stability order for the $\mathbf{ML}^+$ and $\mathbf{ML_2}$ complexes. The difference between the CD spectra of the two types of species is due to the sensitivity of the circular dichroism to the conformational changes in the structure of monensin in the presence of the metal ion. Logically, to unambiguously prove the structure of $[MMon(H_2O)]^+$, it is necessary to find suitable conditions for their isolation, crystallization and characterization.

4.1.2. CD analysis in the visible (Vis-CD) and near-infrared (NIR-CD) wavelength range

Despite the good sensitivity of UV-CD spectroscopy, the quantitative results are subject of re-evaluation (**Table 4.1-1**) due to the similar pattern of the spectra of neutral and charged species, which leads to a possible inaccuracy in determining their stability. For that reason, we developed a complementary method using circular dichroism in the visible (Vis-CD) and near-infrared (NIR) regions to investigate some processes involving the transition metal ions of Co^{2+} and Ni^{2+}. The presence of Vis- and NIR-CD signals proves the interaction between the metal ion and the monensinate anion, since none of the starting components is chirally active by itself in the studied spectral range. The smaller data set simplifies the evaluation of the spectral series obtained upon titration of the monensinate anion with increasing amount of Co^{2+} or Ni^{2+} ions.

First we evaluated the Ni^{2+}-Mon^- system, since the UV-CD results showed a significant stability of nickel complexes, orders of magnitude higher than that of the other divalent metal cations. Spectra of the observed species differ substantially depending on the metal-to-ligand molar ratio: excess monensin leads to a positive maxima at ~ 680 and ~ 1200 nm and a negative minimum at ~ 990 nm, while excess of Ni^{2+} induces a minimum at ~ 750 nm and a maximum at

~ 1080 nm (**Fig. 4.1-6a**). MRA analysis confirmed the existence of the mononuclear mono- and bis-complex species $[NiMon(H_2O)]^+$ and $[NiMon_2(H_2O)]$, for which PSEQUAD calculations yielded the corresponding $lg\beta_1' = 5.94 \pm 0.07$ and $lg\beta_2' = 9.81 \pm 0.11$. These data differ significantly from previous UV-CD values, but are more reliable due to the good distinction in the spectra of the two colored complex species existing in solution.

The observed difference in the stability constants of Ni^{2+}-monensinates obtained in UV- and Vis/NIR-CD measurements provoked our re-evaluation of the Co^{2+}-monensin system as well. The deficit of metal cations leads to the appearance of two maxima (~ 476 nm, ~ 515 nm) and one minimum (~ 554 nm) in the spectra of the studied solutions, corresponding to the formation of the mononuclear bis-complexes (**Fig. 4.1-7**). The excess of Co^{2+} at which the mononuclear mono-complex is observed induces a local maximum (~ 498 nm) and minimum (~ 543 nm). Data analysis shows that the processes can be described by two complex species, with calculated stability constants very close to those obtained by UV-CD spectroscopy: $lg\beta_1' = 5.74 \pm 0.02$ and $lg\beta_2' = 9.93 \pm 0.04$.

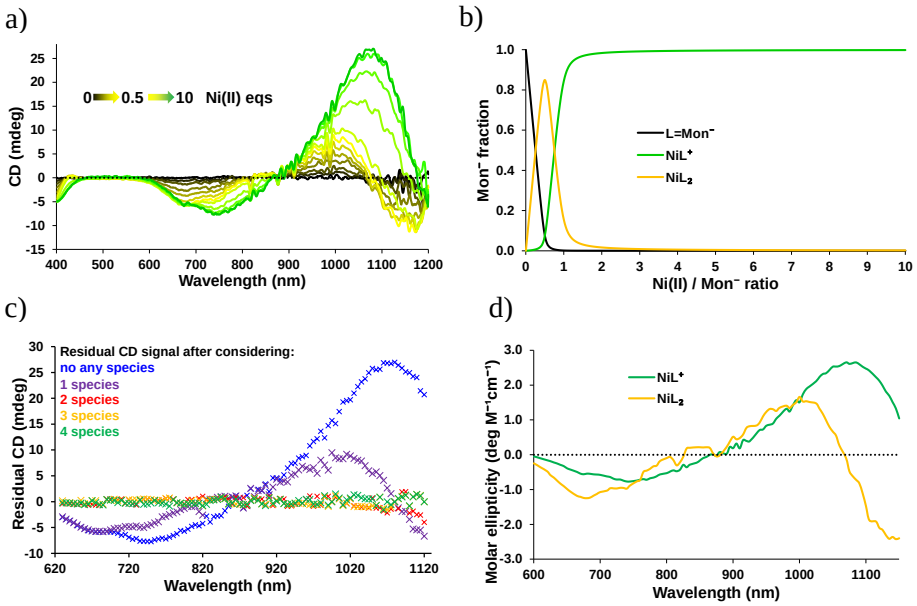

Fig. 4.1-6. a) Titration curves of the Ni^{2+}-monensinate system; b) Distribution diagram of complex species; c) MRA; d) Calculated spectra of $[NiMon(H_2O)]^+$ and $[NiMon_2(H_2O)]$

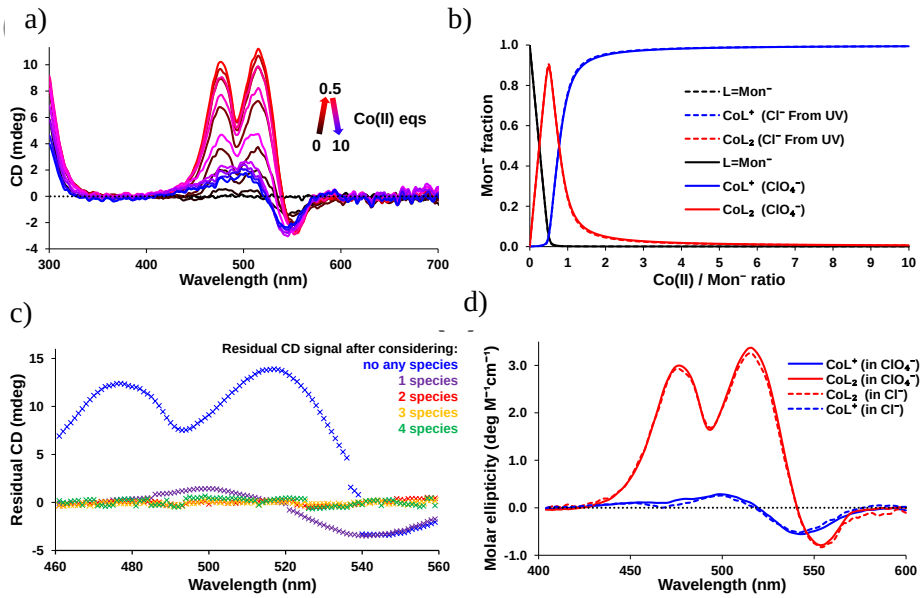

Fig. 4.1-7. a) Titration curves of the Co^{2+}-monensinate system; b) Distribution diagram of complex species; c) MRA; d) Calculated spectra of $[CoMon(H_2O)]^+$ and $[CoMon_2(H_2O)]$

With thus recalculated values of the conditional stability constants for the mono- and bis-monensinates of Co^{2+} and Ni^{2+}, we evaluated the competition processes between the two metal ions for binding to the ligand. In a series of titration experiments, increasing amount of Co^{2+} was added to $[NiMon_2(H_2O)_2]$ and *vice versa*, to the bis-complex of Co^{2+} - Ni^{2+} ions. Taking into account the molar ratio of all participants in the system, the minimum number of complex species in solution and their recently calculated stability, we confirmed the absence of mixed-metal complexes, as well as the fact that all mono- and bis-species should be taken into account when proceeding of competitive processes (**Fig. 4.1-8**). We also applied the developed methodology to study the processes in systems containing "colored" and "colorless" metal ions. The latter are a certain challenge, because the number of "colorless" complex species cannot be estimated by MRA. For this purpose, we monitored the absorption of $[CoMon_2(H_2O)_2]$ at 518 nm and compared the data with its theoretical decrease in the presence of only mono-species as well as in the formation of mono- and bis-complexes with Mg^{2+}, Ca^{2+}, Zn^{2+}. The data showed (**Fig. 4.1-9**) that, similarly to the Co^{2+}-Ni^{2+} systems, here also the presence of mono- and bis-species of the two competing metal ions must be taken into account (**Fig. 4.1-9**), which in turn allowed the calculation of the conditional stability constants of the "colorless" $[MMon(H_2O)]^+$ and $[MMon_2(H_2O)_2]$ (**Table 4.1-3**).

Table 4.1-3. Overall conditional stability constants (lgβ) of "colorless" monensinates (standard deviation is given in parentheses)

Complex species	Zn^{2+}	Mg^{2+}	Ca^{2+}
$[MMon(H_2O)]^+$	6.09 ± 0.02	4.81 ± 0.01	5.18 ± 0.01
$[MMon_2(H_2O)_2]$	10.12 ± 0.02	8.36 ± 0.01	8.40 ± 0.01

The values for the mono- and bis-species containing Zn^{2+} and Mg^{2+} are relatively comparable to those obtained by UV-CD spectroscopy. The study of the Ca^{2+}-monensin system was much more successful, and in all cases the formation of mixed-metal coordination compounds was not observed.

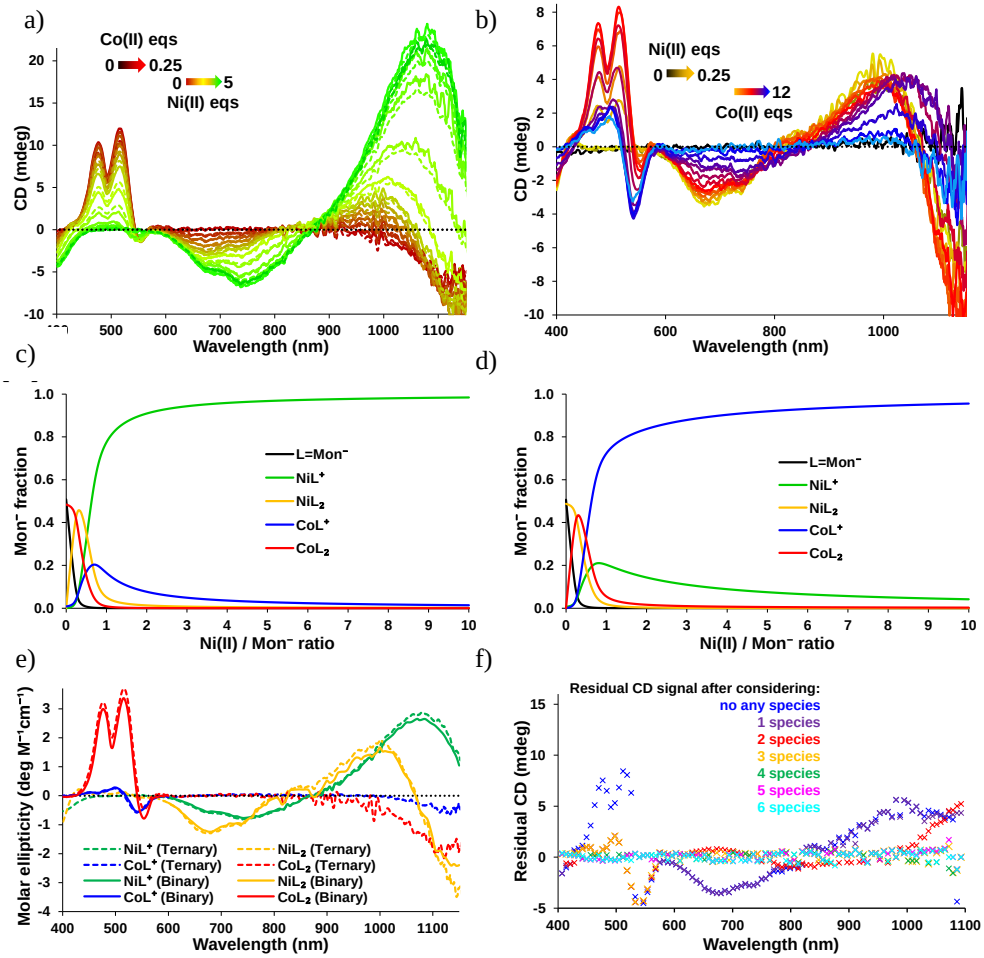

Fig. 4.1-8. Competition between Ni^{2+} and Co^{2+} for binding to monensin. Up – change in CD signals with increasing amount of Ni^{2+} (a) or Co^{2+} (b). In the middle – species distribution in the competing systems Co^{2+}/Ni^{2+} (c) and Ni^{2+}/Co^{2+} (d). Bottom – molar spectra of mono- and bis-complexes calculated in the binary (solid line) and ternary (dashed line) systems (e); residual CD signals at different number of species in solution (f)

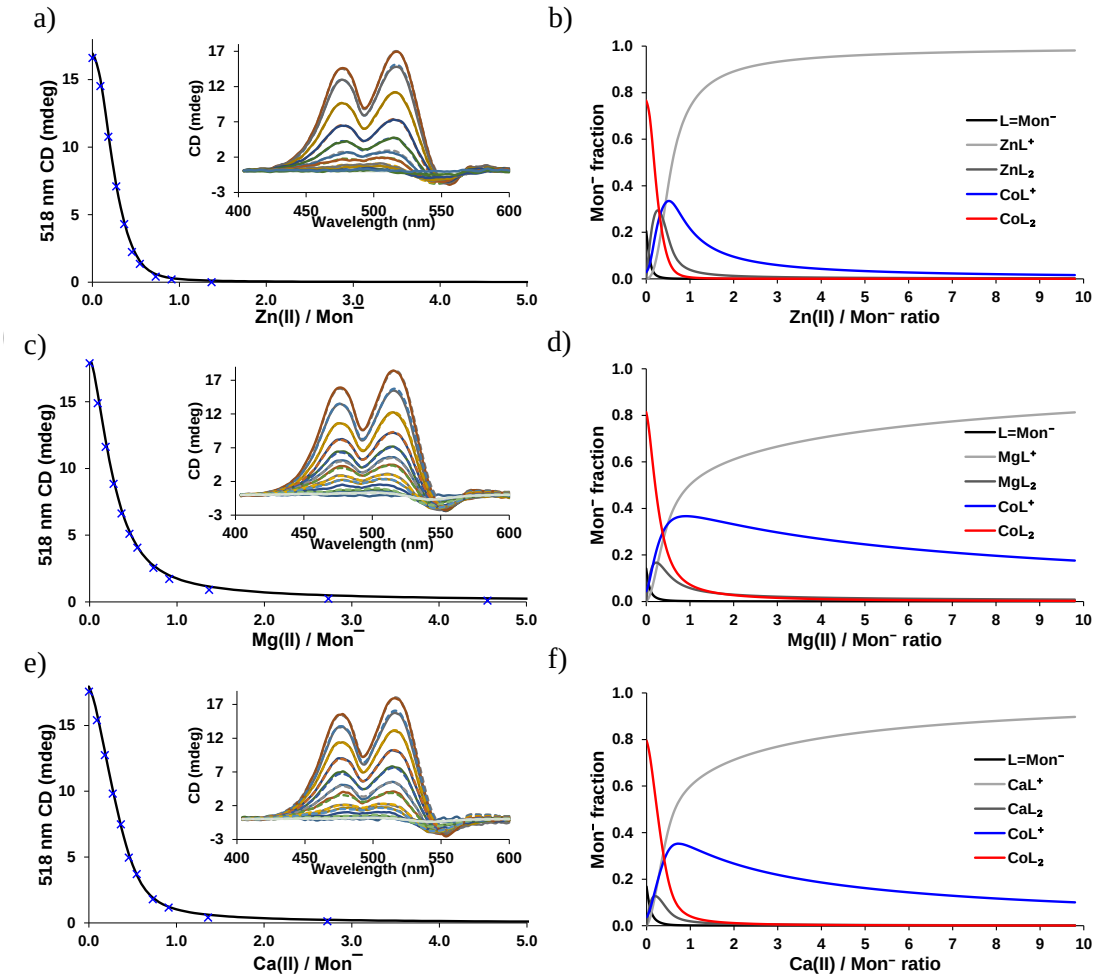

Fig. 4.1-9. Competitive processes between "colorless" metal ions and Co^{2+}. Absorbance' decrease of $[CoMon_2(H_2O)_2]$ at 518 nm upon addition of increasing amounts of Zn^{2+} (a), Mg^{2+} (c), Ca^{2+} (e). Measured values are depicted with blue × symbols, calculated when at least 4 species present – with a solid black line. The inset plots represent the experimental (solid line) and calculated (dashed) spectra. Distribution diagrams of the systems in the presence of Zn^{2+} (b), Mg^{2+} (d), Ca^{2+} (f)

4.1.3. UV-CD spectroscopy of the "lanthanide ion - monensin" systems

The applicability of circular dichroism allowed us to study also the behavior of monensin in the presence of some trivalent lanthanide ions (Gd, La, Nd, Pr, Sm, Eu). For this purpose, the spectral changes in tetraethylammonium monensinate were followed in a series of solutions containing varied metal ion - ligand molar ratios from 1-9 to 3-1 at an optical path of 0,014 mm. The spectral changes in the Sm^{3+}-monensinate system are presented in **Fig. 4.1-10**. The position and sign of the bands at certain Ln^{3+}-monensinate molar ratios are summarized in **Table. 4.1-4**.

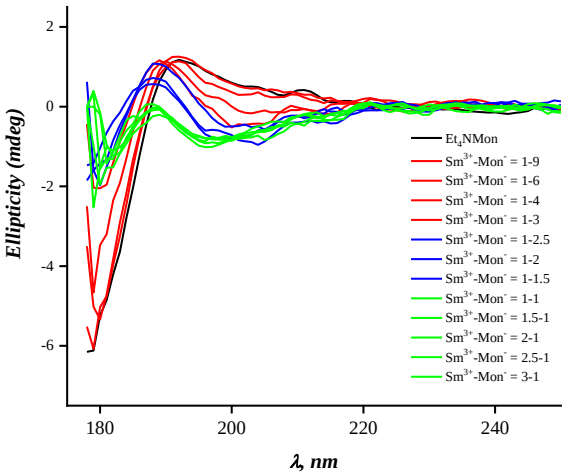

Fig. 4.1-10. SRCD spectra of tetraethylammonium monensinate upon titration with Sm(III) at a constant ligand concentration of 20 mM

Table 4.1-4. Position and sign (+/-) of the SRCD signals of tetraethylammonium monensinate upon titration with trivalent metal ions

Metal ion	Ln^{3+}-Mon^{-} = 1-3	Ln^{3+}-Mon^{-} = 1-2	L^{3+}-Mon^{-} = 1-1
La^{3+}	189 nm (+)	189 nm (+) 200 nm (−)	189 nm (+) 199 nm (−)
Pr^{3+}	190 nm (+) 202 nm (−)	189 nm (+) 200 nm (−)	197 nm (−)
Nd^{3+}	190 nm (+)	189 nm (+) 195-210 nm (−)	189 nm (+) 195-210 nm (−)
Sm^{3+}	189 nm (+) 195-210 nm (−)	188 nm (+) 195-210 nm (−)	190 nm (+) 195-220 nm (−)
Eu^{3+}	190 nm (+)	188 nm (+) 199 nm (−)	189 nm (+) 195-210 nm (−)
Gd^{3+}	190 nm (+)	187 nm (+) 200 nm (−)	190 nm (+) 199 nm (−)

The results show that depending on the molar ratio of the metal ion and monensin, several types of complex species exist in solution, some of which were attributed to the following composition:

- a neutral complex $[MMon_3(H_2O)_3]$ at monensin excess (molar ratio M^{3+}-Mon^{-} from 1-9 to 1-3);

- a positively charged complex $[MMon_2(H_2O)_2]^+$ at M^{3+}-Mon^- = 1-2;

- a positively charged complex $[MMon(H_2O)]^{2+}$ at metal ion-ligand = 1-1.

The inclusion of water molecules in the composition of the complex species was assumed based on previous studies on the monensin structure and its coordination compounds.

Circular dichroism studies lay grounds for the following conclusions:

- for the same lanthanide ion, the spectra of (at least) three types of complex species, although close, differ from each other, and this difference is visible much better in a graphic (**Fig. 4.1-11**) than in tabular form;

- given the ability of lanthanide ions to form diverse structures, the formation of additional coordination species is not excluded;

- at similar M^{3+}-Mon^- molar ratios, the individual lanthanide ions are practically indistinguishable as compared to the monensin complexes with divalent metal ions.

Thus, CD (SRCD)-spectroscopy appears to be a suitable method for studying the specific reaction system Ln^{3+}-Mon^- in solution at different mole ratios of the reagents, but it is inapplicable for distinguishing the corresponding rare earth metal ion. The reason for this is probably the close properties of the lanthanide metal ions as representatives of the f-elements.

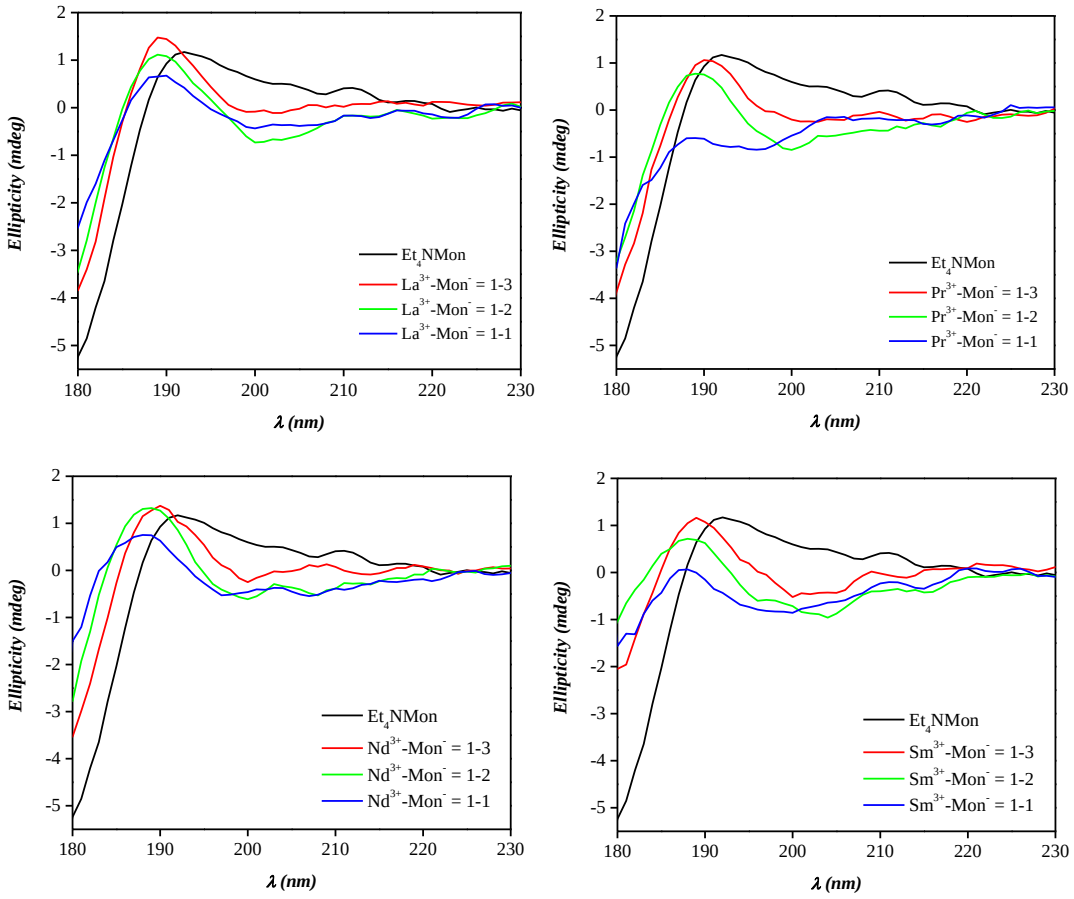

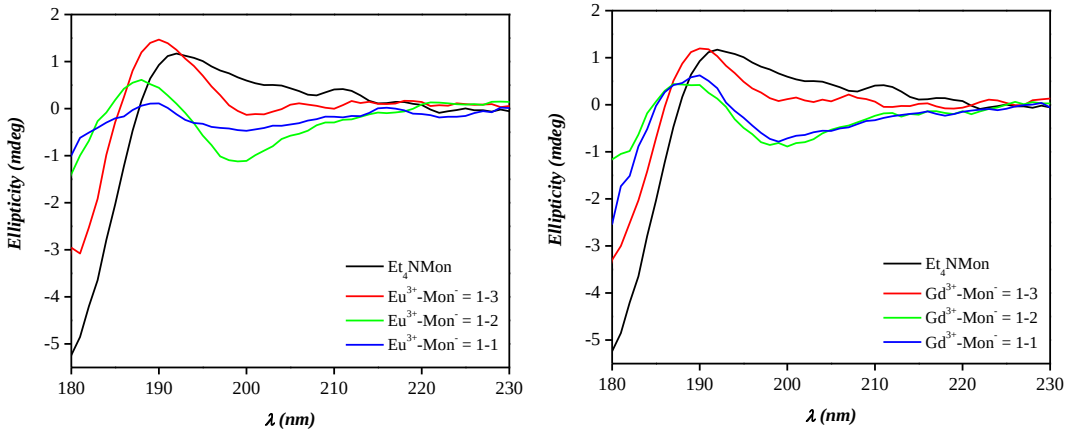

Fig. 4.1-11. SRCD spectra of tetraethylammonium monensinate (black) and the complex species with lanthanide ions (the analytical ligand concentration is kept constant (20 mM))

4.2. Experimental and theoretical CD study of complexes of monensin with monovalent metal cations

The advantages of UV-CD spectroscopy were also used to explore the properties of monensin with monovalent metal ions. Experimental CD and SRCD spectra of monensic acid A (MonH) in the presence of Li^+, Na^+, K^+, Rb^+, Ag^+ and Et_4N^+ were recorded in methanol solutions and compared with computational (theoretical) models. The sign and intensity of the CD signals vary significantly in the studied compounds, despite their close crystal structures. Theoretical modeling based on density functional theory (DFT) and the continuum solvent model, as well as time-dependent density functional theory (TDDFT) simulations, confirm that the CD spectra of monensin complexes are strongly sensitive to the nature of the monovalent ions and can be used for their discrimination.

The CD spectra of MonH and its monovalent derivatives (recorded at 0.2 mm optical pathlength) are presented in **Fig. 4.2-1**. The spectrum of MonH is positive in the range of 190-245 nm with two maxima at 218 and 192 nm, while the replacement of H^+ by Et_4N^+ reduces the intensity of the band at 218 nm (although it remains positive) and leads to a positive maximum at 195 nm. The observed result may be due to the formation of an alternative network of hydrogen bonds in the deprotonated antibiotic. On the other hand, MonH most likely remains in a “closed” conformation, which has been found to be most favorable for the anionic form.

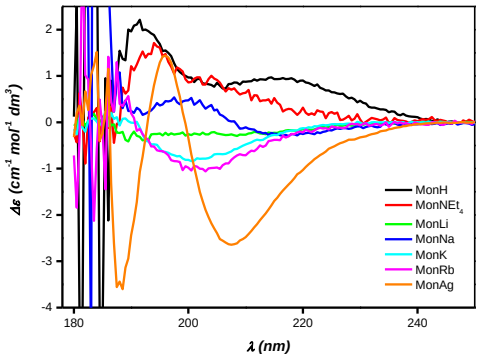

Fig. 4.2-1. Experimental CD spectra of MonH and its derivatives with six monovalent cations (0.2 mm optical pathlength). The intensity in the range 180-192 nm is not reliable; it is presented for comparison with the SRCD spectra

The "trapping" of monovalent metal cations in the monensin cavity leads to significant changes in the CD spectrum of the acidic form of the antibiotic. Complexation with sodium ions is accompanied by the appearance of two bands at 200 nm (positive) and 216 nm (negative). The coordination of lithium ions causes a negative signal in the range 190-230 nm, while the CD spectrum of the silver complex contains positive (196 nm) and negative (208 nm) bands. The potassium and rubidium complexes of monensin are mainly characterized by negative bands with a minimum at 201-203 nm.

Applying SRCD spectroscopy at a shorter optical path (0.014 mm, **Fig. 4.2-2**), we were able to obtain additional information in the far UV-region. SRCD spectra were recorded up to 178 nm due to the limitation due to high absorption values (HT > 5 below this wavelength). The experimental spectra of MonH and $MonNEt_4$ possess a negative signal below 190 nm, and the silver complex shows an intense negative band at 185 nm. Coordination of Li^+ results in the appearance of a negative signal at 187 nm accompanied by a negative shoulder at 200-220 nm. The shape of the spectra of MonK and MonRb differ in the 180-185 nm range, despite the similarities observed in the 190-220 nm range. The monensin sodium complex also possesses a unique spectrum. Comparison between the CD and SRCD spectra shows a very good agreement in the range from 192 to 300 nm. The application of SRCD leads to a higher signal-to-noise ratio, and the use of the shorter optical path (0.014 mm) allow to obtain characteristic signals with high intensity in the 178-192 nm range.

The conformational changes in the monensin molecule upon coordination of the monovalent ions could be the reason for the observed differences in the CD spectra of the coresponding molecular species. These changes, however, are quite small as shown by a PyMol comparison of the structures of monensin A and its metal(I) complexes (**Table 4.2-1**).

From the root mean square deviation (RMSD) data, it can be concluded that the overall conformation of the antibiotic is very similar in each of the complexes. Despite this similarity, also observed in the IR and NMR spectra of the metal(I) monensinates, their CD spectra differ significantly in terms of the bands position and their sign/intensity. However, some trends are observed: 1) the fine structure of MonH differs from that of the metal complexes (RMSD ~ 0.7), which affects the intensity of the CD spectrum; 2) the structure of the MonLi - MonNa and MonK - MonRb pairs is quite close (RMSD ~ 0.2) and is consistent with the close wavelengths of minima and maxima in their CD spectra. Assuming that upon dissolution in methanol the structure of the studied molecular species is preserved, at least some of the observed differences in the CD spectra can be explained by the weak conformational changes that occur in the ligand molecule upon complexation. On the other hand, the crystal structure of MonAg, which is also different from MonH but quite similar to the structures of MonM (e.g., RMSD ~ 0.1 compared to MonNa), has a unique CD spectrum too.

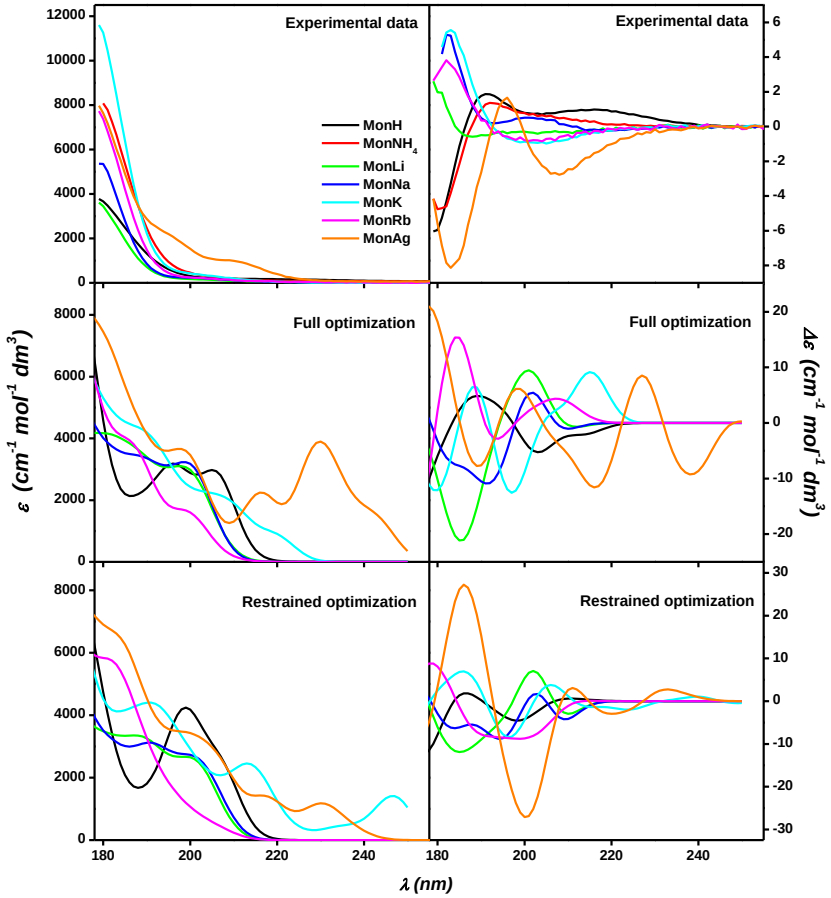

Fig. 4.2-2. Experimental and calculated absorption (left) and SRCD (right) spectra of MonH and MonM (M = Li^+, Na^+, K^+, Rb^+, Ag^+) at 0.014 mm optical pathlenght. B3LYP/PCM/6-311++G**/6-31G** was used in calculation procedures. Results are presented for both the fully and partially optimized geometries of the corresponding compounds

Table 4.2-1. Root-mean-square deviation (RMSD, Å) as a measure of similarity between the 47 core atoms in the "overlaid" structures of MonH and the corresponding monensinates. The known crystal structures are compared both with each other and with the corresponding optimized structures (column 2). Numbers in parentheses refer to the optimized structures

LigAlign comparison	Optimized structure	MonH	MonLi	MonNa	MonK	MonRb
MonH	0.188					
MonLi	0.116	0.715 (0.650)				
MonNa	0.152	0.685 (0.555)	0.187 (0.198)			
MonK	0.438	0.648 (0.472)	0.558 (0.611)	0.404 (0.521)		
MonRb	0.477	0.674 (0.551)	0.658 (0.798)	0.503 (0.646)	0.131 (0.660)	
MonAg	0.460	0.649 (0.283)	0.313 (0.597)	0.134 (0.490)	0.231 (0.567)	0.348 (0.597)

The calculated absorption and CD spectra (**Fig. 4.2-2**) could explain the observed spectral differences, although they do not quantitatively reproduce the experiment. A partial agreement of the theoretical and experimental CD data is observed: for example, both spectra of MonH are negative around 180 nm; the experimentally recorded band has a positive sign at ~185 nm, but calculations predict a negative signal at higher wavelengths, which is not observed experimentally. Part of the discrepancies may be due to the position of the hydrogen atoms, which is not clearly defined by the X-ray structural data. The TDDFT method error and complex conformational and/or hydration equilibria not included in the performed calculations may also be the reason for the observed disagreement between the experimental and theoretical spectra.

On the other hand, the calculations confirm the sensitivity of monensin to the interaction with metal(I) ions, which also affects the observed CD signals. Most transitions up to 200 nm in the monovalent monensinates (except Ag^+ complex) are $\sigma \rightarrow \sigma^*$ (180 nm) or can be considered as such (190-200 nm), while $n \rightarrow \sigma^*$ transitions predominate in the range of 200-206 nm ("n" means a non-bonding orbital (electron pair) of oxygen in a hydroxyl or carboxyl moiety). Most, but not all, of the transitions above 180 nm occur with the participation of the carboxyl moiety. The bands at 210-215 nm are attributed to the $\sigma \rightarrow \pi^*$ and $n \rightarrow \pi^*$transitions, where the π-orbitals

belong primarily to the carboxyl group (the participation of the lone electron pairs of the hydroxyl oxygen can also be accounted for as π). For the silver cation, the situation is different, as all the intense bands at 180, 215, 230 and 242 nm are due to 4d → 5s transitions; the n, π, and σ orbitals of monensin are also involved, but their contribution is significantly weaker.

Despite the calculations performed (based on the known crystal structures) do not reproduce well the experimental CD data, they confirm that the binding of the metal(I) ions is responsible for the observed specific CD absorption with a fine change in monensin conformation. The limited accuracy can be explained by the complicated system, the accumulation of computational error arising from the DFT and TDDFT approximations, the approximate solvent model and the lack of dynamic modeling. In any case, the general similarity of the crystal and fully optimized DFT structures of the monovalent metal monensinates contrasts with their different CD signals. We can conclude, however, that the CD spectroscopy (compared to UV-VIS, IR and NMR) is a sensitive method for evaluating the interactions of monovalent cations with monensin A.

4.3. Theoretical study of competition processes between IA/IB metal cations for binding to monensin or salinomycin

While the polyether antibiotic monensin is known as a sodium ionophore, salinomycin is believed to be selective for potassium ions, although very limited data exist in the literature regarding its affinity towards monovalent cations. On the other hand, depending on the experimental approach, the data on the preferred binding of metal(I) cations vary, thus the position of the alkali cations in the given series is some time disordered. From a third point of view, the structural chemistry of the monovalent metal complexes of monensin is well known compared to the single crystallographic study of sodium salinomycinate. All this together provoked our interest to investigate the possible factors that may influence the selectivity of polyether ionophores towards group IA metal ions using a theoretical approach (DFT/PCM). Furthermore, for sake of comparison, we extended the model to include group IB cations. The properties of metal(I) monensinates were initially evaluated. The obtained results are in line with the experimental data, which gave us reason to apply the same approach to the salinomycin complexes.

4.3.1. General remarks

Alkali metals form spherical monovalent cations, which ionic radius gradually increases with increasing atomic number (**Table 4.3-1**). The ionic charge density (**Table 4.3-2**) decreases in the same direction, thereby weakening the metal ion's affinity for complexation and turning the bulkiest Cs^+ into the weakest (lowest affinity) Lewis acid of the group.

Compared to the physico-chemical properties of the alkaline ions, those of the Cu^+, Ag^+ and Au^+ cations are strongly influenced by the presence of d-orbitals in the outer electron shell, which by hybridizating with the valence s-orbitals reduce their energy, hence - decrease their ionic radius and increase their ability to accept charge. As it is shown in **Table 4.3-1** (last two columns), the charge transfer from the donor groups of the antibiotics to the group IB metal cations is greater (i.e., higher affinity) than that to the corresponding alkali metal ions of the same period. Furthermore, the Wiberg index estimated by the population NBO analysis shows that the bonds between the group IB cations and the donor oxygen atoms are stronger than those for the corresponding group IA representatives: the average value of the Wiberg-index for Cu^+-O, Ag^+-O and Au^+-O is 0.0578, 0.0601 and 0.0917 a.u., respectively, while that of Li^+-O, Na^+-O, K^+-O, Rb^+-O and Cs^+-O is 0.0159, 0.0135, 0.0157 , 0.0063 and 0.0104 a.u., resp.

Table 4.3-1. Structural and electronic characteristics of metal cations of groups IA and IB with coordination number 6

Metal ion	Ionic radius (Å)	Average distance of M-O bond (Å)	Charge transfer to the metal (e) in M^+-(CH_3OCH_3)[a,b]	Charge transfer to the metal (e) in M^+-(CH_3OH)[a,c]
Li^+	0.76 (VI)	2.26	0.286	0.260
Na^+	1.02 (VI)	2.42	0.215	0.198
K^+	1.38 (VI)	2.81	0.166	0.152
Rb^+	1.52 (VI)	2.89	0.142	0.132
Cs^+	1.67 (VI)	3.08	0.129	0.119
Cu^+	0.77 (VI)	2.44	0.360	0.338
Ag^+	1.15 (VI)	2.56	0.300	0.281
Au^+	1.37 (VI)	2.71	0.412	0.381

[a] Calculated from the Hirshfeld population analysis at the B3LYP/6-31+G(d,p) level
[b] CH_3OCH_3 is used as a model for the ether group
[c] CH_3OH is used as a model for the hydroxyl moiety

Table 4.3-2. Charge density of cations of groups IA and IB with varying coordination number and Lewis acidity

Ion	Ionic radii (r, Å)[a]	Charge density[b] (e / Å^3)	Lewis acidity (Valence units)
Li^+	0.59 (IV)	1.16	0.215
Na^+	1.00/1.02 (V/VI)	0.24/0.22	0.159
K^+	1.38 (VI)	0.09	0.108
Rb^+	1.52/1.56 (VI/VII)	0.07/0.06	0.099
Cs^+	-/1.74 (VII/VIII)	-/0.04	0.084
Cu^+	0.60 (IV)	1.10	0.400
Ag^+	1.09/1.15 (V/VI)	0.18/0.16	0.191
Au^+	-/1.37 (II/VI)	-/0.09	-

[a] The respective coordination number(s) of the metal is/are given in parentheses;
[b] Charge density = Ion charge/Ion volume = $1 / (4/3\ \pi r^3)$

4.3.2. Monensin

The structures of the optimized alkali monensinates are presented in **Fig. 4.3-1**. Metal cations with coordination number of 6 are bound to ether and hydroxyl oxygen atoms. The average M-O bond length increases from 2.28 to 3.08 Å, which agrees with the increasing ionic radius of the metal ions (**Table 4.3-1**). This result suggests that the monensinate ion is relatively flexible and its internal cavity, unlike that of other "rigid" macrocycles (e.g., crown ethers), can vary in size, adapting to the spatial requirements of the guest cation.

The preference of monensin for binding to monovalent metal ions was estimated based on the substitution reaction of sodium cations (MonNa) with the rest of IA/IB cations (equation 3, **Table 4.3-3**). The result for the competition of metal ions in solution is a balance between the electronic and the solvation effects. The role of the former can be assessed by monitoring the change in gas-phase Gibbs free energy, ΔG^1 (**Table 4.3-3**). The parameter ΔG^1 depends on the affinity of the metal cation for the ligands (measured as the charge transfer from the ligand to the metal; the greater the charge accepted, the higher the metal affinity). The binding affinity is highest for Li^+ ions and gradually weakens in group IA, and accordingly, the value of ΔG^1 increases from Li^+ to Cs^+. Taking into account the electronic effects, the affinity of metal cations for the monensinate anion decreases in the order $Li^+ > Na^+ > K^+ > Rb^+ > Cs^+$.

The solvation effect, however, affects the affinity order: it remains the same in solvents of low polarity (with a dielectric constant of 2-4), but changes in polar solvents (methanol and

water). The corresponding values of ΔG^{32} and ΔG^{78} for exchange of Li^+ with Na^+ become positive; the free energy for the rest metal ions in these polar solvents decreases but remains positive. Thus, the affinity in methanol follows the order $Na^+ > Li^+ > K^+ > Rb^+ > Cs^+$, which is in good agreement with experimental results showing that monensin A is a sodium ionophore in polar solvents.

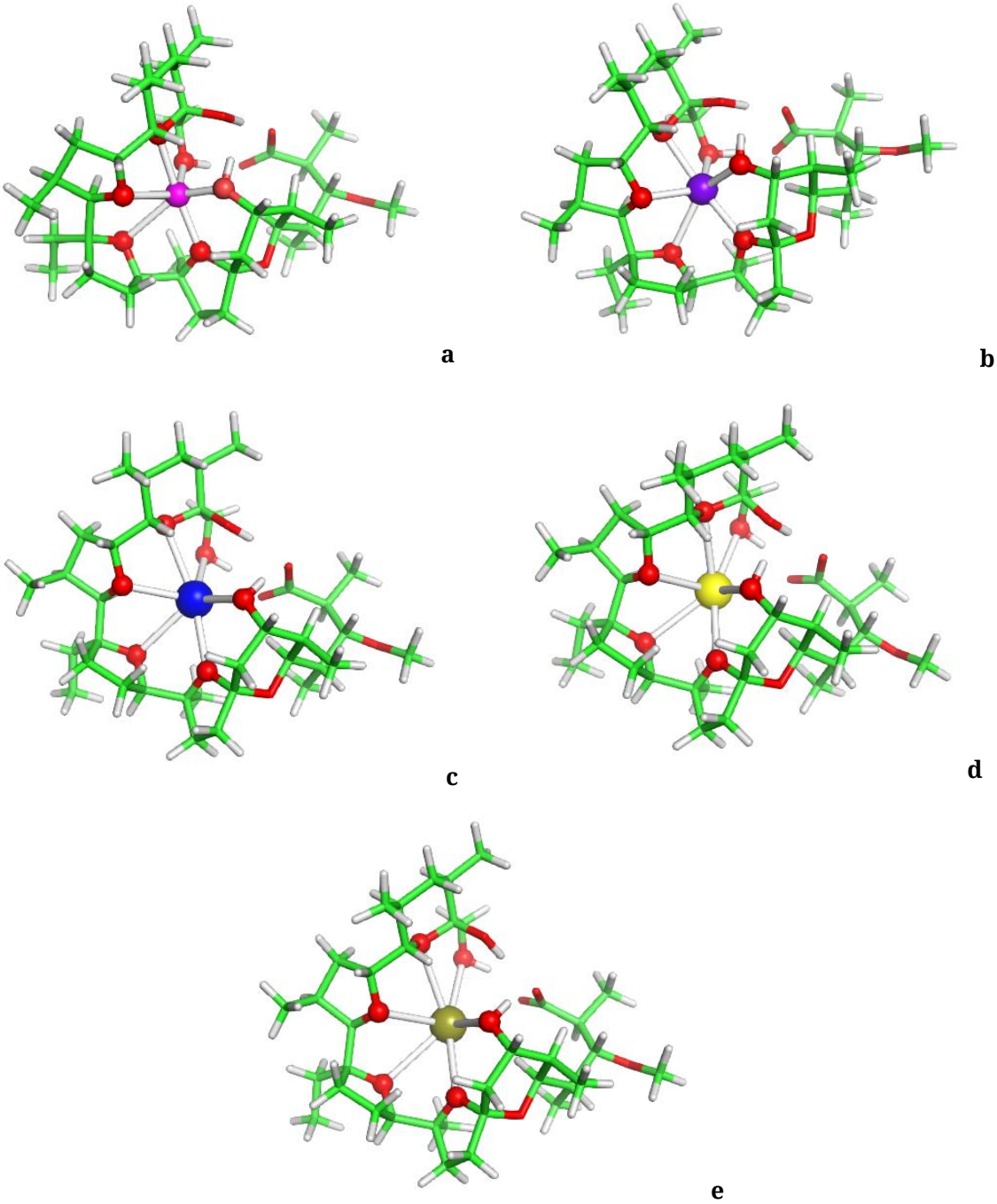

Fig. 4.3-1. B3LYP/6-31+G(d,p) optimized structures of the monensinate anion bound to a) Li^+, b) Na^+, c) K^+, d) Rb^+ and e) Cs^+

Table 4.3-3. Gibbs free energy for the $M^+ \rightarrow Na^+$ exchange (equation 3), ΔG^{ε}, in different polarity environment, ε[a]

Reaction	ΔG^{ε} (kcal/mol)
[Li^+-solution] + [Mon^-Na^+] → [Mon^-Li^+] + [Na^+-solution]	ΔG^1 = -20.5 ΔG^2 = -5.4 ΔG^4 = 0.0 ΔG^{32} = 5.7 ΔG^{78} = 5.9
[K^+-solution] + [Mon^-Na^+] → [Mon^-K^+] + [Na^+-solution]	ΔG^1 = 27.2 ΔG^2 = 17.4 ΔG^4 = 14.0 ΔG^{32} = 9.2 ΔG^{78} = 9.3
[Rb^+-solution] + [Mon^-Na^+] → [Mon^-Rb^+] + [Na^+-solution]	ΔG^1 = 61.7 ΔG^2 = 49.4 ΔG^4 = 44.7 ΔG^{32} = 36.8 ΔG^{78} = 35.4
[Cs^+-solution] + [Mon^-Na^+] → [Mon^-Cs^+] + [Na^+-solution]	ΔG^1 = 76.2 ΔG^2 = 60.7 ΔG^4 = 54.3 ΔG^{32} = 45.3 ΔG^{78} = 43.6
[Cu^+-solution] + [Mon^-Na^+] → [Mon^-Cu^+] + [Na^+-solution]	ΔG^1 = -31.6 ΔG^2 = -2.0 ΔG^4 = 8.7 ΔG^{32} = 15.0 ΔG^{78} = 14.9
[Ag^+-solution] + [Mon^-Na^+] → [Mon^-Ag^+] + [Na^+-solution]	ΔG^1 = 13.5 ΔG^2 = 23.1 ΔG^4 = 26.4 ΔG^{32} = 28.7 ΔG^{78} = 28.3
[Au^+-solution] + [Mon^-Na^+] → [Mon^-Au^+] + [Na^+-solution]	ΔG^1 = 2.4 ΔG^2 = 18.4 ΔG^4 = 24.1 ΔG^{32} = 27.3 ΔG^{78} = 26.6

[a] Estimating the relative metal affinity, that for the reference metal cation Na^+ is taken as 0, while that for the rest metal cations follows the trends in ΔG^{ε}

The optimized structures of monensin complexes with group IB cations are presented in **Fig. 4.3-2**. The smaller ionic radius of the IB ions is consistent with the shorter M-O bond lengths in their complexes with monensin compared to those of the alkali cations (**Table 4.3-1**). The substitution energy of Na^+ c Cu^+, Ag^+, and Au^+ in the gas phase is much more favorable than that

for the corresponding group IA metal ions of the same period (K^+, Rb^+, and Cs^+, respectively; **Table 4.3-3**). The affinity order for all monovalent cations in the gas phase decreases in the order $Cu^+ > Li^+ > Na^+ > Au^+ > Ag^+ > K^+ > Rb^+ > Cs^+$. In solvents with low polarity (eg, $\varepsilon \approx 2$), the affinity order changes in favor of Li^+: $Li^+ > Cu^+ > Na^+ > K^+ > Au^+ > Ag^+ > Rb^+ > Cs^+$. The sequence changes again in polar solvents (methanol), this time in favor of Na^+: $Na^+ > Li^+ > K^+ > Cu^+ > Au^+ > Ag^+ > Rb^+ > Cs^+$.

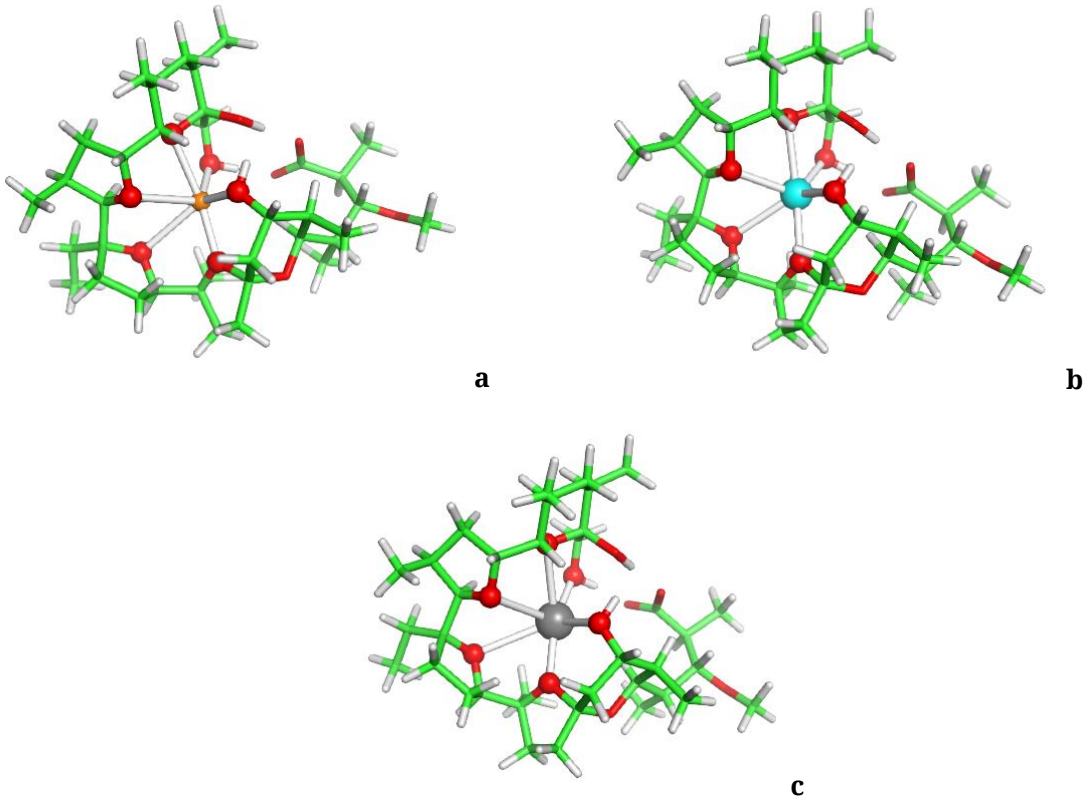

Fig. 4.3-2. B3LYP/6-31+G(d,p) optimized structures of the monensinate anion bound to a) Cu^+, b) Ag^+ and c) Au^+

4.3.3. Salinomycin

The metal(I) complexes of salinomycin were modeled on the basis of the only known crystal structures of sodium salinomycinate (SalNa). Two types of complex species have been experimentally observed, which differ in the number of water molecules coordinated to sodium ions - a complex with one crystalline water (SalNa-W_1) and another one containing two water molecules (SalNa-W_2). The atomic coordinates of the corresponding crystal structures were used for subsequent geometry optimization of the monovalent salinomycinates. Then, in the optimized structures, Na^+ (used as reference) was replaced by the corresponding monovalent

metal ions (M^+) and the resulting SalM-$W_{1/2}$ complexes were subjected to subsequent quantum chemical calculations.

Salinomycin participates in the formation of complexes with alkali metal cations through its oxygen atoms of the ether, hydroxyl, carbonyl and carboxylate groups. Analysis of the obtained structures showed that, like monensin, this antibiotic also possesses a flexible cavity capable to adapt to the specific physicochemical properties of the incoming metal(I) ions. The smallest member of the alkali group, Li^+, accepts its preferred tetrahedral coordination in both the ctructures with one-crystal (W_1, **Fig. 4.3-3**) and two-crystal (W_2, **Fig. 4.3-4**) waters with average Li-O bond length of 1.984/1.962 Å, resp. The complexes with the heavier alkali ions and one crystalline water contain five- (SalNa-W_1), six- (SalK-W_1, SalRb-W_1) and eight-coordinated (SalCs-W_1) cations with increasing metal-oxygen bond length: 2.407, 2.852, 2.985 and 3.211 Å, resp. for Na^+, K^+, Rb^+ and Cs^+. The main trend observed in increasing the coordination number and increasing the length of the metal-oxygen bond with increasing atomic number of the metal ion is analogous in the SalM series with two coordinated water molecules.

Compared to the complexes containing one water molecule, the coordination number of the metal ion differs in the corresponding structures with two water molecules. The metal-oxygen bond lengths in the W_2 series are 2.511 (SalNa-W_2), 2.814 (SalK-W_2), 3.055 (SalRb-W_2), and 3.264 (SalCs-W_2) Å. In both the W_1 and W_2 series, the longer M-O bond is in agreement with the increasing radius of the metal cation: 0.59 Å for tetra-coordinated lithium, 1.00/1.02 Å for penta-/hexa-coordinated sodium, 1.38 Å for hexa-coordinated potassium, 1.52/1.56 Å for hexa-/hepta-coordinated rubidium, and 1.74 Å for octa-coordinated cesium (**Table 4.3-2**). Water molecules remain coordinated to the metal cation in all complexes studied.

The Gibbs free energy was again used to evaluate the thermodynamic effect of competition between Na^+ (serving as a reference) and the other metal cations for salinomycin binding (**Table 4.3-4**). The trend in the changes of ΔG^ε is similar in both series, and the numerical values in most cases are very close.

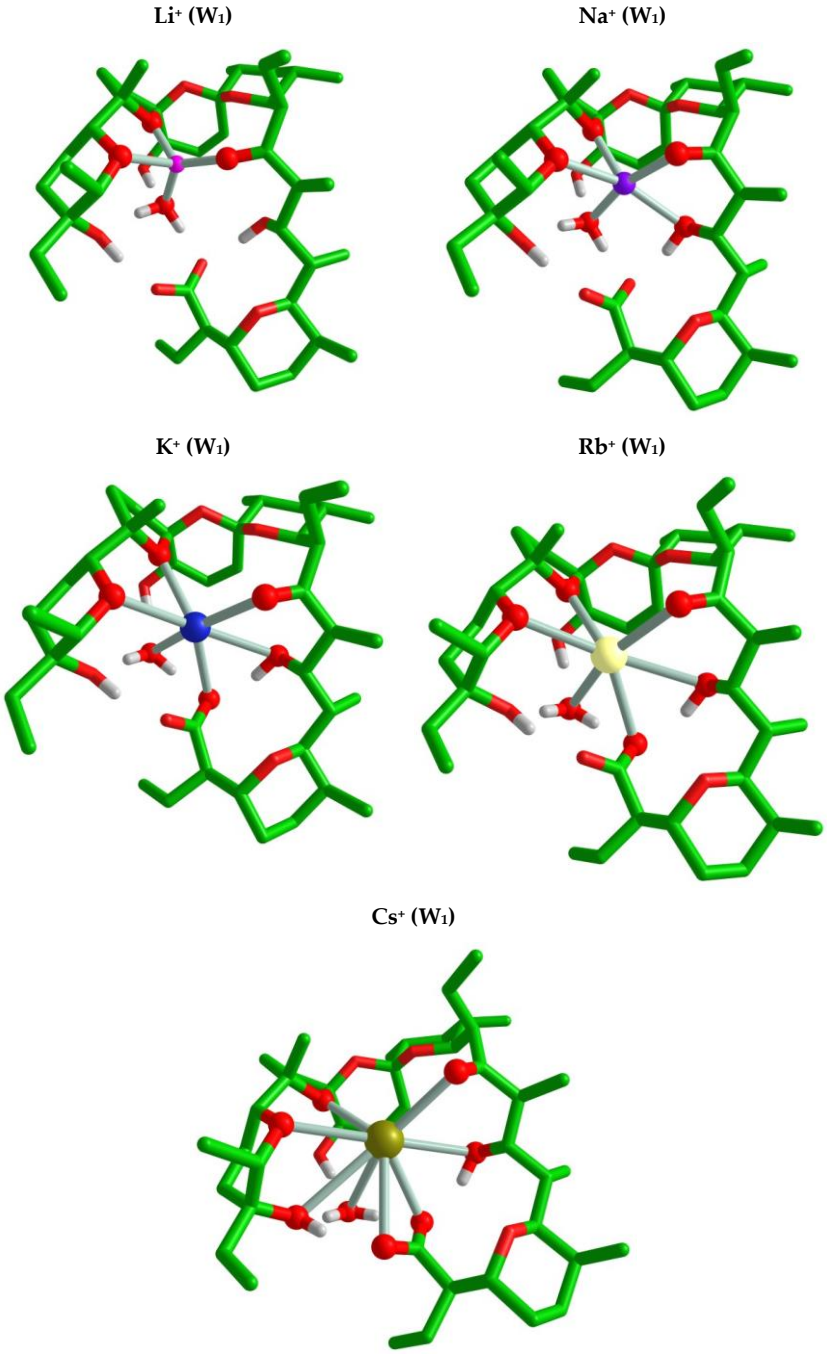

Fig. 4.3-3. B3LYP/6-31+G(d,p) optimized structures of salinomycinate complexes with Li^+, Na^+, K^+, Rb^+ u Cs^+, containing one (W_1) water molecule (hydrogen atoms omitted for clarity)

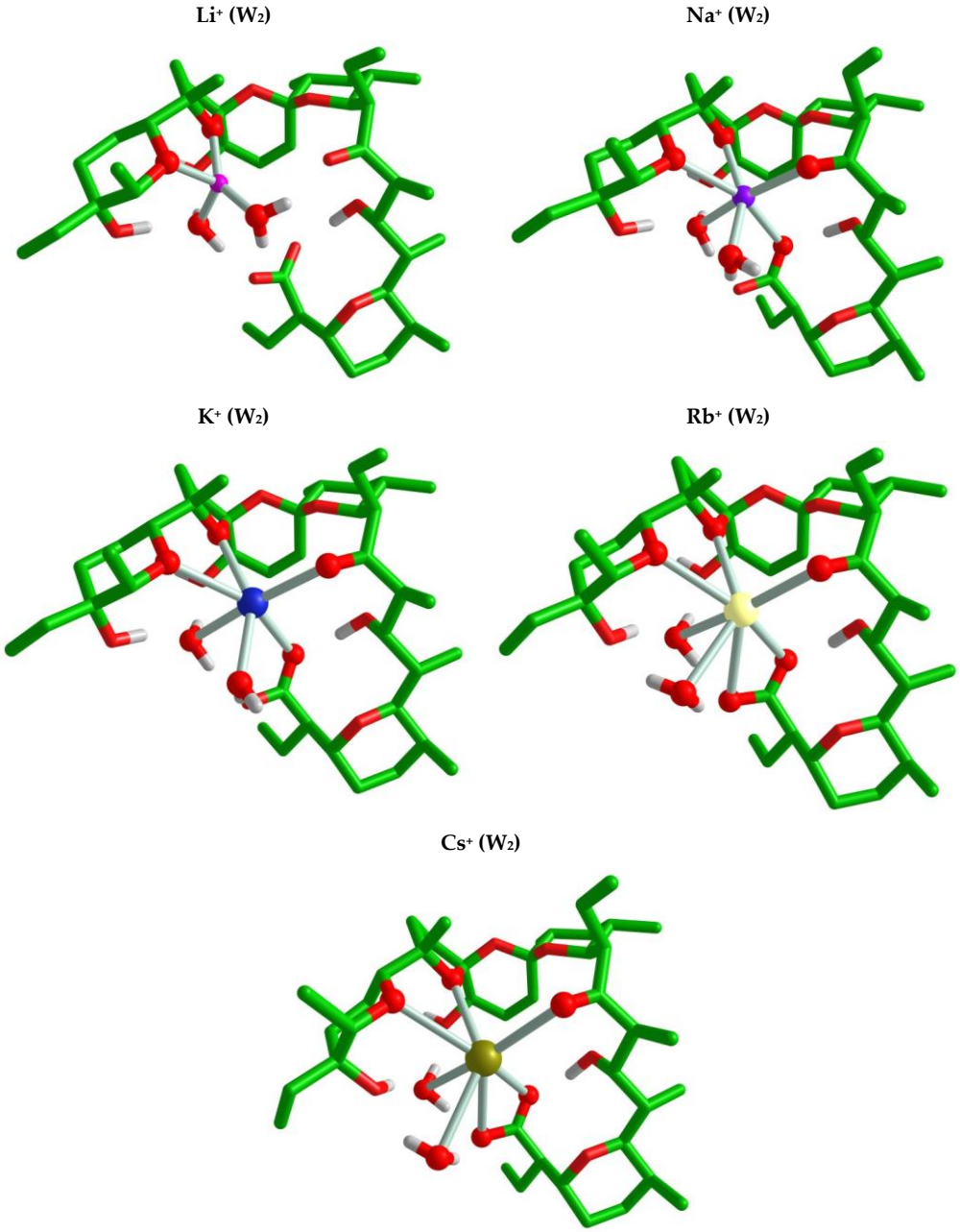

Fig. 4.3-4. B3LYP/6-31+G(d,p) optimized structures of salinomycinate complexes with Li^+, Na^+, K^+, Rb^+ u Cs^+, containing second (W_2) water molecule (hydrogen atoms omitted for clarity)

Table 4.3-4. Gibbs free energy for the substitution M^+/Na^+ reaction for salinomycin (ΔG^ε, kcal/mol) in different polarity environment

Reaction	ΔG^ε	Reaction	ΔG^ε
[Li^+-solution] + [SalNa-W_1] → [SalLi-W_1] + [Na^+-solution]	$\Delta G^1 = -21.6$ $\Delta G^2 = -7.8$ $\Delta G^4 = -3.2$ $\Delta G^{32} = 1.5$ $\Delta G^{78} = 1.4$	[Li^+-solution] + [SalNa-W_2] → [SalLi-W_2] + [Na^+-solution]	$\Delta G^1 = -24.0$ $\Delta G^2 = -10.6$ $\Delta G^4 = -6.5$ $\Delta G^{32} = -1.9$ $\Delta G^{78} = -1.7$
[K^+-solution] + [SalNa-W_1] → [SalK-W_1] + [Na^+-solution]	$\Delta G^1 = 19.8$ $\Delta G^2 = 9.9$ $\Delta G^4 = 6.8$ $\Delta G^{32} = 2.8$ $\Delta G^{78} = 2.8$	[K^+-solution] + [SalNa-W_2] → [SalK-W_2] + [Na^+-solution]	$\Delta G^1 = 20.6$ $\Delta G^2 = 10.0$ $\Delta G^4 = 6.3$ $\Delta G^{32} = 2.7$ $\Delta G^{78} = 2.7$
[Rb^+-solution] + [SalNa-W_1] → [SalRb-W_1] + [Na^+-solution]	$\Delta G^1 = 58.2$ $\Delta G^2 = 46.2$ $\Delta G^4 = 41.6$ $\Delta G^{32} = 34.3$ $\Delta G^{78} = 33.2$	[Rb^+-solution] + [SalNa-W_2] → [SalRb-W_2] + [Na^+-solution]	$\Delta G^1 = 56.1$ $\Delta G^2 = 43.5$ $\Delta G^4 = 38.2$ $\Delta G^{32} = 32.8$ $\Delta G^{78} = 31.2$
[Cs^+-solution] + [SalNa-W_1] → [SalCs-W_1] + [Na^+-solution]	$\Delta G^1 = 71.2$ $\Delta G^2 = 55.7$ $\Delta G^4 = 49.7$ $\Delta G^{32} = 41.4$ $\Delta G^{78} = 40.4$	[Cs^+-solution] + [SalNa-W_2] → [SalCs-W_2] + [Na^+-solution]	$\Delta G^1 = 67.3$ $\Delta G^2 = 51.1$ $\Delta G^4 = 44.7$ $\Delta G^{32} = 38.4$ $\Delta G^{78} = 36.7$
[Cu^+-solution] + [SalNa-W_1] → [SalCu-W_1] + [Na^+-solution]	$\Delta G^1 = -34.2$ $\Delta G^2 = -5.8$ $\Delta G^4 = 4.3$ $\Delta G^{32} = 9.2$ $\Delta G^{78} = 18.0$	[Cu^+-solution] + [SalNa-W_2] → [SalCu-W_2] + [Na^+-solution]	$\Delta G^1 = -31.6$ $\Delta G^2 = -2.9$ $\Delta G^4 = 7.2$ $\Delta G^{32} = 12.0$ $\Delta G^{78} = 11.4$
[Ag^+-solution] + [SalNa-W_1] → [SalAg-W_1] + [Na^+-solution]	$\Delta G^1 = 15.8$ $\Delta G^2 = 25.0$ $\Delta G^4 = 28.2$ $\Delta G^{32} = 29.9$ $\Delta G^{78} = 29.6$	[Ag^+-solution] + [SalNa-W_2] → [SalAg-W_2] + [Na^+-solution]	$\Delta G^1 = 16.0$ $\Delta G^2 = 25.3$ $\Delta G^4 = 28.4$ $\Delta G^{32} = 30.1$ $\Delta G^{78} = 29.5$
[Au^+-solution] + [SalNa-W_1] → [SalAu-W_1] + [Na^+-solution]	$\Delta G^1 = 5.2$ $\Delta G^2 = 20.0$ $\Delta G^4 = 24.8$ $\Delta G^{32} = 27.5$ $\Delta G^{78} = 26.8$	[Au^+-solution] + [SalNa-W_2] → [SalAu-W_2] + [Na^+-solution]	$\Delta G^1 = 0.7$ $\Delta G^2 = 14.5$ $\Delta G^4 = 18.5$ $\Delta G^{32} = 20.1$ $\Delta G^{78} = 18.0$

The smallest alkali cation, Li^+, is the only one that is preferred by salinomycin over Na^+ in low dielectric constant media for the W_1 series and in all solvents for the W_2 series. Heavier alkali ions (K^+, Rb^+, and Cs^+) are weaker competitors of Na^+ and show a positive free energy change in cation exchange that increases with element sequence number. Thus, the affinity of group IA cations for salinomycin can be arranged in the following order: $Li^+ > Na^+ > K^+ > Rb^+ > Cs^+$ (nonpolar solvents) and $Li^+ \geq Na^+ > K^+ > Rb^+ > Cs^+$ (polar solvents). These results are consistent

with the thermodynamic characteristics of alkali ions. The "winner" of group IA, Li^+, is characterized by the highest charge density and high Lewis acidity, and the best charge acceptance ability. These properties gradually weaken for the pecm cations, following the same affinity order given above.

In group IB, the copper cation forms tetrahedral complexes in the W_1 and W_2 series (**Fig. 4.3-5**) with an average Cu-O bond length of 2.220/2.211 Å, resp. Due to the high charge density and strong Lewis acidity, as well as the significant charge-accepting capacity, Cu^+ ions outcompete Na^+ both in the gas phase and in nonpolar solvents such as cyclohexane ($\varepsilon \approx 2$). In more polar solvents, however, the trend changes: due to the solvation effect, the sodium complex becomes dominant (positive values of ΔG^4, ΔG^{32} and ΔG^{78} for Cu^+).

As expected, the coordination number of the metal ion in the silver complexes increases (5 in SalAg-W_1 and 6 in SalAg-W_2), accompanied by the increase of ΔG, which values remain positive within the studied dielectric range (**Table 4.3-4**). In contrast, the coordination number of Au^+ drops sharply to 2 (linear configuration) due to strong relativistic effects. The data show that Au^+ is more competitive than Ag^+ but still cannot outcompete Na^+. Summarizing the results for groups IA and IB, the order of affinity for salinomycin in solvents of low polarity takes the order $Li^+ > Cu^+ > Na^+ > K^+ > Au^+ > Ag^+ > Rb^+ > Cs^+$, while in a medium with a high dielectric constant some disorder is observed: $Li^+ \geq Na^+ > K^+ > Cu^+ > Au^+ > Ag^+ > Rb^+ > Cs^+$.

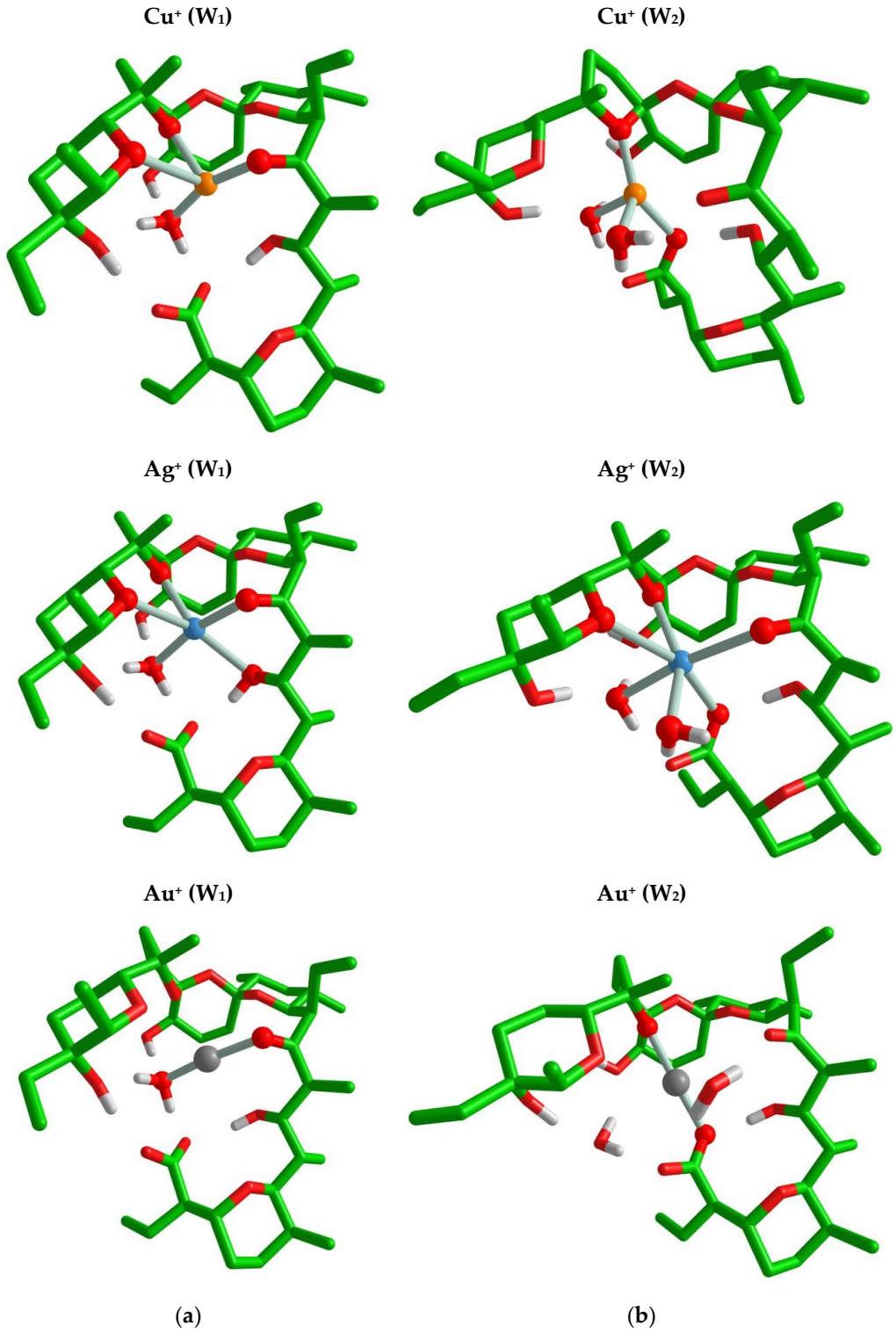

Fig. 4.3-5. B3LYP/6-31+G(d,p) optimized structures of salinomycin with Cu^+, Ag^+ u Au^+, containing (**a**) one (W_1) and (**b**) two (W_2) water molecules

4.4. Summary

The ability of the monensinate anion to interact with di- and tri-valent metal ions was evaluated by UV-CD spectroscopy. In addition to the already known neutral complexes $[MMon_2(H_2O)_2]$ and $[MMon_3(H_2O)_3]$, the formation of positively charged coordination particles in methanol solutions - one with M^{2+} and two with M^{3+} - was proved for the first time using this technique. The stability of the $[MMon(H_2O)]^+$ and $[MMon_2(H_2O)_2]$ species and competition reactions between the divalent metal ions for binding to monensin were assessed by both UV-CD and Vis/NIR-CD. The two approached are complementary with the following characteristics:

UV-CD: 😊 conformational changes in chiral ligands;
😊 study of "colorless" and "colored" metal complexes;
☹ the quantitative results may be unreliable in case of similar conformational changes between two or more species;

Vis/NIR-CD: 😊 induced chirality in complexes with "colored" metal ions;
😊 less experimental data number and simplified computational procedures;
☹ inability to study systems containing only a "colorless" metal ion.

The quantum-chemical calculations performed outline the following factors responsible for the selectivity of monensin and salinomycin towards the monovalent metal cations of groups IA and IB:

- *metal ion radius:* cations with smaller size and higher positive charge density are more competitive than their bulkier counterparts;

- *the metal ion charge accepting ability*: increasing the metal charge accepting ability, especially for d-elements, which translates into increased affinity toward the surrounding ligands (donor atoms), enhances the metal ion selectivity;

- *the dielectric propertied of medium*: the low polarity solvents favor the smaller ions with high ligand affinity (Li^+); in polar solvents characterized by a high dielectric constant, the competitive ability of medium cations, especially Na^+, increases;

- *the size of the internal cavity*, or more precisely – the polyether chain flexibility, is different in the two ionophores and is likely a reason for the coordination number of the metal ions: 6 in all monensin complexes, and varying from 2 to 8 in salinomycin coordination compounds

.

5. Results and Discussion:
Biological activity of polyether ionophores and their metal complexes

To evaluate the effect of the inclusion of metal ions into the structure of polyether ionophores, the biological activity of most of the structurally characterized complexes was evaluated against bacterial strains and/or tumor/non-tumor cell lines of different origin. For some of the coordination compounds, acute toxicity studies were conducted in "*in vivo*" experiments. In addition, a 72-hour treatment of the surviving individuals was carried out in order to evaluate certain biochemical indicators.

5.1. Antibacterial activity

The ability of the target compounds to suppress the bacterial cultures growth was characterized by their minimum inhibitory concentration (MIC, μg/mL, μM) – the lowest concentration at which no visible growth of the strains was observed. The studies were carried out with Gram-positive and Gram-negative microorganisms. The first type of bacteria is sensitive to the action of antibiotics and their metal complexes, while the second is resistant due to peculiarities in their cell wall, preventing the penetration of compounds with a molecular mass greater than 600 kDa.

Two main types of Gram-positive aerobic bacteria have been used over the years – representatives of the genus *Bacillus* and *Kocuria,* and *B. subtilis* (ATCC 6633) and *B. cereus* / *S. lutea* (in various modifications) have been maintained in the laboratory (**Table 5.1-1**). Over time, the methodology used has undergone changes both in terms of the standard used (McFarland) and the nutrient medium. Therefore, the tests of the given metal complexes always included, in addition to the solvent used, the corresponding forms of the antibiotics as controls in the evaluation of the antibacterial activity.

Data on the effect of unmodified antibiotics and their complexes on the growth of the tested strains are summarized in **Table. 5.1-2 – 5.1-4**[2]. In addition, a specific study on the

[2] Agar 1 (NA1) contains 0.1% w/v meat extract, 1% w/v peptone, 0.5% w/v NaCl, 1.5% w/v agar. For monolayer the NA1concentration is 31 g/L;
Agar2 (NA2) contains 5 g/L peptone, 1.5 g/L HM peptone B (beef extract), 1.5 g/L yeast extract, 5 g/L NaCl, 15 g/L agar, final pH 7.4; 28 g/L.
McFarland 3 – 9×10^8 CFU/mL; McFarland 4 – 1.2×10^9 CFU/mL;
Experimental conditions: double layer agar, well size 6 mm, sample volume 20 μL;
[a] McFarland 3; NA1; [b] McFarland 4; NA1; [c] McFarland 4; NA2.

mononuclear bis-complexes of monensin against the Gram-positive anaerobic microorganism *Cl. perfringens spp.* (**Fig. 5.1-1**) was performed.

The results show that the metal salts themselves are non-toxic, with MIC values above 1-5 mM. The inclusion of sodium ions in the composition of monensin (MonNa) does not significantly affect the activity of monensic acid; in most cases, the acidic form of salinomycin is twice as non-toxic as that of MonH.

Table 5.1-1. *B. cereus* and *S. lutea*, used in the study

B. cereus	*B. cereus* ATCC 10876; *B. mycoides spp.*; *B. cereus* 1085 (FDA PCI 213, *B. mycoides*); *B. cereus* ATCC 11778
S. lutea	*S. lutea* ATCC 10054 (FDA PCI 1000); *M. luteus* 159 (FDA PCI 1001); *K. rhizophila* ATCC 9341

Table 5.1-2. Antibacterial activity of polyether ionophores, their metal complexes and some metal salts against *B. subtilis*, strain ATCC 6633 (MIC, μM)

MonNa [a]	23.8		$[YMon_3(H_2O)_3]$ [b]	7.0
$[Mn(MonNa)_2Cl_2]$ [a]	10.8		$[LaMon_3(H_2O)_3]$ [b]	7.0
$[Co(MonNa)_2Cl_2]$ [a]	10.8		$[PrMon_3(H_2O)_3]$ [b]	7.0
$[Cu(MonNa)_2Cl_2]$ [a]	10.7		$[NdMon_3(H_2O)_3]$ [b]	14.0
MonH [a, b]	23.2 - 23.9		$[SmMon_3(H_2O)_3]$ [b]	7.0
$[CoMon_2(H_2O)_2]$ [a]	2.8		$[EuMon_3(H_2O)_3]$ [b]	14.0
$[MnMon_2(H_2O)_2]$ [a]	10.3		$[GdMon_3(H_2O)_3]$ [b]	7.0
$[CaMon_2(H_2O)_2]$ [a]	1.4		$[ErMon_3(H_2O)_3]$ [b]	7.0
$[MgMon_2(H_2O)_2]$ [b]	1.4		MonH [c]	22.7
$[NiMon_2(H_2O)_2]$ [b]	1.4		$[CeMon_2(OH)_2]$ [c]	10.2
$[ZnMon_2(H_2O)_2]$ [a]	1.4		$[CeMon(NO_3)_2(OH)]$ [c]	65.7
SalNa [b]	20		SalH [c]	41.6
SalH [b]	43		$[CeSal_2(OH)_2]$ [c]	18.7
$[CoSal_2(H_2O)_2]$ [b]	5		$[CeSal(NO_3)_2(OH)]$ [c]	60.6
$[NiSal_2(H_2O)_2]$ [b]	10		$MgCl_2.4H_2O$ [a]	5×10^3
$[CuSal_2(H_2O)_2]$ [b]	10		$CaCl_2$ [a]	5×10^3
$[ZnSal_2(H_2O)_2]$ [b]	10		$CoCl_2.6H_2O$ [a]	2×10^3

$Ni(NO_3)_2.6H_2O$ [a]	3×10^3		$MnCl_2.4H_2O$ [a]	5×10^3
$Zn(NO_3)_2.6H_2O$ [a]	3×10^3		$CuCl_2.6H_2O$ [a]	3×10^3
$(NH_4)_2[Ce(NO_3)_6]$ [c]	$> 1.8 \times 10^3$			

Table 5.1-3. Efect (MIC, μM) of polyether ionophores and their complexes *vs B. cereus*

B. cereus ATCC 10876			*B. cereus* 1085 (FDA PCI 213, *B. myc*.)	
MonNa [a]	$> 1.4 \times 10^3$		MonH [b]	11.9
$[Mn(MonNa)_2Cl_2]$ [a]	$> 6 \times 10^2$		$[YMon_3(H_2O)_3]$ [b]	7
$[Co(MonNa)_2Cl_2]$ [a]	$> 6 \times 10^2$		$[LaMon_3(H_2O)_3]$ [b]	7
$MnCl_2.4H_2O$ [a]	$> 5 \times 10^3$		$[PrMon_3(H_2O)_3]$ [b]	7
$CoCl_2.6H_2O$ [a]	$> 4 \times 10^3$		$[NdMon_3(H_2O)_3]$ [b]	3.5
B. mycoides spp.			$[SmMon_3(H_2O)_3]$ [b]	1.8
MonNa [a]	11.9		$[EuMon_3(H_2O)_3]$ [b]	7
$[Cu(MonNa)_2Cl_2]$ [a]	5.4		$[GdMon_3(H_2O)_3]$ [b]	1.8
MonH [a]	11.6 - 11.9		$[ErMon_3(H_2O)_3]$ [b]	3.5
$[CoMon_2(H_2O)_2]$ [a]	1.4		SalNa [b]	10
$[MnMon_2(H_2O)_2]$ [a]	5.1		SalH [b]	21
$[CaMon_2(H_2O)_2]$ [a]	0.7		$[CoSal_2(H_2O)_2]$ [b]	1
$[MgMon_2(H_2O)_2]$ [a]	0.7		$[NiSal_2(H_2O)_2]$ [b]	5
$[NiMon_2(H_2O)_2]$ [b]	0.7		$[CuSal_2(H_2O)_2]$ [b]	2
$[ZnMon_2(H_2O)_2]$ [b]	0.7		$[ZnSal_2(H_2O)_2]$ [b]	1
$CoCl_2.6H_2O$ [a]	2×10^3		*B. cereus* ATCC 11778	
$MnCl_2.4H_2O$ [a]	5×10^3		MonH [c]	5.7
$CuCl_2.6H_2O$ [a]	3×10^3		$[CeMon_2(OH)_2]$ [c]	5.1
$MgCl_2.6H_2O$ [a]	1×10^3		$[CeMon(NO_3)_2(OH)]$ [c]	16.4
$CaCl_2$ [a]	1×10^3		SalH [c]	10.4
$Ni(NO_3)_2.6H_2O$ [a]	3×10^3		$[CeSal_2(OH)_2]$ [c]	4.7
$Zn(NO_3)_2.6H_2O$ [a]	3×10^3		$[CeSal(NO_3)_2(OH)]$ [c]	7.6
			$(NH_4)_2[Ce(NO_3)_6]$ [c]	$> 1.8 \times 10^3$

Table 5.1-4. MIC vales (μM) for monensin, salinomycin, their metal complexes and salts reating *S. lutea*

S. lutea FDA PCI 1000 (ATCC 10054)			*M. luteus* 159 (FDA PCI 1001)	
MonNa [a]	23.8		$[YMon_3(H_2O)_3]$ [b]	7
$[Mn(MonNa)_2Cl_2]$ [a]	10.8		$[LaMon_3(H_2O)_3]$ [b]	7
$[Co(MonNa)_2Cl_2]$ [a]	10.8		$[PrMon_3(H_2O)_3]$ [b]	7
$[Cu(MonNa)_2Cl_2]$ [a]	10.7		$[NdMon_3(H_2O)_3]$ [b]	14
MonH [a. b]	23.2 - 23.9		$[SmMon_3(H_2O)_3]$ [b]	113
$[CoMon_2(H_2O)_2]$ [a]	2.8		$[EuMon_3(H_2O)_3]$ [b]	14
$[MnMon_2(H_2O)_2]$ [a]	10.3		$[GdMon_3(H_2O)_3]$ [b]	28
$[CaMon_2(H_2O)_2]$ [a]	1.4		$[ErMon_3(H_2O)_3]$ [b]	56
$[MgMon_2(H_2O)_2]$ [a]	1.4		SalNa [b]	20
$[NiMon_2(H_2O)_2]$ [b]	> 700		SalH [b]	43
$[ZnMon_2(H_2O)_2]$ [b]	> 700		$[CoSal_2(H_2O)_2]$ [b]	5
			$[NiSal_2(H_2O)_2]$ [b]	10
$MnCl_2.4H_2O$ [a]	5×10^3		$[CuSal_2(H_2O)_2]$ [b]	10
$CoCl_2.6H_2O$ [a]	2×10^3		$[ZnSal_2(H_2O)_2]$ [b]	10
$CuCl_2.6H_2O$ [a]	3×10^3		*K. rhizophila* ATCC 9341	
$MgCl_2.6H_2O$ [a]	5×10^3		MonH [c]	181.4
$CaCl_2$ [a]	5×10^3		$[CeMon_2(OH)_2]$ [c]	326.4
$Ni(NO_3)_2.6H_2O$ [a]	3×10^3		$[CeMon(NO_3)_2(OH)]$ [c]	525.8
$Zn(NO_3)_2.6H_2O$ [a]	3×10^3		SalH [c]	83.2
			$[CeSal_2(OH)_2]$ [c]	37.3
			$[CeSal(NO_3)_2(OH)]$ [c]	30.3
			$(NH_4)_2[Ce(NO_3)_6]$ [c]	$> 1.8 \times 10^3$

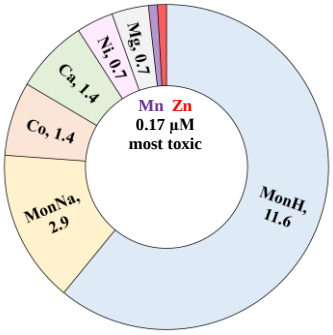

Fig. 5.1-1. Efect of MonNa, MonH and the bis-complexes with divalent metal ions against *Cl. perfringens* (MIC, μM)

Metal ions in the composition of the coordination compounds of monensin and salinomycin affect the antibiotics activity in a heterogeneous way:

- preserve the activity of the starting ligand (MIC is proportional to the number of mole ionophores in the complex);
- potentiate the ability to inhibit bacterial growth (MIC values are significantly lower than those of antibiotics)
- suppress the ionophores effect (higher MIC values compared to unmodified ligands)

In some cases, the same type of complexes show an opposite effect against specific bacterial strains, e.g. nickel(II) and zinc(II) monensinates, which are significantly more effective than MonH against *B. mycoides spp*., but virtually non-toxic against *S. lutea* FDA PCI 1000 (ATCC 10054).

5.2. Cytotoxicity

5.2.1. General remarks

The studies of the effect of the metal ion on the cytotoxicity of monensin or salinomycin were performed on a series of tumor lines of human or animal origin. The experiments were carried out within short- (24-72 h) and long-term (16-26 days) periods, applying different tests:

- MTT, NR, CV to determine the cytotoxic concentration 50 (CC_{50}, μM) and 90 (CC_{90}, μM) – the concentrations at which the test compounds reduce cell viability and proliferation by 50% or 90%;
- staining with AO/PI to monitor the cytopathological changes in the treated lines;
- colony-forming method;
- Comet assay.

The studied cell lines and the target compounds are summarized in **Table. 5.2-1**. Most of the experiments were conducted with solid tumors; the main object of study is monensin and its complexes with biometal ions. The results show that the effect of the compounds is concentration- and time-dependent, and a number of additional factors also affect the response of the cells - their origin, sensitivity and resistance, the method used to assess the cytotoxicity. The deep analysis of all the data collected so far can be a subject of a another independent work. At the present, specific examples of potentiation of the effect of polyether ionophores by metal ions are discussed. Details on the other studies have been published in the corresponding scientific reports.

Table 5.2-1. Cell lines and tested compounds

Cell line		Origin	Compounds
8MGBA	glioblastoma multiforme (brain tumor)	human	MonH, $[MMon_2(H_2O)_2]$ M^{2+} = Mg, Ca, Co, Mn, Ni, Zn
A549	lung cancer	human	MonH, $[MMon_2(H_2O)_2]$ M^{2+} = Mg, Ca, Co, Mn, Ni, Zn
MCF-7	breast cancer	human	MonH, $[MMon_2(H_2O)_2]$ M^{2+} = Mg, Ca, Co, Mn, Ni, Zn
MDA-MB-231	triple negative breast cancer	human	MonH, $[MMon_3(H_2O)_3]$ M^{3+} = La, Nd, Gd, Tb
HepG2	liver cancer	human	MonH, $[MMon_2(H_2O)_2]$ M^{2+} = Mg, Ca, Co, Mn, Ni, Zn
HeLa	cervical cancer	human	MonH, SalH, $[MMon_2(H_2O)_2]$ M^{2+} = Mg, Ca, Co, Mn, Ni, Zn $[CeL(NO_3)_2(OH)]$
A431 and its clones	squamous cell carcinoma	human	MonH, $[MMon_2(H_2O)_2]$ M^{2+} = Mg, Ca, Co, Mn
Lep3	non-tumor embryonic line	human	MonH, SalH, $[MMon_2(H_2O)_2]$ M^{2+} = Mg, Ca, Co, Mn, Ni, Zn $[CeL(NO_3)_2(OH)]$
BV-173	chronic myeloid leukemia (in preblast crisis)	human	SalH, $[MSal_2(H_2O)_2]$ M^{2+} = Co, Cu, Ni, Zn
K-562	chronic myeloid leukemia	human	SalH, $[MSal_2(H_2O)_2]$ M^{2+} = Co, Cu, Ni, Zn
SKW-3	T- cell leukemia	human	SalH, $[MSal_2(H_2O)_2]$ M^{2+} = Co, Cu, Ni, Zn
LSCC-SF-Mc29	hepatoma induced by myelocytomatous virus	chicken	MonH, $[MMon_2(H_2O)_2]$ M^{2+} = Mg, Ca, Co, Mn

LSR-SF-SR	sarcoma induced by Raus sarcoma virus, Schmidt-Rupin strain	rat	MonH, $[MMon_2(H_2O)_2]$ M^{2+} = Mg, Ca, Co, Mn $[MMon_3(H_2O)_3]$ M^{3+} = La, Nd, Gd, Tb
Zajdela	chemically induced liver cancer	rat	MonH, $[MMon_2(H_2O)_2]$ M^{2+} = Mg, Ca, Co, Mn, Ni, Zn

5.2.2. Uterine cervical carcinoma (HeLa)

The proliferation and viability of the HeLa cell line were studeid in a series of experiments with MonH and the mononuclear bis-monensinates of Mg^{2+}, Ca^{2+}, Mn^{2+}, Co^{2+}, Ni^{2+} u Zn^{2+} (**Fig. 5.2-1**). Despite the apparent isostructurality, almost all complexes show higher, but different, toxicity compared to monensic acid except $[MgMon_2(H_2O)_2]$ (72 h). For comparison, the effect of the same compounds (under similar conditions) was also evaluated against the non-tumor line Lep3 of human origin. The results showed that nickel(II) and zinc(II) bis-monensinates possess a significantly better selectivity index SI = CC_{50} (Lep3) / CC_{50} (HeLa) = 4.3 ($[NiMon_2(H_2O)_2]$ and 3.0 ($[ZnMon_2(H_2O)_2]$), which distinguishes them from all other compounds (SI = 0.1-1.1).

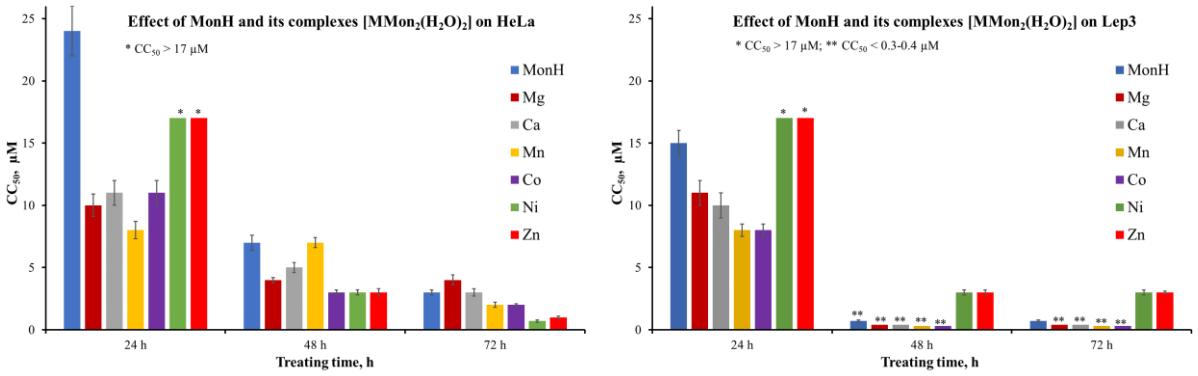

Fig. 5.2-1. CC_{50} (μM) of monensic acid and its mononuclear bis-complexes with Mg^{2+}, Ca^{2+}, Mn^{2+}, Co^{2+}, Ni^{2+} and Zn^{2+} (MTT assay, 24-72 h treatment)

The combination of HeLa and Lep3 lines was also tested against the cerium(IV) mono-complexes $[CeL(NO_3)_2(OH)]$ (**Table 5.2-2**). In addition to being highly toxic against cells isolated from the cervix cancer, the coordination compounds are also significantly more selective than some of the approved chemotherapeutics. The doble staining of HeLa with AO/PI (**Fig 5.2-2**) corroborates the MTT experimental data, confirming the cytotoxicity of the compounds and their ability to induce apoptosis. The untreated HeLa line (control) is visualized as a dense

monolayer and the cells possess a bright green nucleus and weak cytoplasmic fluorescence. Treatment with the target compounds resulted in a greatly reduced monolayer compared to the control, bright green nuclear fluorescence, swollen cells, vacuolization, and chromatin condensation. The additional increase of the concentration of the tested compounds increases the number of apoptotic cells.

Table 5.2-2. Cytotoxicity (CC_{50}, μM) of cerium(IV) complexes [$CeL(NO_3)_2(OH)$] against tumor HeLa and non-tumor Lep3 cell lines (MTT test, 72 h)

Compound	HeLa	Lep3	SI (Lep3/HeLa)
[$CeMon(NO_3)_2(OH)$]	< 0.53	6.31	> 12.62
[$CeSal(NO_3)_2(OH)$]	2.73	> 9.71	> 3.56
cisplatin	28	1.63	0.058
oxaliplatin	15	2.39	0.159
epirubicin	32	1.36	0.043

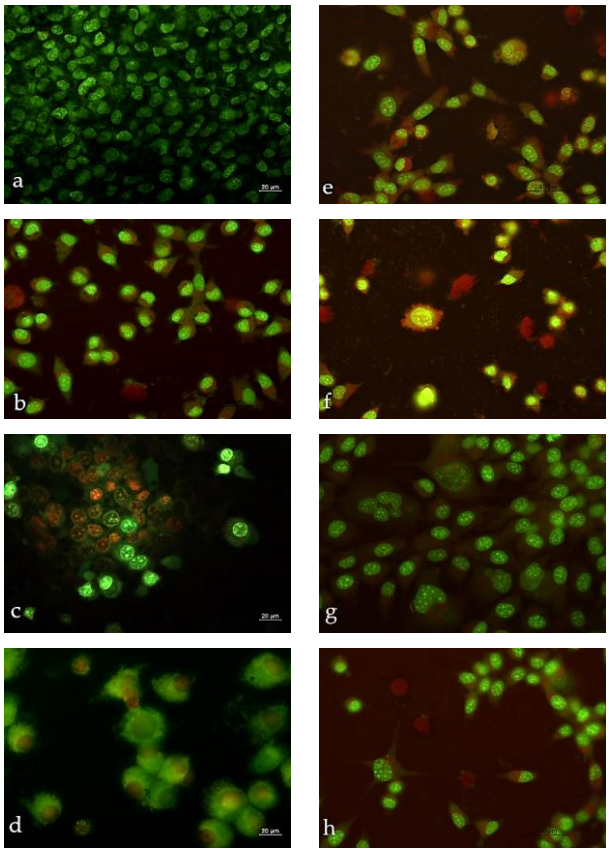

Fig. 5.2-2. Cytopathological changes in HeLa cells after double staining with AO/PI (72 h): (a) untreated cells (control); (b) MonH, 0.5 mg/mL; (c) MonH, 1 mg/mL; (d) MonH, 5 mg/mL; (e) SalH, 0.5 mg/mL; (f) SalH, 1 mg/mL; (g) [$CeMon(NO_3)_2(OH)_2$], 0.5 mg/mL; (h) [$CeSal(NO_3)_2(OH)_2$], 0.5 mg/mL (bar = 20 μm)

5.2.3. Leukemia cells (BV-173, K-562, SKW-3)

The cytotoxicity of salinomycin and mononuclear bis-complexes $[MSal_2(H_2O)_2]$ (M^{2+} = Co, Cu, Ni, Zn) was evaluated against three leukemic cell lines (**Fig. 5.2-3**, **Table 5.2-3**). The cobalt(II) and copper(II) complexes show better activity compared to nickel(II) and zinc(II) salinomycinates, and are significantly more toxic than SalH and SalNa. The metal salts are the most non-toxic, causing a 50% reduction in cell viability at significantly higher concentrations compared to the metal complexes. The myeloid cell lines BV-173 and K-562 show higher hemosensitivity to the tested compounds with nanomolar CC_{50} values compared to the SKW-3 cell line isolated from lymphoid T-cell leukemia.

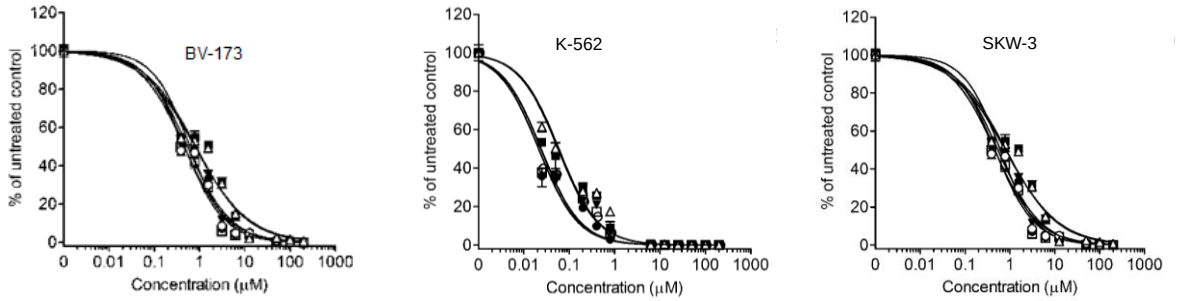

Fig. 5.2-3. Effect of SalH (Δ), SalNa (■) and complexes $[MSal_2(H_2O)_2]$ with Co^{2+} (○), Cu^{2+} (▲), Ni^{2+} (□), Zn^{2+} (●) against human tumor cell lines (MTT, 72 h)

Table 5.2-3. Cytotoxicity of salinomycin and its complexes

Compound / Cell line	CC_{50} (μM)		
	BV-173	K-562	SKW-3
SalH	0.052	0.059	0.830
SalNa	0.033	0.056	0.791
$[CoSal_2(H_2O)_2]$	0.012	0.021	0.461
$[CuSal_2(H_2O)_2]$	0.034	0.024	0.544
$[NiSal_2(H_2O)_2]$	0.012	0.022	0.468
$[ZnSal_2(H_2O)_2]$	0.061	0.024	0.612
$Co(NO_3)_2.6H_2O$	31.27	21.71	14.74
$Ni(NO_3)_2.6H_2O$	125.60	19.70	107.00
$Cu(CH_3COO)_2.H_2O$	67.56	10.83	51.89
$Zn(NO_3)_2.6H_2O$	64.71	52.81	73.34

5.3. Toxicological studies

The potentiated antibacterial and cytotoxic properties of polyether ionophores expressed by their metal complexes raised the question of the *in vivo* effect of these compounds. In this Section the results from the initial assessment of the toxicity of monensin and salinomycin complexes with biometal ions on laboratory animals (white male ICR mice) and their effect on the clinical parameters of the survivals are presented.

5.3.1. Acute toxicity (LD_{50})

The median lethal dose LD_{50} (acute toxicity indicator, **Table 5.3-1**) is determined according to the Prozorovsky's method for the following compounds:

- MonNa and $[M(MonNa)_2Cl_2]$ (M^{2+} = Mn, Co);
- MonH and $[MMon_2(H_2O)_2]$ (M^{2+} = Co, Zn);
- SalNa and $[MSal_2(H_2O)_2]$ (M^{2+} = Mg, Ca, Co, Zn).

Table 5.3-1. LD_{50} values of MonH, MonNa, SalNa and their metal complexes

Compound	LD_{50} (confidence interval)	
	mg / kg b.w.	μmol / kg b.w.
MonNa *	> 100	> 144
$[Mn(MonNa)_2Cl_2]$ *	> 79.4	> 52
$[Co(MonNa)_2Cl_2]$ *	> 31.6	> 21
MonH	87.0 (63-120)	130 (94-179)
$[CoMon_2(H_2O)_2]$ *	> 31.6	> 22
$[ZnMon_2(H_2O)_2]$	34.2 (23-51)	24 (16-35)
SalNa	21.6 (15-32)	28 (19-41)
$[MgSal_2(H_2O)_2]$	25.8 (21-32)	17 (13-21)
$[CaSal_2(H_2O)_2]$	20.5 (17-25)	13 (11-16)
$[CoSal_2(H_2O)_2]$	44.7 (38-60)	27 (23-37)
$[ZnSal_2(H_2O)_2]$	108.0 (73-160)	67 (46-100)

* It was not possible to determine the $LD5_0$ within the studied concentration range

The complexes $[CaSal_2(H_2O)_2]$ and $[MgSal_2(H_2O)_2]$ are the most toxic, and monensic acid is the most non-toxic among the compounds for which the LD_{50} value has been determined unambiguously. The zinc(II) complexes of monensin and salinomycin differ significantly in their

toxicity both to each other and to the parent antibiotics: MonH is five times less toxic than $[ZnMon_2(H_2O)_2]$, while SalH is more toxic compared to $[ZnSal_2(H_2O)_2]$.

Depending on the particular substance, a different clinical picture is observed in the treated experimental animals. The death in acute experiments with MonH and MonNa is not characterized by a change in the animals behavior. This is not the case, however, with the $[ZnMon_2(H_2O)_2]$ complex, namely – adynamia, bradypnea, loss of postural reflex, clonic seizures are observed.

The treatment with low doses of SalNa during the first 2-3 hours is accompanied by increased physical activity, while at high doses decreased physical activity and tachypnea were observed. Later ataxia, loss of postural reflex and aggressive behavior in survived animal groups were noticed. The cobalt(II) and zinc(II) salinomycinates do not cause significant changes in the animal status at the beginning – the animals are agitated with increased physical activity. After several hours, considerable alterations are obserced – mice become oppressed, drowsy and lose postural reflex. In the group treated with calcium(II) and magnesium(II) complexes tremor, disorientation and ataxia are observed.

5.3.2. Clinical indicators

The complexes of salinomycin with Mg^{2+} and Ca^{2+} showed the highest toxicity and for this reason we investigated their effect on the survivals through additional biochemical analyses. For this purpose, a three-day treatment with the same dose of the compound used during the acute toxicity experiments was carried out. Representative data for the parameters ALB, TP, AST, ALT, ALP, LDH, CR, URE upon treatment with $[MgSal_2(H_2O)_2]$ and $[CaSal_2(H_2O)_2]$ are presented in **Table 5.3-2**.

Table 5.3-2. Representative biochemical indices of survivals (72 h treatment, *per os*)

Compound	Dose, mg/kg b.w.	ALB, g/L	TP, g/L	AST, U/L	ALT, U/L	ALP, U/L	LDH, U/L	CR, μmol/L	URE, mmol/L
$[MgSal_2(H_2O)_2]$	20.0	36.6	-	640	91	362	1435	43.4	-
	25.0	29.4	-	173	68	203	1888	-	-
	31.6	33.0	-	385	83	330	905	62.2	-
	50.1	28.1	-	510	93	391	1750	-	-
$[CaSal_2(H_2O)_2]$	10.0	35.8	-	178	58	228	796	-	-

	12.6	34.3	60.0	240	95	216	-	66.5	12.7
	15.8	34.8	64.5	173	73	316	-	60.5	11.5
	20.0	43.7	-	175	95	219	954	37.2	-
	25.0	40.3	55.6	280	108	317	1571	40.4	10.2
	31.6	37.9	51.1	705	305	412	-	44.1	-
	39.8	34.6	63.4	255	70	129	-	55.3	13.9
	50.1	50.3	-	385	170	324	1255	43.1	-
Controls (range)	low	23	50	95	32	150	695	27	5
	high	34	74	474	105	326	2634	59	17

"-" – nor determined

From the results obtained, it can be concluded that the 72-hour treatment (once a day) with salinomycin complexes does not significantly affect most of the measured clinical parameters of the animals and the differences with the control group are not significant. The normal values of serum creatinine and urea are indicative that there is no acute kidney damage manifesting as renal failure. The increased ALB in the group treated with $[CaSal_2(H_2O)_2]$ could refer to animal dehydration. The increased AST values measured for some individuals suggest possible myocardial damage, since the mechanism of toxicity of the tested compounds is associated with myocardial ion channel disturbances. Liver function appears normal during the testing period. From the biochemical analysis, it can be concluded that the three-day treatment with the tested salinomycin complexes did not affect the liver and kidney functions of the experimental animals. A possible myocardial dysfunction is suggested, but to gain a deeper insight into the mechanism of toxicity, long-term chronic and subchronic toxicity studies should be conducted.

5.4. Summary

The experimental data reveals that the properties of a therapeutic candidate cannot be unambiguously and "automatically transferred" from one biological object to another. For a complete antibacterial characterization of a given compound, targeted research is required, which includes a wide range of microorganisms of different origin, accompanied (if possible) by studying of its mode of action. The latter requires more in-depth experiments, which are not the subject of the present work. The essence of the obtained results is the initial assessment of the activity of the complex compounds, which revealed their potential as effective antimicrobials.

The studies on the antitumor properties of polyether ionophores and their metal derivatives confirm the knowledge that the structural modification of natural biologically active compounds through complex formation is a successful approach in medicinal chemistry and can be applied to the development of novel pharmaceutical agents. Although this group of antibiotics has not found application in human medicine (due to potential cardiotoxicity), the data indicate that ionophores and their coordination compounds are of interest in the search for effective, and possibly selective, chemotherapeutics.

From the conducted preliminary trial on the effect of ionophorous antibiotics and their complexes, it can be concluded that the tested compounds do not significantly affect the studied clinical parameters during a three-day treatment:

- the observed deviations from the reference values for the most indicators are insignificant;

- the liver and kidney functions of the treated animals are preserved;

- isolated examples of dehydration and myocardial damage have been registered.

From the clinical signs of toxicity observed and based on the preliminary biochemical data obtained it can be suggested that the lethal outcome is associated with central nervous system toxicity and breath insufficiency. From a statistical point of view, the confirmation of this hypothesis requires additional experiments with a large number of laboratory animals.

6. Conclusions

1. 32 neutral "classical" and 7 "non-classical" complexes of the natural polyether ionophores monensin and salinomycin were isolated and structurally characterized:

- in the "classical" complexes, the antibiotics act identically through carboxylate and hydroxyl functions, forming mononuclear bis- and tris complexes with metal ions of the second and fourth oxidation state (bis-) and with trivalent ions of the rare earth elements (tris-);
- in the "non-classical" complexes, the ionophores are polydentate ligands, and their биндинг is specific for each individual coordination състем depending on the nature of the metal ion and the antibiotic form.

2. The ability of monensin and salinomycin to complex metal ions in solution has been studied by circular dichroism spectroscopy and theoretical models. It has been found that monensin can exist as positively charged coordination species in the presence of di- and trivalent metal cations. The theoretical modeling of the competition processes between monovalent metal ions for binding to monensin corroborate the experimentally observed phenomena, which laid ground to apply the same approach to the salinomycinate systems.

3. The inclusion of a metal ion in the composition of the coordination compounds of monensin and salinomycin affects the biological activity of the parent ligands in a different way: it retains, potentiates or reduces the effectiveness of the polyether ionophores. These results show that each therapeutic candidate should undergo as much as possible detailed characterization of its properties at *in vitro* and *in vivo* (laboratory models) conditions before reaching the phase of clinical trials in volunteers.

7. Achievements

While developing the present Thesis, the following results were achieved for the first time, which are primarily of a fundamental nature and contribute to the understanding of the matter nature and some specific phenomena:

1. It has been proven that the monovalent polyether ionophores monensin and salinomycin interact with metal cations in higher oxidation state until the formation of neutral coordination compounds. This fact can explain the influence of the close environment of antibiotics on their antibacterial activity.

2. Circular dichroism spectroscopy is an advantegeous thecnique when investigating the fate of the chiral monensin in solution. Thanks to it, the formation of a series of positively charged complex species has been proven, which was not possible by the use of other spectral methods. Moreover, the CD spectroscopy in the ultraviolet range allows to discriminate between the "colorless" metal ions such as those of alkaline elements, Mg^{2+}, Ca^{2+}, Zn^{2+}, Cd^{2+}, and its application in the visible wavelenght range allow to study both "color" systems (Co^{2+}, Ni^{2+}), as well as the competition processes of "color-colorless" metal cations.

3. Until now, the biological characterization of the discussed monensin and salinomycin complexes is the exlusive result of the efforts of Bulgarian researchers. The obtained data are promising and disclose the potential of carboxylic ionophores (alone or as coordination compounds) in the therapy of diseases of different origin.

8. Publications on Dissertation topic

The present Thesis relies on 27 original scientific papers, of which 21 publications were published in refereed and indexed journals and 4 as monograph chapters. The publications were not used obtaining the PhD degree.

Publication	Bibliographic data	Quartile	Points
Dorkov *et al.*, 2008	Synthesis, structure and antimicrobial activity of manganese(II) and cobalt(II) complexes of the polyether ionophore antibiotic sodium monensin A. J. Inorg. Biochem. 102(1):26-32	Q1	25
Pantcheva *et al.*, 2008	First divalent metal complexes of the polyether ionophore monensin A: X-ray structures of $[Co(Mon)_2(H_2O)_2]$ and $[Mn(Mon)_2(H_2O)_2]$ and their properties. Curr. Drug Discov. Technol. 5(2):154-161	Q3	15
Pantcheva *et al.*, 2009a	Crystal structure and properties of the copper(II) complex of sodium monensin A. J. Inorg. Biochem. 103(10):1419-1424	Q1	25
Pantcheva *et al.*, 2009b	Divalent metal complexes of the monovalent polyether ionophorous antibiotic monensin. In: Insights into Coordination, Bioinorganic and Applied Inorganic Chemistry, M. Melník, P. Segľa, M. Tatarko (Eds.), Press of Slovak University of Technology, Bratislava, pp. 257-268. ISBN 978-80-227-3085-4	monograph chapter	15
Ivanova *et al.*, 2010	Crystal structures and spectral properties of new Cd(II) and Hg(II) complexes of monensic acid with different coordination modes of the ligand. Centr. Eur. J. Chem. 8(4):852-860	Q3	15
Pantcheva *et al.*, 2010a	First solid state alkaline-earth complexes of monensic A acid: X-ray crystal structure of $[M(Mon)_2(H_2O)_2]$ (M = Mg, Ca), spectral properties and cytotoxicity against Gram-positive bacteria. BioMetals 23(1):59-70	Q1	25
Pantcheva *et al.*, 2010b	Nickel(II) and zinc(II) dimonensinates: crystal structure, spectral properties and bactericidal activity. Inorg. Chim. Acta 363:1879-1886	Q2	20
Alexandrova *et al.*, 2011	Cytotoxic and antiproliferative activities of monensic acid and its metal(II) complexes against drug sensitive and multidrug resistant human tumor cell lines. Intern. J. Biol. Biomed. Eng. 5(2):93-101	Q4	12*
Ivanova *et al.*, 2011	Cd(II) and Pb(II) complexes of the polyether ionophorous antibiotic salinomycin. Chem. Centr. J. 5:52	Q2	20
Mitewa *et al.*, 2011	Antitumor activity of the polyether ionophorous antibiotic monensin and its metal(II) complexes. In:	monograph chapter	15*

	Recent Researches in Modern Medicine. Braissant, O., Wakamatsu, H., Kuo-Kang, I., Allegaert, K., Lenbury, Y., Wachholtz, A. (Eds.), WSEAS Press, pp. 439-444. ISBN: 978-960-474-278-3		
Pantcheva & Mitewa, 2011	Polyether ionophores: coordination properties, antibacterial / antitumor activity and acute toxicity of their metal complexes. In: New Trends in Coordination, Bioinorganic and Applied Inorganic Chemistry. Melník, M., Segľa, P., Tatarko, M. (Eds.), STU Press, Bratislava, pp. 452-465. ISBN 978-80-227-3509-4	monograph chapter	15*
Alexandrova *et al.*, 2012	Cytostatic and cytotoxic properties of monensic acid and its biometal(II) complexes against human tumor / non-tumor cell lines. Cent. Eur. J. Chem. 10(5):1464-1474	Q2	20
Ivanova *et al.*, 2012	Synthesis, spectral properties, antibacterial and antitumor activity of salinomycin complexes with the transition metal ions Co(II), Ni(II), Cu(II) and Zn(II). J. Chem. Chem. Eng. David Publ. 6(6):551-562		
Pantcheva *et al.*, 2013	In vitro activity of biometal(II) complexes of monensin against virus-induced transplantable animal tumors. Biotechn. & Biotechn. Equipmn. 27(2):3703-3708	Q3	15
Zhorova *et al.*, 2013	Cytotoxicity of monensic acid and its biometal(II) complexes against anaerobic bacterial strain *Clostridium perfringens spp.* Biotechn. & Biotechn. Equipmn. 27(6):4308-4310	Q3	15
Atanasov *et al.*, 2014	Preliminary study on *in vivo* toxicity of monensin, salinomycin and their metal complexes. Bulg. Chem. Comm. 46(2):236-239	Q4	12
Nedzhib *et al.*, 2016	Circular dichroism is sensitive to monovalent cation binding in monensin complexes. Chirality 28(5):420-428	Q2	20
Pantcheva *et al.*, 2019a	Spectral properties and biological activity of La(III) and Nd(III) monensinates. Open Chemistry 17:1423-1434	Q3	15
Pantcheva et el., 2019b	Coordination compounds of polyether ionophore monensin with gadolinium(III) ions. In: Nanoscience & Nanotechnology, vol. 19(1), pp. 40-46, Balabanova, E., Mileva, E. (Eds.). ISSN: 1313-8995		
Alexandrova *et al.*, 2020	Study on *in vitro* toxicity of biometal(II) monensinates against rat Zajdela liver tumour. Chem. Didact. Ecol. Metrol. 25(1):125-132	Q4	12*
Dudev *et al.*, 2020	Factors governing the competition between group IA and IB cations for monensin A: a DFT/PCM study. RSC Advances 10:5734-5741	Q1	25

Pantcheva *et al.*, 2020	New insights into coordination chemistry of monensin towards divalent metal ions. Inorg. Chim. Acta 505:119481	Q2	20
Dudev *et al.*, 2022	A DFT/PCM study on the affinity of salinomycin to bind monovalent metal cations. Molecules 57(2):532	Q1	25*
Pantcheva *et al.*, 2022a	Alkaline-earth metal(II) complexes of salinomycin – spectral properties and antibacterial activity. Phys. Sci. Rev. / In: Chemical Sciences for the New Decade. Ramasami, P. (Ed.) vol. 2. Biochemical and Environmental Applications, pp.65-78. Walter de Gruyter GmbH, Berlin / Boston. ISBN 978-3-11-078358-2	monograph chapter	15*
Pantcheva et al., 2022b	Spectral properties of copper(II) bis-monensinate. C. R. Acad. Bulg. Sci. 75(4):519-526	Q3	15*
Kis *et al.*, 2023	Circular dichroism spectroscopic studies on solution chemistry of M(II)-monensinates in their competition reactions. Inorganics 11(8):334	Q2	20*
Petkov *et al.*, 2023	Novel cerium(IV) coordination compounds of monensin and salinomycin. Molecules 28(12):4676	Q1	25*

* The publications were not used acquiring “assoc. prof.” or “professor” academic positions, resp.